ChemComm

FEATURE ARTICLE

Cite this: *Chem. Commun.*, 2019, **55**, 6629

Small-molecule fluorescent probes for specific detection and imaging of chemical species inside lysosomes

Jun-Long Zhu,[a] Zheng Xu,[b] Yangyang Yang[c] and Lin Xu *[ad]

In the past few years, the preparation of novel small-molecule fluorescent probes for specific detection and imaging of chemical species inside lysosomes has attracted considerable attention because of their wide applications in chemistry, biology, and medical science. This feature article summarizes the recent advances in the design and preparation of small-molecule fluorescent probes for specific detection of chemical species inside lysosomes. In addition, their properties and applications for the detection and imaging of pH, H_2O_2, HOCl, $O_2^{\bullet-}$, lipid peroxidation, H_2S, HSO_3^-, thiols, NO, $ONOO^-$, HNO, Zn^{2+}, Cu^{2+}, enzymes, *etc.* in lysosomes are discussed as well.

Received 29th April 2019,
Accepted 7th May 2019

DOI: 10.1039/c9cc03299a

rsc.li/chemcomm

1. Introduction

Lysosomes are important cell organelles that contain more than 50 degradative enzymes, which usually have optimal activity in an acidic environment of pH 4.5–5.5.[1] The acidic microenvironments in lysosomes can activate these enzyme functions to facilitate the degradation of proteins.[2] For a long time, lysosomes were considered merely to be cellular waste bags as well as the stomachs of the cells. Nowadays, lysosomes are described as advanced organelles which play critical roles in cellular homeostasis and the mediation of a variety of physiological processes, such as protein degradation and plasma membrane repair.[3] Pieces of evidence have shown that lysosomes are associated with the pathogenesis of diseases such as storage disorders, cancer, neurodegenerative disorders, and cardiovascular diseases.[4]

Recent research has indicated that the chemical species (such as pH, H_2O_2, HOCl, $O_2^{\bullet-}$, lipid peroxidation, H_2S, HSO_3^-, thiol, NO, $ONOO^-$, HNO, Zn^{2+}, Cu^{2+}, enzyme, *etc.*) inside lysosomes seriously affect the status and function of these organelles.[5] For example, a lysosomal proton is associated with many cellular events, including apoptosis, autophagy, and cell maturation.[6] H_2S inside lysosomes could cause cell death in association with the activation of calpain proteases and lysosomal destabilization.[7] Excessive H_2O_2 in lysosomes would lead to lysosomal dysfunction or even rupture.[8] HOCl could induce apoptosis of cultured cells through the rupture of lysosomes.[9] Zn^{2+} plays an important role in lysosome dysfunction and the autophagy lysosome pathway.[10] The level of Cu^{2+} in lysosomes is closely related to a number of neurodegenerative diseases, including Wilson's disease (WD), Menkes disease (MD) and Alzheimer's disease (AD).[11] Therefore, specific detection and imaging of chemical species inside lysosomes would be very meaningful for the understanding of intracellular reaction kinetics and mechanisms, and further assisting the development of diagnostic and treatment strategies. Compared with traditional analytical techniques such as atomic absorption spectrometry, inductively coupled plasma atomic emission spectrometry, and

Lin Xu

Lin Xu received his PhD degree in Chemistry from the East China University of Science and Technology (ECUST, Shanghai) in 2012 under the supervision of Professor Xuhong Qian. Subsequently, he joined the East China Normal University (ECNU, Shanghai) as an assistant professor and was promoted to an associate professor and a professor in 2014 and 2018, respectively. He carried out two-year postdoctoral research at the University of Cambridge with Prof. Jonathan Nitschke during 2015–2017. His research interests focus mainly on supramolecular fluorescent chemistry.

---

[a] *Shanghai Key Laboratory of Green Chemistry and Chemical Processes, School of Chemistry and Molecular Engineering, East China Normal University, 3663 N. Zhongshan Road, Shanghai, P. R. China. E-mail: lxu@chem.ecnu.edu.cn*

[b] *Medicinal Chemistry, Monash Institute of Pharmaceutical Sciences, Monash University, Victoria, Australia*

[c] *Shanghai Key Laboratory of Chemical Biology, School of Pharmacy, East China University of Science and Technology, Shanghai, P. R. China*

[d] *State Key Laboratory of Fine Chemicals, Dalian University of Technology, Dalian 116024, China*

electrochemical methods, fluorescence probes have been recognized as one of the most efficient molecular tools in biological systems due to their high sensitivity and selectivity, easiness of manipulation, real-time imaging, high spatiotemporal resolution, and nondestructive detection.[12] Therefore, during the past few years, a great number of small-molecule fluorescent probes for the specific detection and imaging of chemical species inside lysosomes have been developed, which provide important concentration and distribution information of the chemical species within lysosomes. Considering the fact that significant progress has been made in this field, it is crucial and urgent to summarize the recent development of such fluorescent probes. In this feature article, we will summarize and discuss the recent advances in small-molecule fluorescent probes for specific detection of chemical species, such as pH, H_2O_2, HOCl, $O_2^{\bullet -}$, lipid peroxidation, H_2S, HSO_3^-, thiol, NO, $ONOO^-$, HNO, Zn^{2+}, Cu^{2+}, and enzymes, inside lysosomes.

2. General methods for delivering small-molecule fluorescent probes to lysosomes

Despite the fact that various kinds of small-molecule fluorescent probes for specific detection and imaging of chemical species inside lysosomes have been reported, there are only a few methods to deliver molecular probes to cellular lysosomes so far. The most common approach is the incorporation of weakly alkaline groups, such as morpholine, as the guiding unit to target the probe molecules into the lysosome since these acidotropic groups can help the probes selectively accumulate in acidic lysosomes through the protonation of the amine groups in a cellular acidic environment.[13] Thus, usually, this kind of lysosome-specific probes contain a fluorophore as well as an amine-containing side group. For instance, LysoTracker Red is one of the commonly-used commercial lysosome probes, which has a BODIPY fluorophore and a weak basic side chain that can accumulate in acidic lysosomes.[14] The other way to target the probes into lysosomes is by using a rhodamine group, which acts as not only the fluorophore but also the lysosome anchor.[15] Under neutral or basic conditions, the spirolactam of rhodamine remains closed and the rhodamine derivatives are nonfluorescent. However, under acidic conditions such as within lysosomes, a proton leads to spirolactam ring-opening, which exhibits strong fluorescence emission and results in the accumulation of probes in lysosomes.

Based on the above strategies, various kinds of small-molecule fluorescent probes for specific detection and imaging of chemical species such as protons, NO, H_2S, H_2O_2, HOCl, HNO, His, Zn^{2+}, Cu^{2+}, and enzymes inside lysosomes have been reported. In order to make it easy to understand, in this feature article, we classified these fluorescent probes depending on the type of the guests they recognized.

3. Small-molecule fluorescent probes for the detection of lysosomal pH

As previously mentioned, lysosomes contain more than 50 degradative enzymes that play critical roles in cellular metabolism. The acidic microenvironments in lysosomes (pH 4.5–5.5) can activate these enzyme functions to facilitate the degradation of proteins. However, the minor pH fluctuation of lysosomes may induce lysosome malfunction and consequently result in lysosomal storage diseases. Therefore, it is essential to precisely monitor lysosomal pH inside living cells in order to investigate cellular functions and understand physiological and pathological processes.

The spirocyclic structure of rhodamine is sensitive to the pH of the solutions.[16] For example, under basic conditions, it remains in the spirocyclic form that is non-fluorescent and colorless. While in acidic solutions, the ring-open form displays strong fluorescence and pink color. More importantly, these probes based on rhodamine usually exhibit a pK_a value ranging from 4 to 6, which is suitable for studying acidic lysosomes. Therefore, the rhodamine framework is popular for studying the pH of lysosomes.

Han *et al.* reported a rhodamine 6G-based fluorescent probe **1** (Scheme 1).[17] Analogous to commercial lysotrackers which often consist of a fluorophoric core linked to a weak base moiety, probe **1** also contains an amino group in order to preferentially accumulate in acidic organelles. The pH titration displayed that probe **1** was almost nonfluorescent at pH 7.0 or above because of its stable "ring-closed" form while the fluorescence was significantly enhanced as the pH decreased. The fluorescence intensity of probe **1** at pH 4.0 was 1500-fold brighter than that at pH 7.0, and was 100 fold brighter than that at pH 6.5, which indicated that probe **1** was a sensitive acid responsive probe capable of sensing minute pH changes in the range of pH 6.0–4.0 (Fig. 1a). The high sensitivity of probe **1** to protons and its high selectivity over interfering species that could be present inside cells such as Na^+, K^+, Ca^{2+}, Co^{2+}, Cu^{2+}, Fe^{3+}, Zn^{2+}, Mg^{2+}, HOCl, and H_2O_2

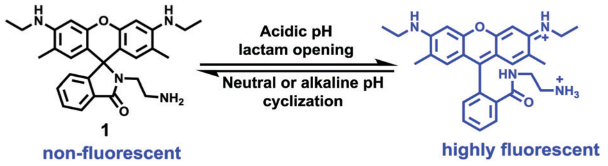

Scheme 1 Fluorescent probe **1** for pH.

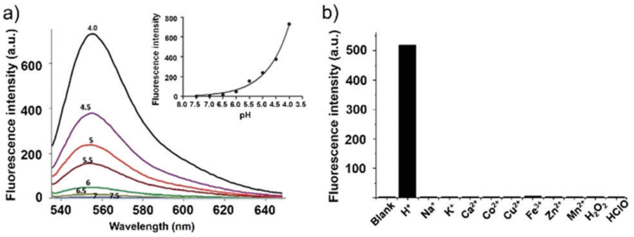

Fig. 1 (a) Fluorescence emission spectra of probe **1** at various pH values; the inset shows the pH titration curve of probe **1** (Ex@535 nm and Em@552 nm); (b) selectivity of probe **1** for pH over selected interferences in Dulbecco's Modified Eagle Medium (DMEM). Fluorescence emission intensity of probe **1** in DMEM containing H_2O_2 (5 mM), HOCl (5 mM) or various cations (1 mM) as compared to pH (0.1 mM) (Ex@533 nm, Em@553 nm). Copyright 2011 Royal Society of Chemistry.

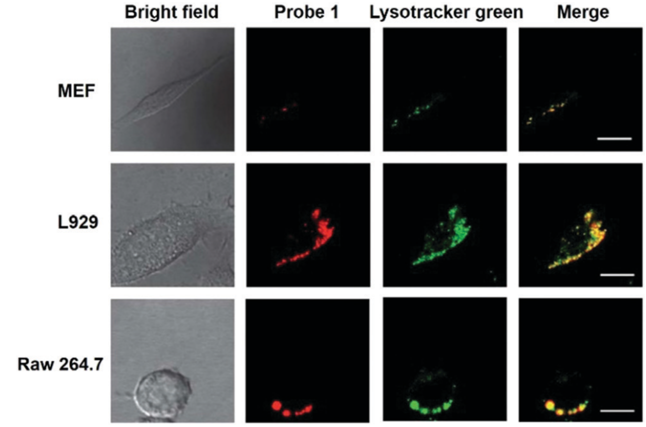

Fig. 2 Intracellular distribution of probe **1** as compared to lysotracker green. MEF, L929 and Raw 264.7 cells were respectively co-cultured with probe **1** and lysotracker green, washed with HBBS buffer, and then analyzed with confocal fluorescence microscopy to pinpoint the locations of probe **1** and lysotracker green inside cells. Merging of the fluorescence of probe **1** (shown in red) and lysotracker green (in green) was shown in yellow. Bars, 10 mm. Copyright 2011 Royal Society of Chemistry.

indicated that probe **1** was a potential selective pH sensor for applications in live cells (Fig. 1b). The double staining experiments showed that probe **1** stained the lysosomes in cells of mouse embryonic fibroblast (MEF), L929, and mouse leukaemic monocyte macrophage (Raw 264.7). Moreover, the distribution of probe **1** colocalized with lysotracker green, suggesting that probe **1** selectively stain lysosomes in live cells (Fig. 2). Further, it was found that probe **1** exhibited high stability against photobleaching and long retention time in lysosomes, allowing tracking of morphological alteration of lysosomes from start to finish in the process of TNF-a triggered cell death.

Zhang and Mao *et al.* designed a new rhodamine-morpholine fluorescent probe **2**, which contains a morpholine group as the lysosome tracker (Scheme 2).[18] The investigation of the fluorescence responses of probe **2** at various pH values showed that it was almost nonfluorescent at pH 7.4 because of its stable "ring-closed" form, but the fluorescence intensity of probe **2** was significantly enhanced as the H^+ concentration increased to induce the opening of the spirolactam ring, which displayed a 140-fold increase in the emission intensities within the pH range of 7.4–4.5 (Fig. 3a). Moreover, probe **2** had a pK_a of 5.23, which was valuable for studying lysosomal pH (Fig. 3b). The confocal fluorescence imaging experiment showed that probe **2** and LysoSensor Green displayed large overlaps, which suggested that probe **2** selectively stained lysosomes in live cells (Fig. 4). More importantly, probe **2** was successfully applied to detect the chloroquine-induced increase in lysosomal pH and monitor the lysosomal pH changes during apoptosis in live cells, which indicated that probe **2** could detect lysosomal pH changes in real time.

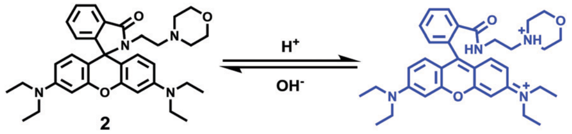

Scheme 2 Fluorescent probe **2** for pH.

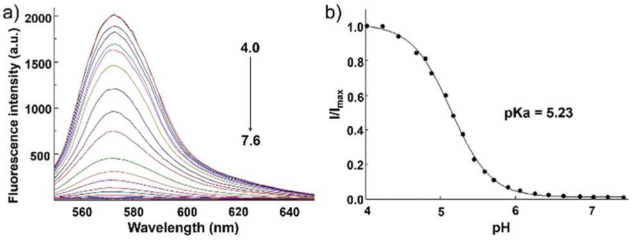

Fig. 3 (a) Fluorescence spectra of probe **2** (10 μM) at various pH values in Britton–Robinson buffer solution (40 μM), λ_{ex} = 525 nm, (b) pH titration curve of probe **2**, λ_{ex} = 525 nm, λ_{em} = 573 nm. Copyright 2014 Elsevier.

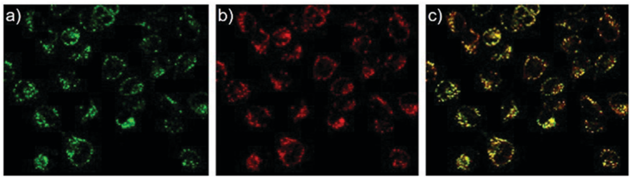

Fig. 4 Cells were stained with (a) 1 mM LysoSensor Green, (b) 10 mM probe **2**. (c) Areas of colocalization appear in yellow. Probe **2** and LysoSensor Green were excited at 543 nm and 488 nm, respectively. The fluorescence images were recorded at 550–650 nm and 495–515 nm. Copyright 2014 Elsevier.

Zhao and Miao *et al.* reported a rhodamine B-based pH probe **3**, which was synthesized from rhodamine B and cysteine ethyl ester (Scheme 3).[19] As shown in Fig. 5a, probe **3** was nearly non-fluorescent at pH 7.51. However, significant fluorescence enhancement was observed with decreasing pH from 7.51 to 3.53 (more than 150-fold increase), which demonstrated the formation of a ring-open structure of probe **3** induced by H^+ under acidic conditions. In addition, the result revealed that

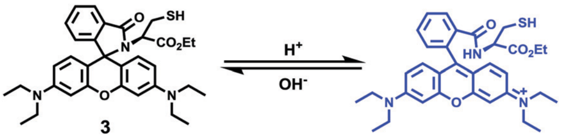

Scheme 3 Fluorescent probe **3** for pH.

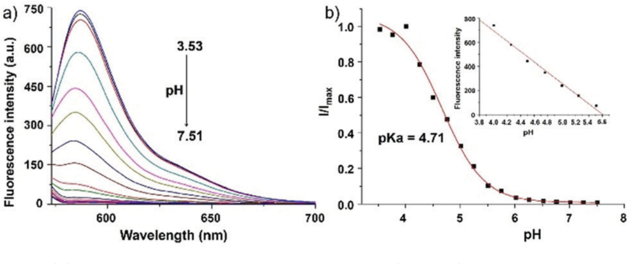

Fig. 5 (a) Fluorescence spectra of probe **3** (10 μM) in buffer at various pH values; (b) fluorescence intensity at 584 nm with pH values according to the fluorescent pH titration (pH 3.53–7.51), λ_{ex} = 563 nm. The inset shows the linear relationship of fluorescence intensity at 584 nm and pH values from 4.0 to 5.5 (*R* = 0.98101). Copyright 2013 Elsevier.

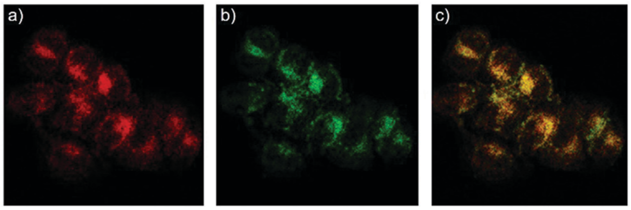

Fig. 6 Confocal fluorescence images of living HeLa cells co-stained with 1 μM probe **3** and 0.25 μM LysoSensor Green. (a) Red emission from probe **3**; (b) green emission from LysoSensor Green; (c) overlay of (a) and (b); areas of co-localization appear in yellow. Copyright 2013 Elsevier.

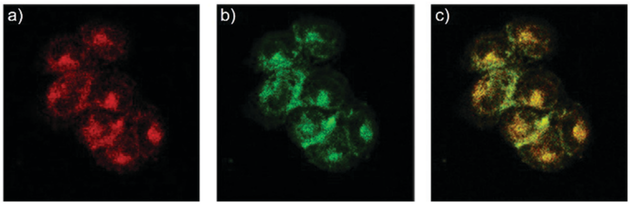

Fig. 8 Fluorescence microscopy images of living HeLa cells co-stained with 1 μM probe **4** and 0.25 μM LysoSensor green. (a) Red emission from probe **4**; (b) green emission from LysoSensor green; (c) overlay of (a) and (b); areas of colocalization appear in yellow. Copyright 2014 Elsevier.

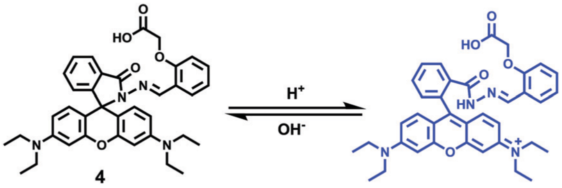

Scheme 4 Fluorescent probe **4** for pH.

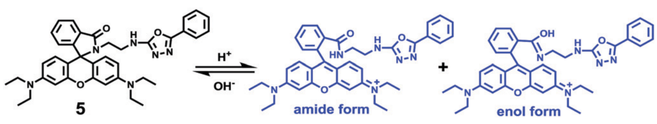

Scheme 5 Fluorescent probe **5** for pH.

probe **3** with a pK_a of 4.71 was suitable for studying acidic organelles (Fig. 5b). The fluorescence imaging experiments showed that the distribution of probe **3** colocalized with LysoSensor Green, which suggested that probe **3** could selectively stain lysosomes in living cells (Fig. 6). The lysosome-specificity of probe **3** might be due to *N*,*N*-diethyl groups of **3**. Moreover, it was found that probe **3** could serve as a fluorescent indicator for lysosomal pH and monitor lysosomal pH changes in living cells.

After that, Zhao and Miao *et al.* further reported a rhodamine B-based probe **4** for detecting H^+ (Scheme 4).[20] The fluorescence response of probe **4** to pH was similar to that of probe **3**, while probe **4** has a pK_a of 5.72, which is higher than that of probe **3** (Fig. 7). The result indicated that the detection range of probe **4** could cover both normal and abnormal lysosome pH. Confocal fluorescent microscopy images displayed that the distribution of red fluorescence from probe **4** colocalized with green fluorescence from LysoSensor Green, which suggested that probe **4** selectively stained lysosomes in living cells (Fig. 8). Moreover, the fluorescence microscopy images of living HeLa cells co-incubated with bafilomycin A1 (BafA1) and probe **4** indicated that probe **4** could be used as a fluorescent indicator for lysosomal pH and to monitor lysosomal pH changes in living cells.

Zhao and Miao *et al.* also designed and synthesized a new rhodamine-based probe **5**, which exhibited a highly selective and sensitive response to acidic pH (Scheme 5).[21] The fluorescence intensity of probe **5** gradually increased about 46-fold from pH 6.7 to 4.4 with a pK_a value of 5.05. Based on the ^1H NMR spectra, the authors suggested that two open-ring structural forms, the amide form and the enol form, of probe **5** existed in the acidic solution simultaneously. Probe **5** could monitor intracellular pH in living HeLa as well as HUVEC cells. Moreover, it was suggested that probe **5** was valuable to measure pH changes in lysosomes as well since the fluorescence of the probe in cells weakened upon the addition of bafilomycin A1 or chloroquine that could induce a pH value increase in lysosomes.

Yu and Li *et al.* prepared two rhodamine B-based probes **6** and **7** *via* click reaction (Scheme 6).[22] 1,2,3-Triazole was introduced as an ideal bridge to improve the biocompatibility and water solubility of probes **6** and **7**. The difference between probes **6** and **7** was that **7** comprised one more amide bond, which might serve as additional protonate groups under acidic conditions. The investigations of the fluorescent response of probes **6** and **7** to pH showed that the fluorescence of probe **6** increased about 35 fold from pH 7.6 to 4.0 while that of probe **7** increased about 75 fold from pH 8.0 to 4.4 (Fig. 9). Moreover, the pK_a values of the two probes were calculated as 4.79 and

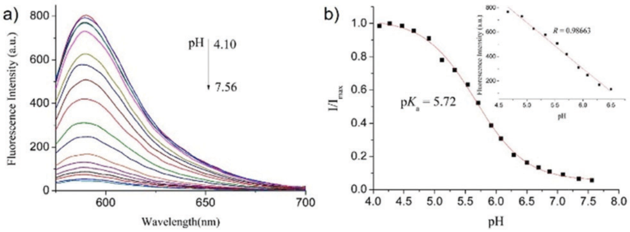

Fig. 7 (a) Fluorescence spectra of probe **4** (10 μM) in aqueous solution (Britton–Robinson buffer–EtOH, 9 : 1, v/v) with different pH values; (b) pH titration curve of probe **4**, λ_{ex} = 563 nm, λ_{em} = 589 nm. The inset shows the linear relationship of fluorescence intensity at 589 nm and varying pH values from 4.6 to 6.5. Copyright 2014 Elsevier.

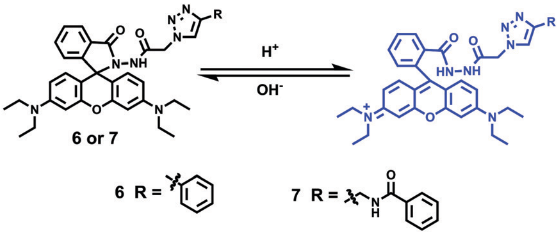

Scheme 6 Fluorescent probes **6** and **7** for pH.

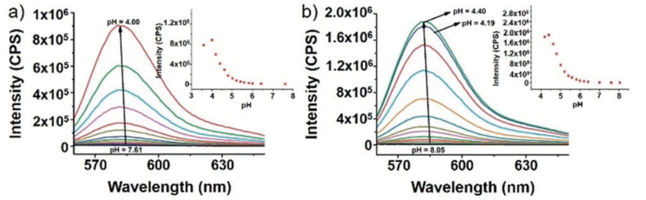

Fig. 9 (a) Fluorescence spectral changes of probe **6** (5 μM) in Britton–Robinson buffer (B–R buffer) solution at different pH values (λ_{ex} = 540 nm), and the maximum emission intensity was measured at 583 nm. Inset: Plot of the emission fluorescence intensity at 583 nm; pH 3.60, 4.00, 4.19, 4.40, 4.62, 4.80, 5.01, 5.21, 5.41, 5.59, 5.82, 6.00, 6.21, 6.42, 7.01, and 7.61. (b) Fluorescence spectral changes of probe **7** (5 μM) in B–R buffer solution at different pH values (λ_{ex} = 540 nm), and the maximum emission intensity was measured at 583 nm. Inset: Plot of the emission fluorescence intensity at 583 nm; pH 3.60, 4.00, 4.19, 4.40, 4.62, 4.80, 5.01, 5.21, 5.41, 5.59, 5.82, 6.00, 6.21, 6.42, 7.01, 7.61, and 8.05. Copyright 2014 Royal Society of Chemistry.

5.23 for probes **6** and **7**, respectively. Interestingly, confocal laser scanning microscopy analysis indicated that the subcellular regions stained with probe **6** not only matched those stained with LysoTracker Green very well but also matched well with MitoTracker Green staining, while the subcellular regions stained with probe **7** only matched well with LysoTracker Green staining (Fig. 10). These results revealed that probes **6** and **7** had different locations in living cells. Moreover, compared with the two commercial dyes LysoTracker Green and MitoTracker Green, probes **6** and **7** were much less toxic, and it was suggested that probes **6** and **7** were more beneficial for biological applications in this regard.

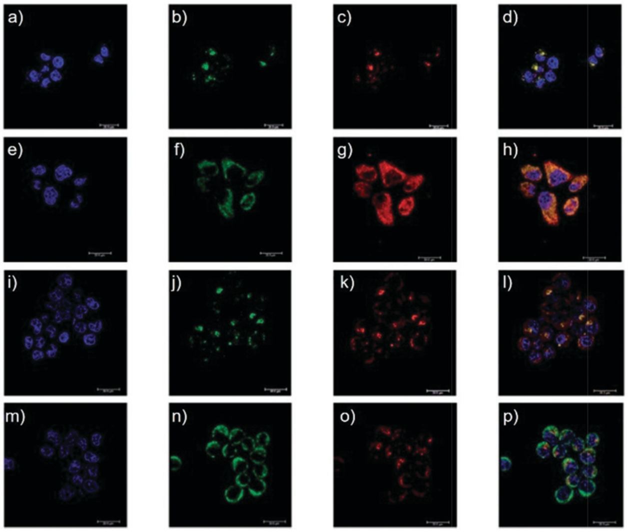

Fig. 10 Confocal microscopy images of the intracellular distribution of lysosomes (incubation 30 min). (a–d) HeLa cells were stained with one drop of NucBlue (blue channel), 1 μM LysoTracker Green (green channel) and 5 mM probe **6** (red channel). (e–h) HeLa cells were stained with one drop of NucBlue (blue channel), 1 μM MitoTracker Green (green channel) and 5 μM probe **6** (red channel). (i–l) HeLa cells were stained with one drop of NucBlue (blue channel), 1 μM LysoTracker Green (green channel) and 5 μM probe **7** (red channel). (m–p) HeLa cells were stained with one drop of NucBlue (blue channel), 1 μM MitoTracker Green (green channel) and 5 μM probe **7** (red channel). Blue channel: λ_{ex} = 405 nm, λ_{em} = 420–470 nm; green channel: λ_{ex} = 488 nm, λ_{em} = 500–540 nm; red channel: λ_{ex} = 552 nm, λ_{em} = 565–620 nm. Copyright 2014 Royal Society of Chemistry.

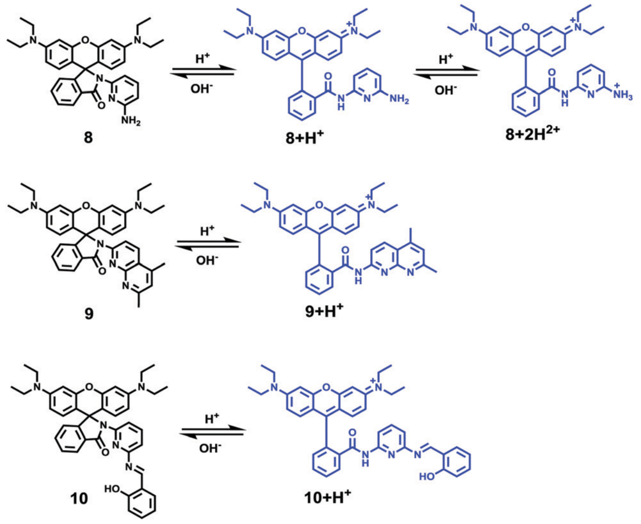

Scheme 7 Fluorescent probes **8**, **9** and **10** for pH.

Li and Liu *et al.* prepared a series of rhodamine B-based probes **8**, **9**, and **10** (Scheme 7).[23] For these probes, the functional group of 2,6-diaminopyridine was introduced and the amine side chains were protected with a flexible Schiff base or a rigid naphthyridine based on the considerations that a compound containing amine will not only have good solubility in both water and lipids but will also help the probe to accumulate selectively in an acidic environment such as a lysosome. The neutral solution of probes **8**, **9**, and **10** was almost colorless and non-fluorescent; however, with decreasing pH from 7 to 3.67, these probes exhibited a remarkable fluorescence emission peak at 590 nm with the solution changing from colorless to pink. It was found that the large straight line slope for probes **8**, **9**, and **10** was in the pH range from 4.34 to 5.35, 4.34 to 5.13, and 4.16 to 5.25, respectively (Fig. 11), which indicated that these probes have promising properties to study the pH of lysosomes in biological systems. Moreover, all of the probes could detect

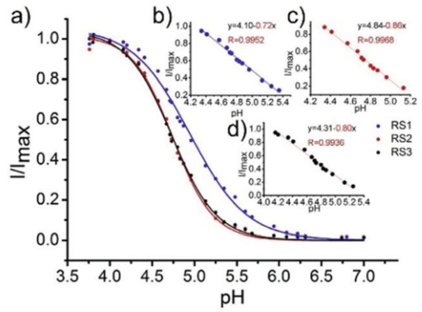

Fig. 11 (a) Sigmoidal fitting of the maximum emission fluorescence intensity at 590 nm for probes **8**, **9** and **10**. Inset: (b) The linearity of probe **8** in the pH range of 4.34–5.35. (c) The linearity of probe **9** in the pH range of 4.34–5.13. (d) The linearity of probe **10** in the pH range of 4.16–5.25. Copyright 2015 Elsevier.

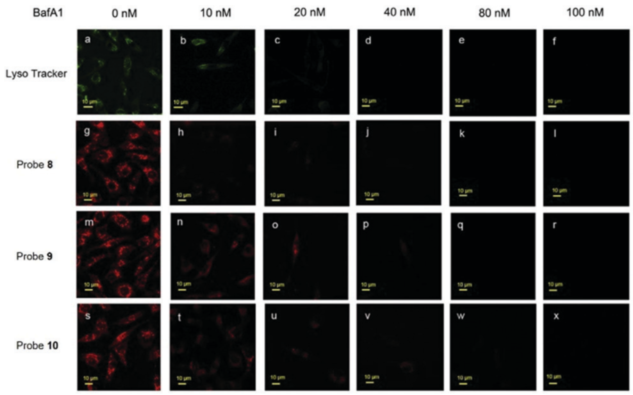

Fig. 12 Lysosomal pH dependent staining of A549 cells with probe **8** (10 μM), probe **9** (10 μM), probe **10** (10 μM) and LysoTracker green DND-26 (0.5 μM). A549 cells pretreated with or without Bafilomycin A1 for about 5 h and then analyzed by confocal microscopy. The intracellular fluorescence of probes **9** and **10** is shown in red and that of LysoTracker green DND-26 is shown in green. Copyright 2015 Elsevier.

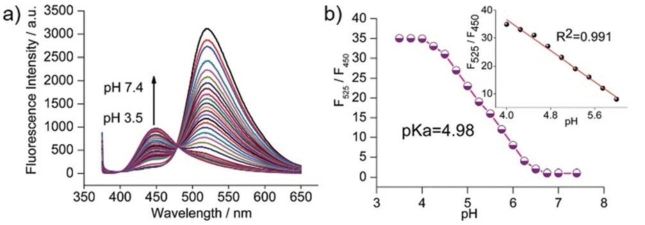

Fig. 13 (a) Fluorescence emission spectra of probe **11** (1 μM) in PBS buffer (10 mM) at different pH values. (b) Plot of F_{525}/F_{450} (the ratio of the fluorescence intensity of probe **11** at λ_{em} = 525 nm and λ_{em} = 450 nm) *versus* pH. Inset: The linear relationship between F_{525}/F_{450} and pH in the pH range of 4.0–6.3. Copyright 2015 Royal Society of Chemistry.

pH changes with high selectivity both at pH 7.0 and pH 4.2. Confocal microscopy images of living A549 cells co-stained with probes **8**, **9**, and **10** indicated that all of the probes could selectively stain lysosomes in living cells while probe **9** was the most promising one in terms of cell permeability and pH sensitivity *in vivo*. Furthermore, lysosomal pH dependent staining of A549 cells with probes **8**, **9**, **10**, and the commercially available lysosome specific staining probe LysoTracker green DND-26 demonstrated that probes **9** and **10** could sensitively respond to lysosomal pH changes but probe **8** performed inferior to probes **9**, **10**, and LysoTracker (Fig. 12). The results revealed that probes **9** and **10** could be used for real-time monitoring of lysosomal pH changes sensitively. MTT assays suggested that probes **9** and **10** exhibited no obvious toxicity to the A549 cells but probe **8** was highly toxic to the cells. The authors described that the different performances including the quantum yield, cytotoxicity, cell membrane permeability and sensitivity for staining lysosomes of probes **8**, **9**, and **10** were attributed to the different lone pair electron distribution of the N atoms in the lactam of probes **8**, **9**, and **10**.

Zhang *et al.* designed a rhodamine B-based fluorescent probe **11** for the detection of lysosomal pH (Scheme 8).[24] In probe **11**, the morpholine group served as a targeting unit for lysosomes, the xanthene derivative exhibited a pH-modulated open/close reaction of the spirocycle, and the *o*-hydroxy benzoxazole moiety displayed a pH modulated excited-state intramolecular proton transfer (ESIPT) process. When the pH values changed from 3.5 to 7.4, the fluorescence intensity of probe **11** at 525 nm decreased significantly accompanied by a large increase in the fluorescence intensity at 450 nm (Fig. 13a), which provides the basis for achieving a ratiometric (F_{525}/F_{450}) detection of pH. Moreover, probe **11** exhibited an excellent F_{525}/F_{450} linearity in the pH range of 4.0–6.3 with a pK_a value of 4.98, which made **11** a promising ratiometric fluorescent probe for an accurate measurement of lysosomal pH (Fig. 13b). The confocal fluorescence microscopy studies showed that probe **11** could selectively stain lysosomes in living cells. Moreover, a strong fluorescence in the green channel and no obvious fluorescence in the blue channel were observed when HeLa cells were incubated with probe **11** for 30 min. However, upon the addition of chloroquine, the fluorescence intensity of the HeLa cells exhibited a time-dependent decrease in the green channel accompanied by a significant time-dependent increase in the blue channel (Fig. 14). The results proved that probe **11** could image the dynamic changes in lysosomal pH.

Zhao and Miao *et al.* reported a rhodamine B-based fluorescent probe **12**, in which the positive charge was introduced to contribute to the solubility and its sensitivity to the pH environment (Scheme 9).[25] At pH > 6.0, probe **12** was non-fluorescent. However, the decrease in pH gave rise to both an increase in fluorescence intensity at 580 nm and a discernible fluorescence color change concomitantly (Fig. 15a). Moreover, probe **12** exhibited a pK_a value

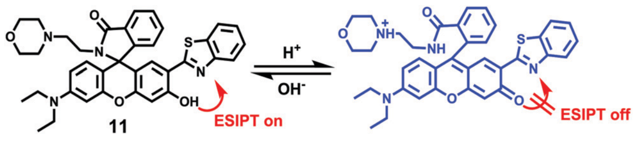

Scheme 8 Fluorescent probe **11** for pH.

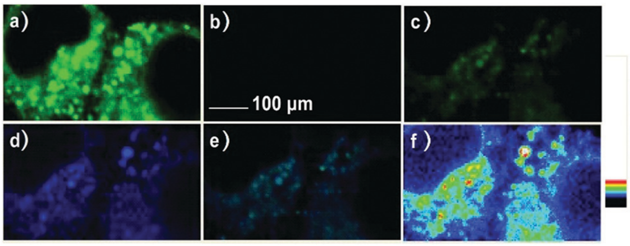

Fig. 14 Fluorescence images of probe **11** in HeLa cells before and after chloroquine stimulation. (a–c) Images of the stained cells before chloroquine simulation. (a) Fluorescence image from the green channel with HeLa cells incubated with probe **11** (1 μM). (b) Fluorescence image from the blue channel. (c) Pseudocolor image of (a) and (b). (d–f) Images of the cells in (a–c) exposed to 80 μM chloroquine for 10 min. (d) Fluorescence image from the green channel. (e) Fluorescence image from the blue channel. (f) Pseudocolor image of (d) and (e). The probe was excited at 405 nm and the fluorescence was collected at: blue channel 415–470 nm and green channel 485–550 nm. Scale bar: 100 μm. Copyright 2015 Royal Society of Chemistry.

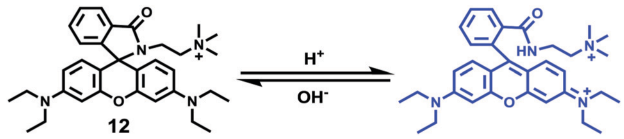

Scheme 9 Fluorescent probe **12** for pH.

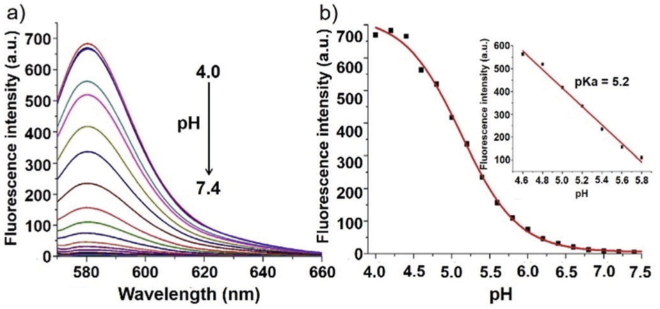

Fig. 15 (a) Change in the fluorescence spectra of probe **12** (1 μM) in aqueous solution containing DMSO (B–R buffer : DMSO = 95 : 5, v/v) with decreasing pH from 7.4 to 4.0 (λ_{ex} = 560 nm). (b) Sigmoidal fitting of the pH-dependent fluorescence intensity at 580 nm. Inset: The good linearity in the pH range of 4.6–5.8. Copyright 2015 Elsevier.

of 5.2 and displayed good linearity (R^2 = 0.98905) between fluorescent intensity at 580 nm and pH ranging from 4.6 to 5.8, which implied that probe **12** could serve as a functional pH probe for weak acidic organelles like lysosomes (Fig. 15b). Confocal fluorescence imaging of living HeLa cells co-stained with probe **12** and Lysosensor^{TM} Green DND-189 suggested that probe **12** could specifically label lysosomes in cells (Fig. 16). Fluorescence microscopy imaging of living HeLa cells pretreated with chloroquine revealed that probe **12** could be used as an indicator in the monitoring of pH changes of lysosomes in living cells with a fast response.

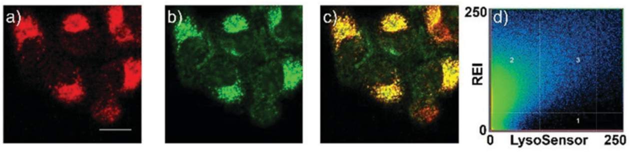

Fig. 16 Confocal fluorescence imaging of living HeLa cells co-stained with probe **12** (5 μM) and LysoSensor Green (1 μM) for 1 h. (a) Red emission from probe **12**; (b) green emission from LysoSensor Green; (c) overlay of (a) and (b); areas of co-localization appeared in yellow; (d) the correlation of LysoSensor Green and probe **12** intensities. Copyright 2015 Elsevier.

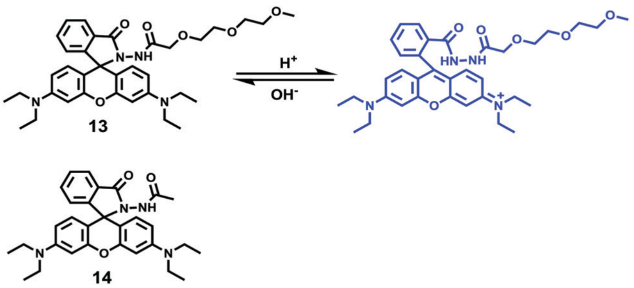

Scheme 10 Fluorescent probes **13** and **14** for pH.

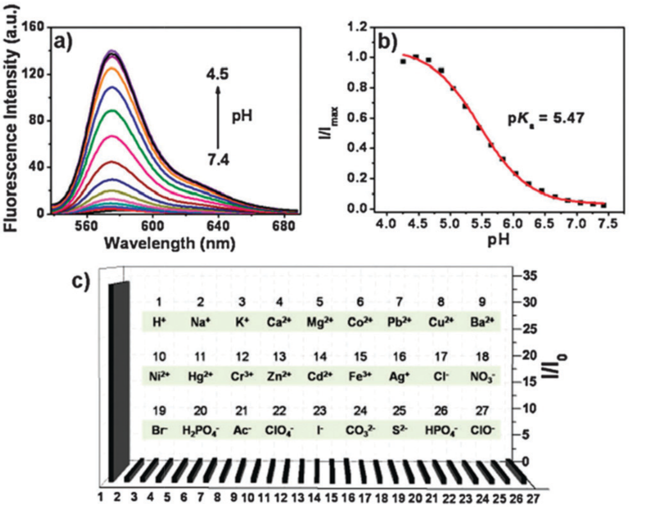

Fig. 17 (a) Fluorescence spectra of probe **13** at various pH values in Britton–Robinson buffer solution, λ_{ex} = 525 nm. (b) pH titration curve of probe **13**, λ_{ex} = 559 nm, λ_{em} = 578 nm. (c) Fluorescence responses (578 nm) of probe **13** to miscellaneous ions in water: 50 μM for H^+, 200 μM for the other ions. Copyright 2012 Royal Society of Chemistry.

Peng and Fan *et al.* reported a rhodamine-based pH fluorescent sensor **13**, in which a novel lysosome-locating group methylcarbitol was first introduced.[26] Moreover, a contrasting molecule **14** lacking the methylcarbitol group was synthesized as well (Scheme 10). Probe **13** was almost nonfluorescent at pH 7.4 while its fluorescence was significantly enhanced as the H^+ concentration increased (Fig. 17a). Within the pH range of 7.4–4.5, a 50-fold increase in the emission intensities was observed. The pH titration curve of **13** yielded a pK_a of 5.47 indicating that probe **13** could detect minute pH changes in the 4.5–6.0 range, which covered both normal and abnormal lysosome pH (Fig. 17b). Moreover, no observable fluorescence enhancement of probe **13** in the presence of chemical species such as Na^+, K^+, Ca^{2+}, Mg^{2+}, Co^{2+}, Pb^{2+}, Ni^{2+}, Hg^{2+}, Cr^{3+}, Zn^{2+}, Cd^{2+}, Fe^{3+}, Ag^+, Cu^{2+}, Cl^-, NO_3^-, Br^-, $H_2PO_4^-$, Ac^-, ClO_4^-, I^-, CO_3^{2-}, S^{2-}, HPO_4^{2-}, and OCl^- suggested that probe **13** exhibited high selectivity for H^+ (Fig. 17c). Confocal fluorescence microscopy results demonstrated that probe **13** was able to stain the acidic vesicles but its contrasting molecule **14** without the methylcarbitol group could not. Confocal fluorescence imaging of living cells co-stained with probe **13** and LysoSensor™ Green DND-189 indicated that **13** selectively stained lysosomes in live cells (Fig. 18). Fluorescence images of **13** in mouse macrophages stimulated with chloroquine indicated that probe **13** was a lysosomal pH-responsive sensor in cell biology. Furthermore, probe **13** could be used to monitor changes in the acidity of lysosomes during apoptosis in live cells.

Han and Yang *et al.* prepared a ratiometric pH probe **15** based on a fluorescence resonance energy transfer (FRET) mechanism through the conjugation of rhodamine 6G-lactam (R6G-lactam) with dansyl chloride *via* diethylenetriamine (Scheme 11).[27] This probe was expected to selectively accumulate in lysosomes in

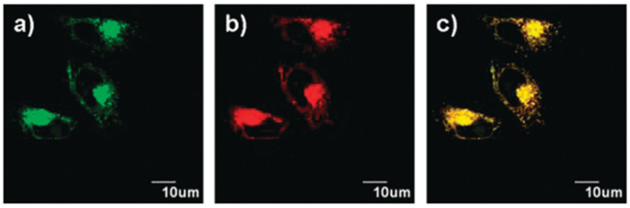

Fig. 18 Probe **13** co-localizes to lysosomes in live MCF-7. Cells were stained with: (a) 1 μM LysoSensor Green, (b) 10 μM Probe **13**. (c) Areas of co-localization appear in yellow. Probe **13** and LysoSensor Green were excited at 559 nm and 488 nm, respectively. The fluorescence images were recorded at 575–620 nm (Probe **13**) and 495–515 nm (LysoSensor Green), respectively. Copyright 2012 Royal Society of Chemistry.

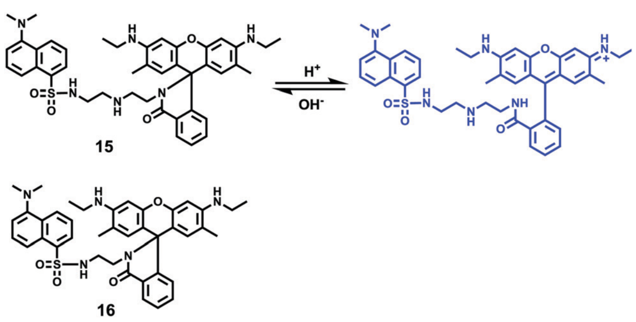

Scheme 11 Fluorescent probe **15** for pH.

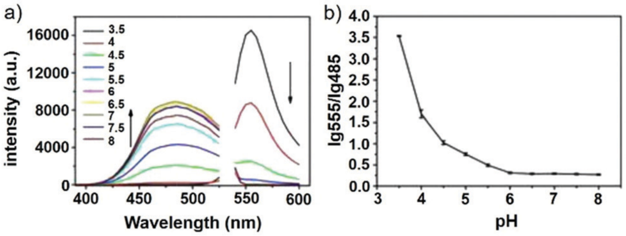

Fig. 19 pH dependent ratiometric fluorescence emission of probe **15**. (a) Fluorescence emission spectra of probe **15** (10 μg mL^{-1}) at pH 3.5–8.0 under dual-wavelength excitation (λ_{ex}@300 nm for dansyl group, 532 nm for R6G-lactam). (b) pH titration curves of lg ratios between fluorescence emission of R6G-amide (I_{555nm}) and that of dansyl group (I_{485nm}). Copyright 2013 Elsevier.

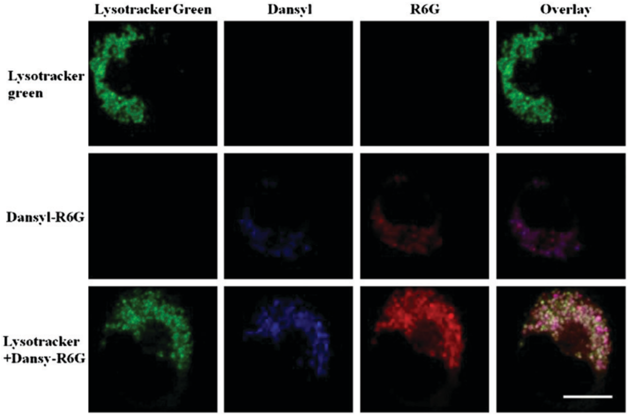

Fig. 20 Staining of lysosomes with probe **15**. L929 cells were respectively stained with probe **15** (1 μg mL^{-1}), Lysotracker green (0.4 μg mL^{-1}), or both. Intracellular R6G-amide fluorescence is shown in red, dansyl fluorescence is shown in blue and that of Lysotracker green is marked in green. Bar, 10 μm. Copyright 2013 Elsevier.

living cells *via* protonation of the amine-containing linker. The fluorescence emission centered at 555 nm, characteristic of R6G-lactam, was 800 fold brighter at pH 4.0 relative to that at pH 6.5 (Fig. 19a). In contrast to the dramatic increase of R6G-lactam fluorescence at acidic pH, the dansyl moiety exhibited decreased fluorescence emission at 485 nm. Fig. 19b revealed that subtle acidification in the range of pH 5.5–3.5 resulted in pronounced changes in the ratios of R6G-amide fluorescence intensity (I_{555nm}) to that of the dansyl group (I_{485nm}). It was suggested that probe **15** could be used as a molecular pH-meter for monitoring subtle acidic pH changes. Confocal microscopic analysis of L929 cells co-stained with **15** and LysoTracker Green DND-26 showed that probe **15** was exclusively confined in lysosomes (Fig. 20). The analog, **16**, where R6G-lactam was linked with the dansyl moiety by ethylenendiamine, distributed both intra- and extra-lysosomally, which suggested that diethylenetriamine linker of probe **15** played a critical role in targeting lysosomes. Confocal fluorescence microscopy demonstrated that probe **15** could determine the pH of individual lysosomes and the overall lysosomal pH in living cells. Moreover, probe **15** was proved to be highly efficient in differentiating apoptosis *vs.* necrosis cells.

Peng *et al.* reported a naphthalimide–rhodamine FRET system **17** as a ratiometric and intracellular pH probe, in which 1,2,3-triazole was identified as an ideal bridge and biocompatible (Scheme 12).[28] As shown in Fig. 21a, probe **17** displayed a green fluorescence colour

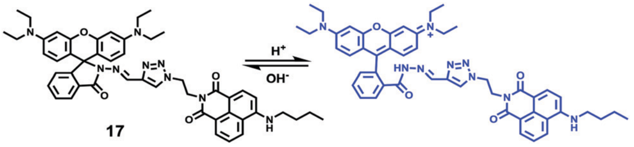

Scheme 12 Fluorescent probe **17** for pH.

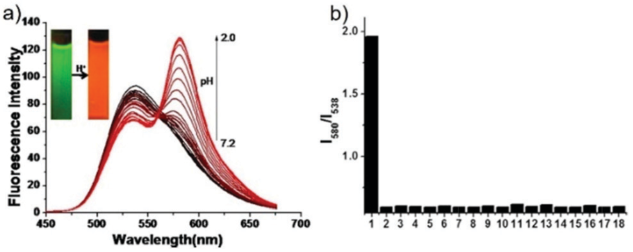

Fig. 21 (a) Emission spectra of probe **17** (5 μM) at pH approximately ranging from 7.2 to 2.0 upon addition of HCl (1 M) in solution (methanol/HEPES = 9/1, v/v, pH 7.2). Inset: Change in fluorescence of probe **17** (5 μM) upon addition of H^+ (100 μM). Excitation wavelength is 430 nm. Slit: 5 nm/2.5 nm. (b) Selectivity of probe **17** for pH over selected cation interferences. The ratios of fluorescence emission intensity of probe **17** (5 μM) at 580 nm and 538 nm (F_{580nm}/F_{538nm}) containing various cations (333 μM) as compared to H^+ (200 μM) in the solution (methanol/HEPES = 9/1, v/v, pH 7.2). 1: H^+, 2: Blank, 3: Na^+, 4: Ca^{2+}, 5: Mg^{2+}, 6: Zn^{2+}, 7: Cd^{2+}, 8: Ba^{2+}, 9: Fe^{3+}, 10: Fe^{2+}, 11: Cr^{3+}, 12: Pb^{2+}, 13: Cu^{2+}, 14: Hg^{2+}, 15: Mn^{2+}, 16: Ni^{2+}, 17: Co^{2+}, 18: NH_4^+. Copyright 2013 Elsevier.

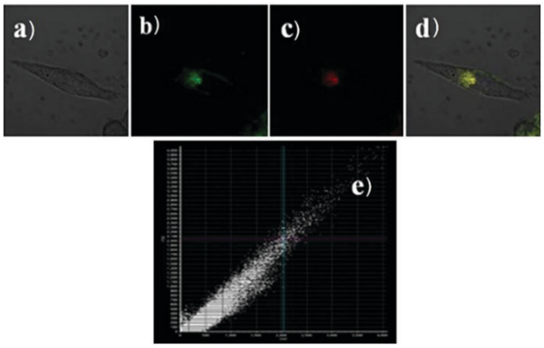

Fig. 22 Intracellular distribution of probe **17** (10 μM) as compared to lysosensor green (1 μM). (a) Bright field image; (b) fluorescence image of lysosensor green; (c) fluorescence image at 580 ± 15 nm of probe **17**; (d) merging of b and c; (e) co-localization coefficient of probe **17** and lysosensor green is 99.9% in the same cell. Excitation wavelength of lysosensor green and probe **17** respectively is 488 nm and 405 nm. Copyright 2013 Elsevier.

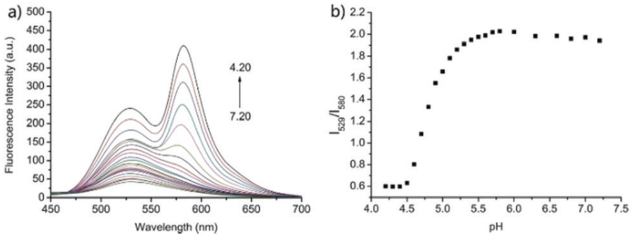

Fig. 23 (a) Fluorescence spectra of probe **18** (5 μM) in the B–R buffer/EtOH (9/1, v/v) solution at different pH values (7.20, 7.00, 6.80, 6.60, 6.30, 6.00, 5.80, 5.70, 5.60, 5.50, 5.40, 5.30, 5.20, 5.10, 5.00, 4.90, 4.80, 4.70, 4.60, 4.50, 4.40, 4.30, and 4.20); and (b) the plot of the emission ratios of *R* at I_{529}/I_{580} *versus* pH values; λ_{ex} = 390 nm. Copyright 2015 Royal Society of Chemistry.

when pH > 6.2. However, the intensity of the green fluorescence band centered at 538 nm gradually decreased and a new pink fluorescence band centered at 580 nm gradually increased when the pH changed from 7.20 to 2.00. The ratiometric calibration curve of I_{580nm}/I_{538nm} indicated that the pK_a of **17** was 2.79. As shown in Fig. 21b, probe **17** exhibited a selective response to H^+ in the presence of metal ions or amino acids. Co-localization experiments suggested that probe **17** was cell membrane permeable and localized in lysosomes (Fig. 22).

Zhao and Miao *et al.* prepared a ratiometric pH probe **18** comprising a naphthalimide donor and a rhodamine acceptor based on the FRET mechanism (Scheme 13).[29] Probe **18** displayed very weak fluorescence at 529 nm at pH 7.20. As the pH value decreased from 7.20 to 4.20, the emission band of naphthalimide centred at 529 nm enhanced gradually accompanied by a new peak evolved at 580 nm strikingly (Fig. 23a). The interesting observation that both emission intensities of the naphthalimide (529 nm) and rhodamine (580 nm) moieties increased along with the pH decrease might be attributed to the integration of PET and FRET processes. At pH 7.20, the photo-induced electron transfer (PET) process of piperazine nitrogen quenched the fluorescence of the naphthalimide moiety. However, the addition of H^+ prohibited the PET process *via* protonation of the nitrogen, which induced the enhancement of the fluorescence intensity of the naphthalimide. In the meantime, the H-bonding interaction between protonated piperazine N and rhodamine lactam O induced the ring-opening process of the rhodamine spirocycle, thus the FRET process from the naphthalimide donor to the rhodamine acceptor occurred accordingly. The ratio of fluorescence intensities (I_{529nm}/I_{580nm}) of **18** showed a significant change from pH 4.50 to 5.50 and the pK_a of **18** was calculated to be 4.82 (Fig. 23b). The co-localization fluorescence imaging experiments indicated that probe **18** could detect lysosomal pH changes and selectively stain lysosomes in living cells, which was confirmed by the excellent colocalization of the red emission of **18** with the green emission of LysoSensor Green DND-189 (Fig. 24).

Based on a similar mechanism to the above case, Zhao and Miao *et al.* synthesized a FRET-based fluorescent probe **19**, embracing a coumarin donor and a rhodamine acceptor, for detecting pH values (Scheme 14).[30] As shown in Fig. 25a, probe

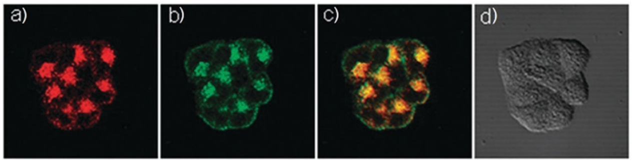

Fig. 24 Fluorescence microscopy images of living HeLa cells co-stained with probe **18** (5 μM) and LysoSensor Green DND-189 (1 μM). (a) Red emission of probe **18** (560–700 nm), (b) green emission of LysoSensor Green DND-189, (c) overlay of (a) and (b), and (d) a bright field image. Excitation wavelength of probe **18** and LysoSensor Green DND-189 was 405 nm and 488 nm, respectively. Copyright 2015 Royal Society of Chemistry.

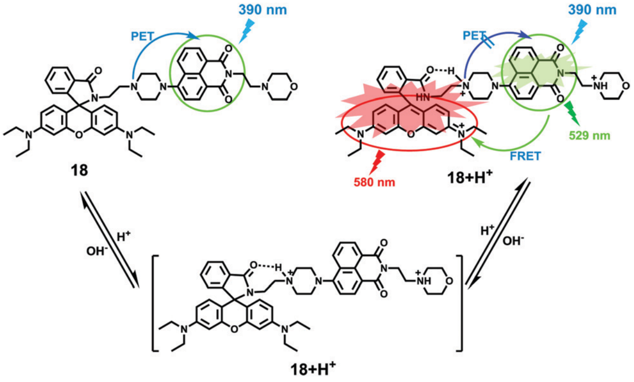

Scheme 13 Fluorescent probe **18** for pH.

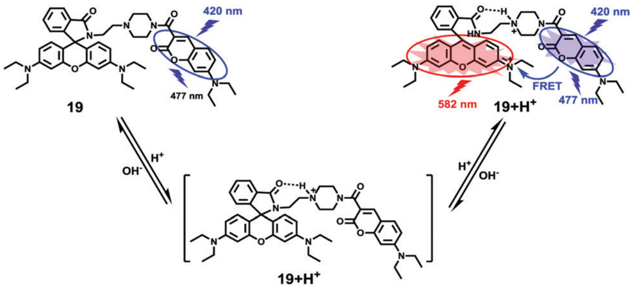

Scheme 14 Fluorescent probe **19** for pH.

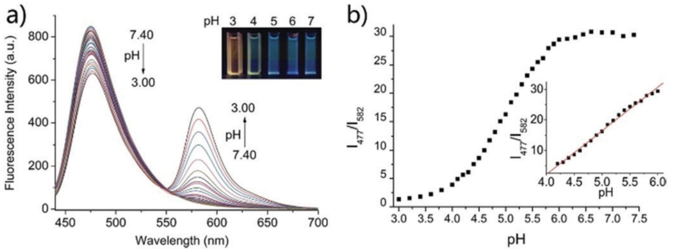

Fig. 25 (a) Fluorescence spectra of probe **19** (1 μM) in solution (B–R buffer/EtOH = 7/3, v/v) at different pH values (3.00, 3.20, 3.40, 3.60, 3.80, 4.00, 4.10, 4.20, 4.30, 4.40, 4.50, 4.60, 4.70, 4.80, 4.90, 5.00, 5.10, 5.20, 5.30, 5.40, 5.50, 5.60, 5.70, 5.80, 5.90, 6.00, 6.15, 6.30, 6.45, 6.60, 6.80, 7.00, 7.20, and 7.40). Inset: The photographs of probe **19** at diverse pH values under UV irradiation; incubation time: 2 h; (b) fluorescence emission ratios (I_{477}/I_{582}) *versus* pH values according to the fluorescence pH titration. Inset: The good linearity in the pH range of 4.20–6.00 (R = 0.99763). λ_{ex} = 420 nm. Copyright 2015 Royal Society of Chemistry.

19 exhibited a strong blue emission at 477 nm at pH 7.40, which was mainly attributed to the optical properties of the coumarin moiety. As pH decreased from 7.40 to 3.00, the fluorescence intensity of the coumarin moiety decreased gradually accompanied by a new red emission peak of the rhodamine moiety appearing at 582 nm and showing an 18-fold increase. The decrease of coumarin emission (477 nm) and the concomitant increase of rhodamine emission (582 nm) along with the pH decrease were attributed to the FRET process from the coumarin moiety (donor) to the rhodamine moiety (acceptor). The pH titration of probe **19** showed that the ratios of fluorescence intensities (I_{477nm}/I_{582nm}) were linearly proportional to the pH value in the range of 4.20–6.00 and the pK_a of the probe was calculated to be 4.98 (Fig. 25b). Moreover, fluorescence microscopy images of HeLa cells co-stained with probe **19** and LysoSensor® Green DND-189 indicated that probe **19** could selectively stain the lysosome in living cells (Fig. 26). Meanwhile, the probe exhibited desirable anti-interference ability against many analytes (metal cations, amino acids and the ATP) and displayed satisfactory photostability and low cytotoxicity in HeLa cells.

Ge and Sun *et al.* prepared a pH probe **20** based on rosamine, which is the decarboxylated analogue of rhodamine (Scheme 15).[31] Probe **20** was non-fluorescent in neutral environments resulting from the photoinduced electron transfer (PET) by the electron donating amine-containing side chain. However, a 400-fold enhancement of the emission intensity was observed when the pH was reduced from 8.0 to 3.0 and a 13-fold increase was observed in the pH range of 4.0–6.0, indicating that probe **20** was a particularly sensitive pH probe (Fig. 27a). The pK_a of probe **20** was calculated to be 4.73, which indicated that probe **20** was suitable for detecting and imaging pH in lysosomes (Fig. 27b). Confocal microscopic analysis of HeLa cells co-stained with **20** and LysoSensor Green DND-26 showed that probe **20** could be used effectively as a lysosome-specific sensor for monitoring changes in lysosomal pH during physiological and pathological processes (Fig. 28).

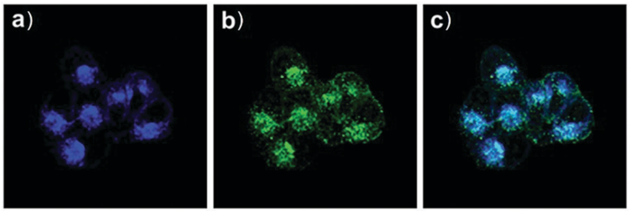

Fig. 26 Fluorescence microscopy images of HeLa cells co-stained with probe **19** (2 μM) and LysoSensor Green DND-189 (1 μM). (a) Blue fluorescence of probe **19** (450–550 nm); (b) green fluorescence of LysoSensor Green DND-189; (c) merged image of (a) and (b). The excitation wavelength of probe **19** and LysoSensor Green DND-189 was 405 nm and 488 nm, respectively. Copyright 2015 Royal Society of Chemistry.

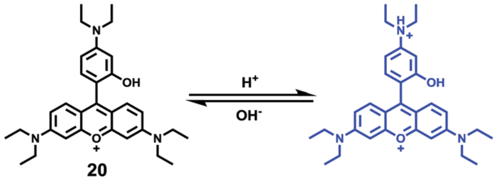

Scheme 15 Fluorescent probe **20** for pH.

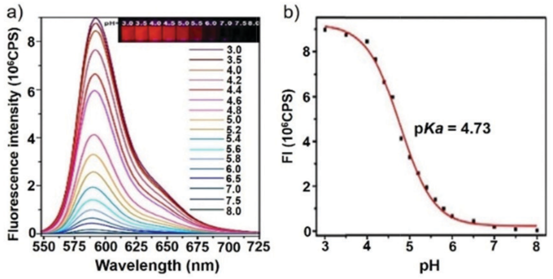

Fig. 27 (a) Fluorescence spectra of probe **20** (10 μM) under different pH values in Na_2HPO_4–citric acid buffer solution; the inset shows color changes of probe **20** at pH 3.0 and 8.0. (b) Fluorescence spectra of probe **20** (10 μM) at various pH values in Na_2HPO_4–citric acid buffer solution, λ_{ex} = 535 nm; the inset shows fluorescence changes of probe **20** at various pH values under UV light excitation at 365 nm. Copyright 2014 Elsevier.

Ying *et al.* reported a series of BODIPY-based pH probes **21a–d** (Scheme 16).[32] As expected, these probes were almost non-fluorescent at neutral pH 7.0, due to photo-induced electron transfer (PET) from the aniline moiety to the BODIPY fluorophore. With pH lowering, the fluorescence intensities of these probes **21a–d** increased gradually. Interestingly, these probes displayed tunable pK_a values ranging from 3.2 to 5.2 because of the different substitution of the *N*-alkyl group on the aniline moiety and the substituent on the BODIPY fluorophore (Fig. 29).

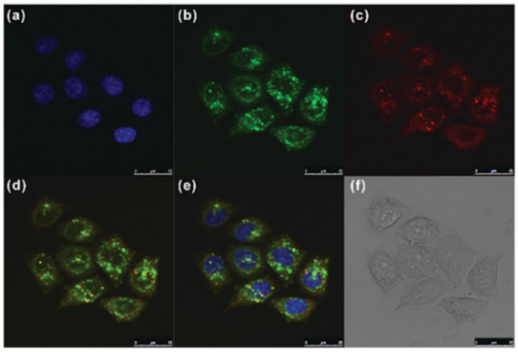

Fig. 28 Fluorescence images of HeLa Cells. (a) Fluorescence image of HeLa cells with Hoechst 33342 (1.0 μM); (b) fluorescence image of HeLa cells with LysoTracker Green DND-26 (1.0 μM); (c) fluorescence image of HeLa cells with probe **20** (10 μM); (d) merged image of (b) and (c); (e) merged image of (a)–(c); (f) bright-field transmission image of the cells. The fluorescence images were excited at 405 nm, 488 nm and 543 nm, and recorded at 435–480 nm (Hoechst 33342), 505–550 nm (LysoSensor Green DND-26) and 580–625 nm (probe **20**), respectively. Copyright 2014 Elsevier.

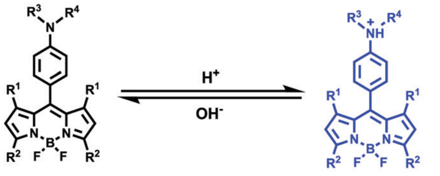

21a (R^1, R^2, R^3, R^4 = CH_3);
21b (R^1, R^2 = CH_3, R^3, R^4 = CH_2CH_3);
21c (R^1, R^2 = CH_3, R^3 = CH_2CH_3, R^4 = $CH_2CH_2CH_2CO_2Me$);
21d (R^1 = H, R^2 = $CH_2CH_2CO_2Me$, R^3, R^4 = CH_2CH_3)

Scheme 16 Fluorescent probes **21a–c** for pH.

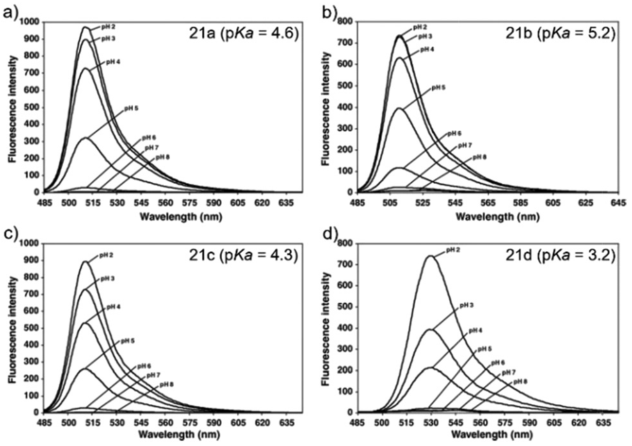

Fig. 29 Fluorescence emission spectra (λ_{ex} = 480 nm) of probes **21a–d** as a function of pH. Probes **21a–d** were prepared at 100 nM concentration at varying pH buffer. 100 mM NH_4OAc was used to make pH 2–4 buffers; PBS was used to make pH 5–8 buffers. Copyright 2011 Elsevier.

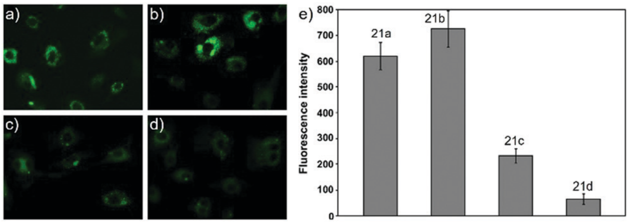

Fig. 30 The cell images and relative fluorescence intensities of pH probes **21a–d**. Cell imaging labeled with probes **21a–d** is shown in (a–d), respectively. (e) The fluorescence intensities were averaged in triplicate. Copyright 2011 Elsevier.

The cell images clearly showed that probes **21a–d** selectively labeled the acidic organelle lysosomes. Moreover, their fluorescence intensities in the acidic lysosomes were varied based on the pK_a of the pH probes, for example, probe **21b** with pK_a = 5.2 displayed the highest fluorescence intensity, but probe **21d** with pK_a = 3.2 showed the lowest fluorescence intensity. Furthermore, it was demonstrated that these probes especially probe **21b** was useful for noninvasive monitoring of lysosomal pH changes during physiological and pathological processes (Fig. 30).

Liu, Tiwari, and Luo *et al.* prepared a series of BODIPY-based near-infrared fluorescent probes **22a–c** for the detection of lysosomal pH (Scheme 17).[33] In these probes, piperazine residues were used to manipulate the fluorescent responses to pH *via* the modulation of the intramolecular charge transfer (ICT) effect and potential photo-induced electron transfer (PET) of piperazine moieties at 3,5-positions to BODIPY cores at different pH values. Moreover, tri(ethylene glycol)methyl ether residues attached to piperazine moieties were used to enhance the hydrophilic properties of the probes and improve the water solubilities of the probes. Fluorescent probes **22a**, **22b** and **22c** displayed very sensitive responses to pH. For example, a decrease of pH values from 9.98 to 2.20 caused a significant increase in fluorescence intensities at 715 nm of fluorescent probes **22a**, **22b** and **22c** with 75-, 88- and 102-fold enhancements, respectively (Fig. 31). The pK_a values of probes **22a**, **22b** and **22c** were calculated to be 2.91, 3.19 and 3.57, respectively. Live cell imaging of probes **22a**, **22b** and **22c** both in breast cancer cell line MDA-MB-231 and normal endothelial cell line HUVEC-C suggested that probes **22a**, **22b** and **22c** were able to target lysosomes in a manner similar to Lyso-Sensor Green DND-189 and distinguish between different regions inside cells based on pH (Fig. 32 and 33). Probe **22a** showed the highest fluorescence intensity among all three probes.

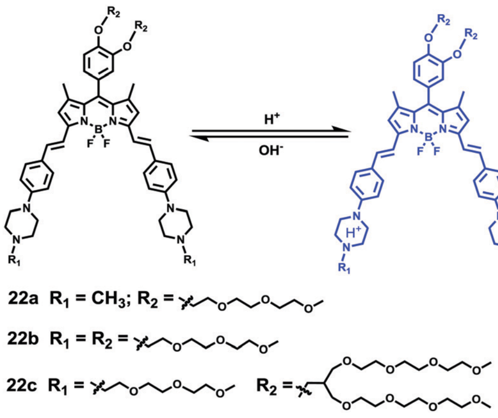

Scheme 17 Fluorescent probes **22a–c** for pH.

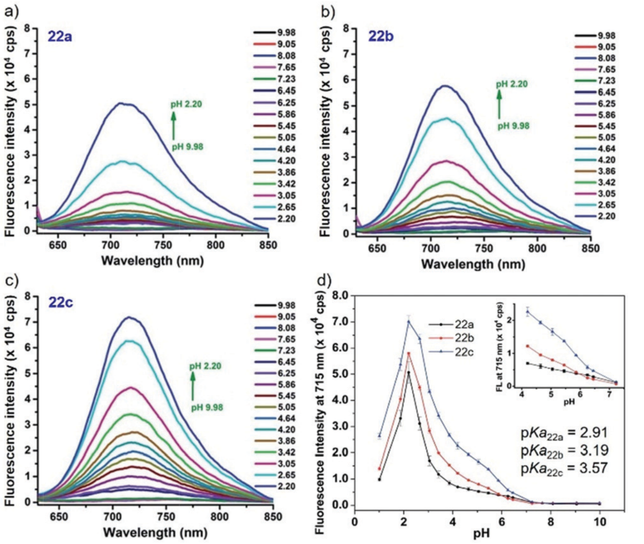

Fig. 31 (a–c) Emission spectra of fluorescent probes **22a–c** (5 μM) in buffer solution at different pH values. (d) Fluorescent responses of probes **22a–c** to different pH values in buffer solutions. Inset: Zoomed fluorescence intensity responses of probes **22a–c** to pH in the window between cytoplasm pH and lysosomal pH. Copyright 2015 Royal Society of Chemistry.

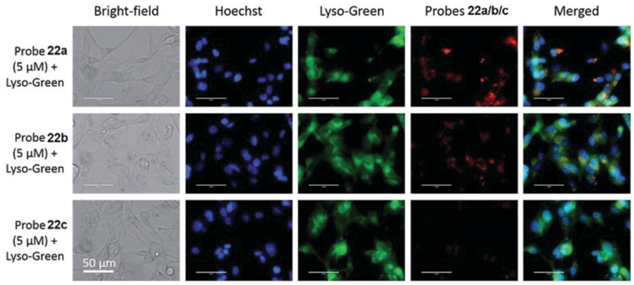

Fig. 32 Fluorescence images of MDA-MB-231 cells incubated with fluorescent probes **22a–c**. Cells incubated with 5 μM of respective probes for 2 h, post serum starvation (2 h) and imaged for co-localization with 1 μM LysoSensor Green and (1 μg mL^{-1}) Hoechst 33342 stains. All images were acquired at 60× magnification using an inverted fluorescence microscope (AMF-4306, EVOS$_{\text{fl}}$, AMG). Copyright 2015 Royal Society of Chemistry.

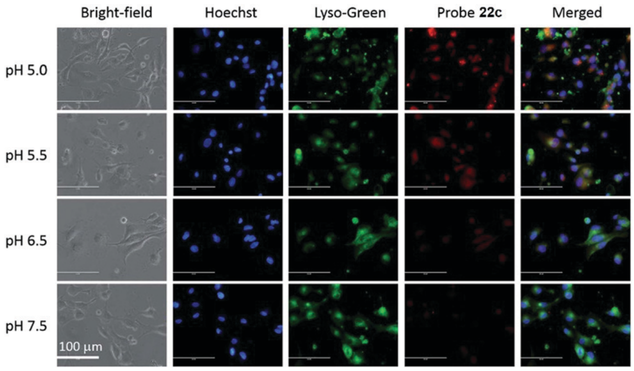

Fig. 33 Fluorescence images of HUVEC-C cells incubated with 15 μM probe **22c** at different pH values; 1 μM LysoSensor Green and 1 μg mL^{-1} Hoechst 33342 were used as co-stains. Images were acquired using an inverted fluorescence microscope (AMF-4306, EVOS$_{\text{fl}}$, AMG) at 40× magnification. Copyright 2015 Royal Society of Chemistry.

However, probe **22c**, the most hydrophilic compound among these three probes, displayed poor fluorescent signals. The possible reason was that probes **22a** and **22b** were more hydrophobic and less steric hindered than probe **22c**, therefore they could more easily bind or interact with lipophilic structures such as micelles, liposomes, and membranes in lysosomes. Live cell fluorescence imaging of probes **22a–c** at different intracellular pH values indicated that probe **22c** was sensitive to pH not only in buffer solution but also inside the living cells. More importantly, compared with commercial probe LysoSensor, probe **22c** was more sensitive to pH. For instance, probe **22c** displayed very weak fluorescence in cells near physiological pH whereas its fluorescence intensity was significantly enhanced as pH decreased from 7.5 to 5.0. However, probe LysoSensor Green did not display any evident change of fluorescence at different pH values.

Li *et al.* reported a pH sensitive fluorescent probe **23** based on a 4-acylated naphthalimide fluorophore (Scheme 18).[34] In probe **23**, D-Phe–L-Phe was used to regulate the pK_a and partition coefficient of the probe and *N*,*N*-dimethylethylamine was selected as the PET donor for its acidotropic property towards lysosomes. Probe **23** displayed weak fluorescence under neutral and basic conditions. However, the emission of probe **23** significantly increased as the pH decreased to acidic levels (Fig. 34). The appropriate pK_a of probe **23** was 6.48, which was suitable for detecting in the pH range of 7.3–4.5. ES-2 cells were co-stained with commercial markers, including Lyso Tracker Red (LT Red), Mito Tracker Green (MT Green) and Golgi Tracker Red (GT Red), which demonstrated that probe **23** could specifically label lysosomes in ES-2 cells (Fig. 35). Moreover, the signal to noise ratio of probe **23** in lysosome imaging was much higher than that of LT Red.

Tian *et al.* reported a series of pH sensitive probes **24a**, **24b** and **24c** based on naphthalimide derivatives (Scheme 19).[35]

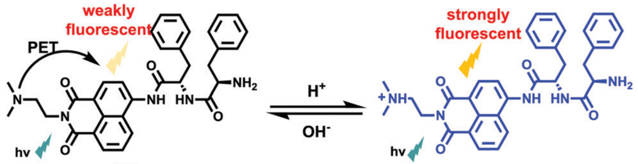

23

Scheme 18 Fluorescent probe **23** for pH.

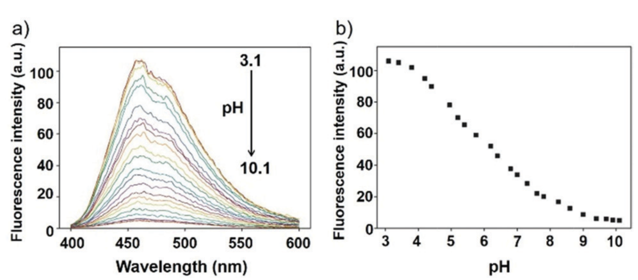

Fig. 34 (a) The fluorescence change of probe **23** in Britton–Robinson buffer at different pH values; (b) the fluorescence intensity at 460 nm depending on different pH values, λ_{ex} = 360 nm. Copyright 2013 Royal Society of Chemistry.

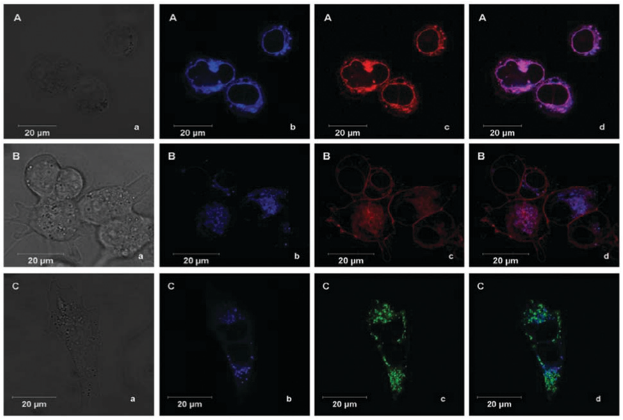

Fig. 35 Colocalization images of ES-2 cells incubated with probe **23** and the three commercial trackers. The four images in each row show: (a) bright-field images; (b) cells stained by probe **23**, (λ_{ex} = 405 nm); (c) cells stained by LT Red (λ_{ex} = 555 nm), GT Red (λ_{ex} = 555 nm) and MT Green (λ_{ex} = 488 nm) in rows A, B and C, respectively; (d) merged images. All images were taken under a 63× oil immersion objective. Copyright 2013 Royal Society of Chemistry.

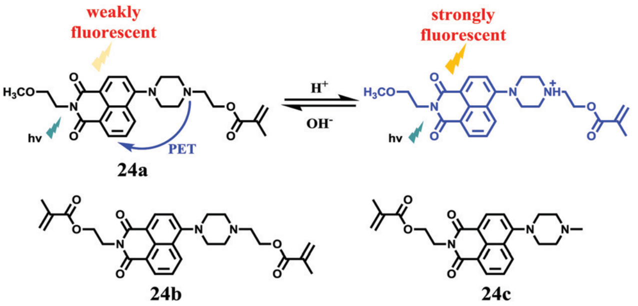

Scheme 19 Fluorescent probes **24a–c** for pH.

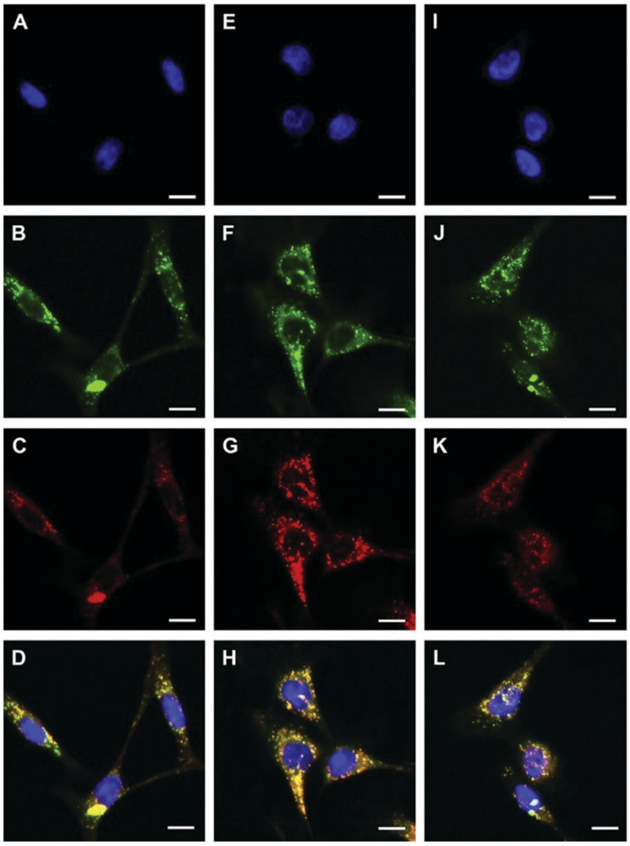

Fig. 37 Confocal fluorescence images of probe **24a** (B), **24b** (F) and **24c** (J) in CP-A cells co-stained with nuclei staining Hoechst 33342 (A, E and I) and LysoTracker Red (C, G and K), respectively. The scale bar represents 10 mm. D is the overlay of A, B and C. H is the overlay of E, F and G. L is the overlay of I, J and K. Copyright 2010 Elsevier.

The acidity of lysosomes enabled a protonation of amino groups, and thus made probes emit brightly in lysosomes by inhibiting the photo-induced electron transfer from the amino groups to the fluorophores (Fig. 36a). Through studies in U87MG, HeLa, CP-A, and CP-D cells with confocal fluorescence microscopy, **24a**, **24b** and **24c** were proved to be permeable and accumulated majorly in the lysosome (Fig. 37). More interestingly, these pH probes possess methacrylate moieties enabling these compounds to be used as monomers and further polymerized with other monomers for thin film preparation. Film **25** composed of the sensing moiety **24c** has been successfully used as an extracellular pH sensor to monitor pH changes during the metabolism of prokaryotic *Escherichia coli* (*E. coli*). Monitoring results showed that the pH values measured with film **25** correlated well with those measured using a glass pH electrode.

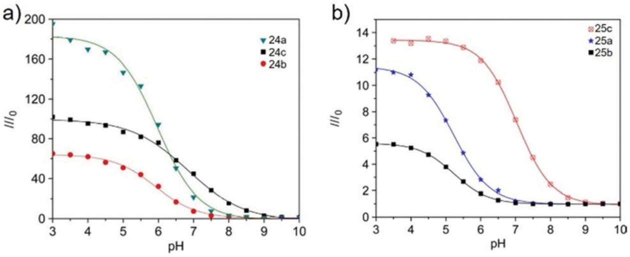

Fig. 36 (a) Fluorescence intensity (at 517 nm) ratios of probes **24a–c** from pH 3 to pH 10. I_0 is the fluorescence intensity at pH 10. Excitation wavelength for emission spectra was 405 nm. Concentrations of the sensors were 5 μM. (b) Fluorescence intensity (at 517 nm) ratios of thin films **25a–c** from pH 3 to pH 10. I_0 is the fluorescence intensity at pH 10. Excitation wavelength for emission spectra was 405 nm. Copyright 2010 Elsevier.

Ge and Lu *et al.* prepared two benzophenoxazine-based fluorescent probes **26a** and **26b** (Scheme 20).[36] The (2-hydroxyethyl)pyridin-1-ium-3-yl group was chosen for the pH-activatable OFF–ON emission response. Moreover, electronic groups, including a cyano or a hydroxyl group, were attached to the central fused heterocycles of benzo[*a*]-phenoxazines to modify the pK_a values for lysosome labelling. Fluorescence emission experiments revealed that they were highly sensitive and selective pH probes (Fig. 38). However, the pK_a value of each was 5.0 and 5.8, which showed that the attachment of the hydroxyl group has a small effect on pK_a. Moreover, probe **26a** exhibited excellent selectivity to protons over other competitive species that may be present in biological systems (Fig. 39). Additionally, probe **26a** with HeLa cells showed that it could be used as a lysosome-tracker both in

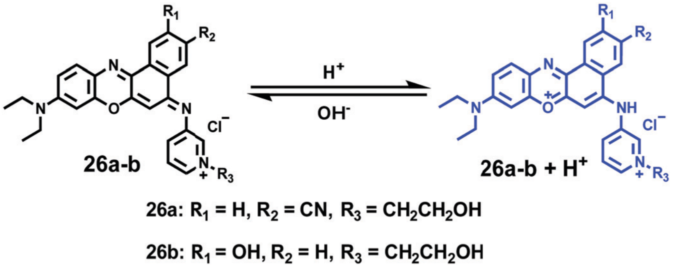

Scheme 20 Fluorescent probes **26a** and **26b** for pH.

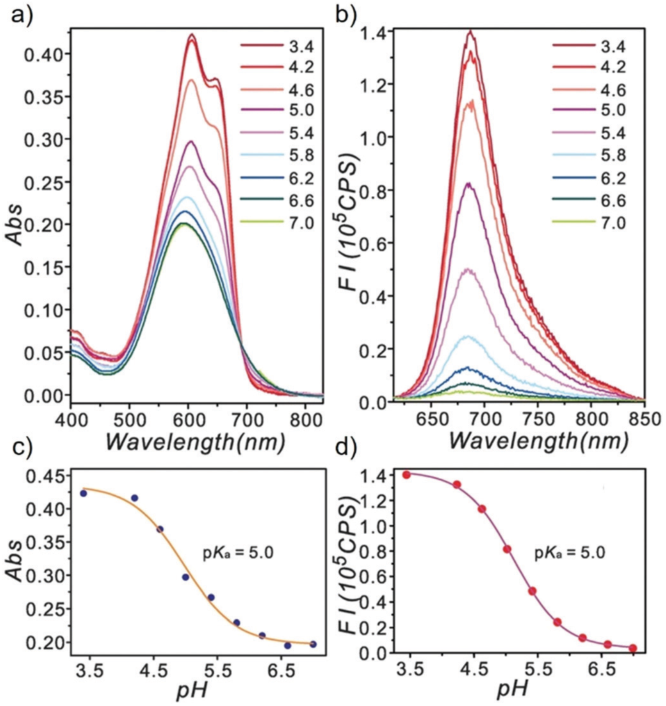

Fig. 38 Optical responses of probe **26a** towards various pH values with disodium hydrogen phosphate–citric acid buffers containing 1% DMSO. (a) Absorption spectra; (b) emission spectra (λ_{ex} = 600 nm); (c) absorption changes with different pH values monitored at 607 nm; (d) fluorescence intensity changes with different pH values monitored at 686 nm. Copyright 2013 Royal Society of Chemistry.

long wavelength (633 nm) and NIR (650–790 nm) regions (Fig. 40), while probe **26b** can only be used as a cytoplasm pH probe.

Kim *et al.* presented a series of ratiometric two-photon (TP) pH probes (**27a–c**, **28**) derived from benzimidazole, which has an ideal pK_a value (pK_a ≈ 5.5) for acidic organelles and thus was used as a proton binding site of these probes (Scheme 21).[37] These benzimidazole derivatives had pK_a values ranging from 4.9 to 6.1, and their spectra showed a marked blue-to-green emission colour change in response to a pH decrease (Fig. 41). Among these derivatives, **28** was lysosomal-targeted by introducing a tertiary amine substituent to **27a** (pK_a ≈ 10). The pK_a value of **28** was 5.82 in one-photon mode and 5.86 in two-photon mode. Probe **28** could locate in lysosomes selectively with the Pearson colocalization coefficient = 0.95 when it was co-labelled with Lysotracker Red DND-99 (LTR) in HeLa cells. The ratiometric

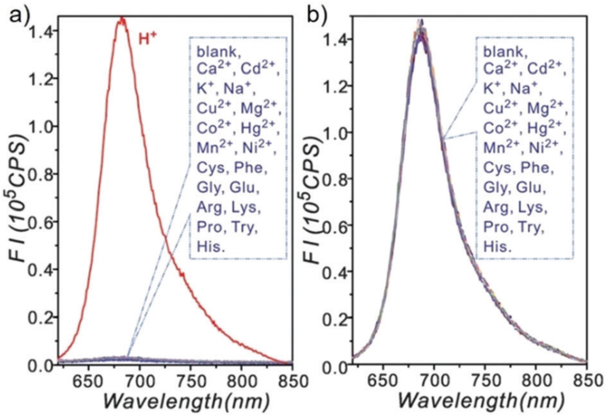

Fig. 39 Fluorescence responses of **26a** (10 μM) to different analytes; K^+ (100 mM), Na^+ (100 mM), Ca^{2+} (0.5 mM), Cd^{2+} (0.3 mM), Cu^{2+} (0.3 mM), Mg^{2+} (0.5 mM), Co^{2+} (0.3 mM), Hg^{2+} (0.3 mM), Mn^{2+} (0.3 mM), Ni^{2+} (0.3 mM), Cys (0.1 mM), Phe (0.1 mM), Gly (0.1 mM), Glu (0.1 mM), Arg (0.1 mM), Lys (0.1 mM), Pro (0.1 mM), Try (0.1 mM) and His (0.1 mM) were included. (a) Tested in disodium hydrogen phosphate-citric acid buffer (pH 7.0). (b) Tested in citric acid buffer (pH 1.6). Copyright 2013 Royal Society of Chemistry.

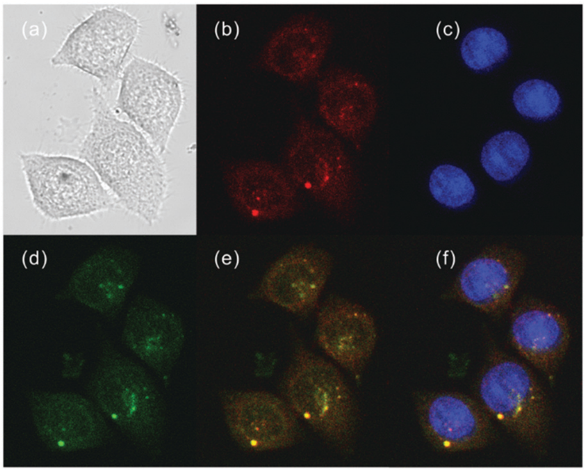

Fig. 40 Fluorescence images of HeLa cells (blue channel emission was collected in the range 410–480 nm upon excitation at 405 nm, green channel emission was collected in the range 505–550 nm upon excitation at 488 nm, and red channel emission was collected in the range 650–790 nm upon excitation at 633 nm). (a) The bright-field image; (b) image with Hoechst 33342 (50 nM); (c) image with LysoTracker Green DND-26 (50 nM); (d) image with probe **26a** (10 μM); (e) overlay of (b) and (d); (f) overlay of (b), (c) and (d). Copyright 2013 Royal Society of Chemistry.

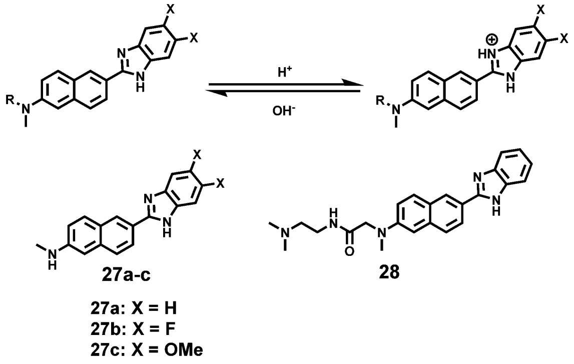

Scheme 21 Fluorescent probes **27a–c** and **28** for pH.

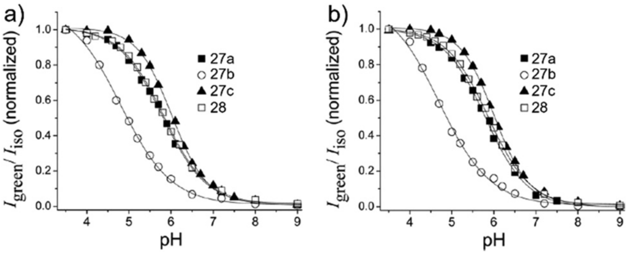

Fig. 41 (a) Plots of I_{green}/I_{iso} *versus* pH for probes **27a–c** and **28** determined in one-photon mode. The excitation wavelength is 360 nm. (b) Plots of I_{green}/I_{iso} *versus* pH for probe **27a–c** and **28** determined in two photon mode. Data in (b) are normalized at the maximum I_{green}/I_{iso}. The excitation wavelength for two-photon mode is 740 nm. Copyright 2013 American Chemical Society.

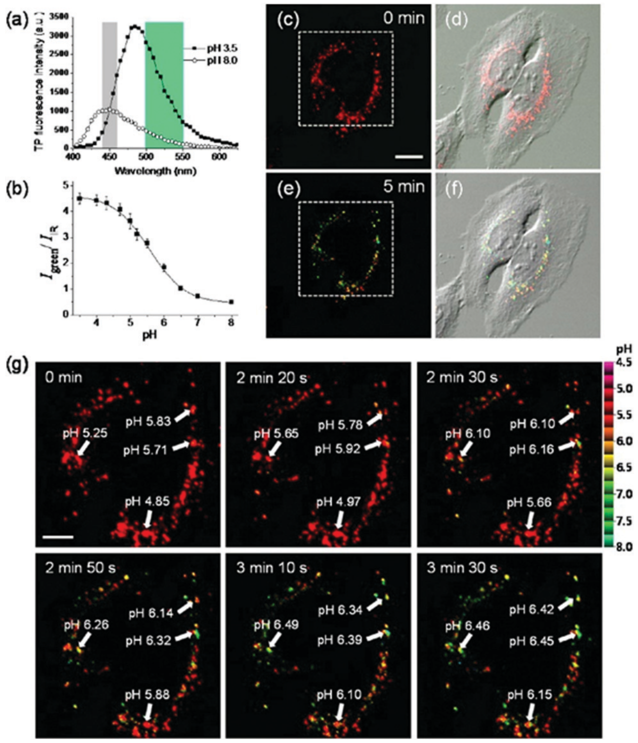

Fig. 42 (a) Two-photon excited fluorescence spectra of ionophore-treated HeLa cells labeled with 3 μM probe **28** at pH 3.5 and pH 8.0. (b) Two photon I_{green}/I_{IR} titration with pH in ionophore-treated and **28**-labeled HeLa cells. (c and e) Pseudocolored ratiometric TPM images (I_{green}/I_{IR}) of HeLa cells incubated with 3 μM **28** before (c) and after (5 min) (e) addition of 5 mM NH_4Cl to the imaging solution, and (d and f) merged images with the corresponding DIC images. (g) Enlargement of a white box in (c) showing the changes of pH with time. The numbers in (g) are the estimated pH values in the region of interest indicated by white arrows. Excitation wavelength is 740 nm. Scale bars are (c) 20 μm and (g) 8 μm. Cells shown are representative images from replicate experiments (*n* = 25). Copyright 2013 American Chemical Society.

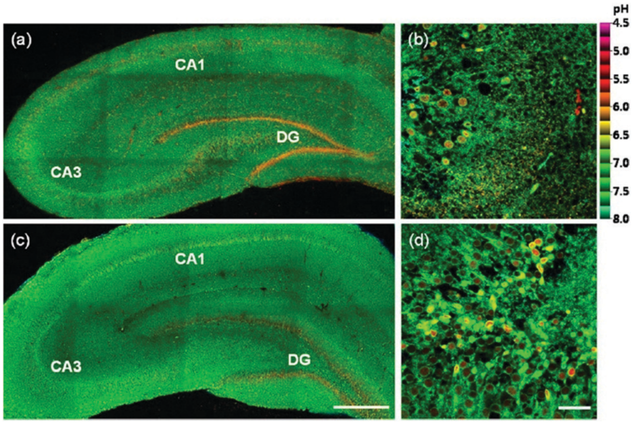

Fig. 43 Pseudocolored ratiometric TPM images (I_{green}/I_{IR}) of a rat hippocampal slice stained with 30 μM (a and b) **28** and (c and d) **27a**. (a and c) 120 TPM images along the *z*-direction at depths of approximately 90–180 μm were accumulated to visualize the overall pH distribution with 10× magnification. (b and d) Higher magnification images (63×) in the regions of DG. Excitation wavelength is 740 nm. Scale bars are (a and c) 300 μm and (b and d) 47 μm. Copyright 2013 American Chemical Society.

TPM image of **28**-labeled HeLa cells showed the various pH values separately and real-time pH changes inside of the lysosome compartment (Fig. 42). Moreover, **28** was capable of direct, real-time estimation of the pH values in living mouse brain tissues through use of two-photon microscopy. Fluorescence images of a fresh slice of rat hippocampus stained with **28** showed that the acidic pH was more distributed in the DG than in CA regions. Additionally, images at a higher magnification clearly showed that acidic spots stained with **28** were much clearer than those stained with **27a** (Fig. 43).

After proving the usage of quinoline derivatives as fluorophores to design fluorescent probes, Xue and Jiang *et al.* designed a quinoline-based fluorescent probe **29** for ratiometric detection of lysosomal pH (Scheme 22).[38] A weak electron-withdrawing acetamido was introduced at the 2-position of quinolone, which could enhance the charge-transfer process and import a diverse proton receptor. In the meantime, a basic dimethylethylamino moiety was also attached to the tail of the 4-position on the quinoline fluorophore as the lysosome anchor through protonation. Probe **29** can ratiometrically and selectively respond to pH changes with an emission shift of 76 nm and calculated pK_a of 4.20 ± 0.015 (Fig. 44). With **29** and LysoTracker Red DND-99 in NIH 3T3 cells, it was shown that **29** could be efficiently localized to lysosomes with a Pearson's colocalization coefficient of 0.81. Moreover, as oxidation can induce alkalization of lysosomes and acidification of cytoplasm, **29** was used to evaluate the efficiency of redox agents (Fig. 45). Probe **29** imaged and monitored

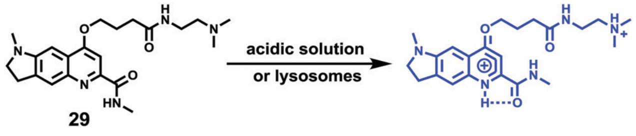

Scheme 22 Fluorescent probe **29** for pH.

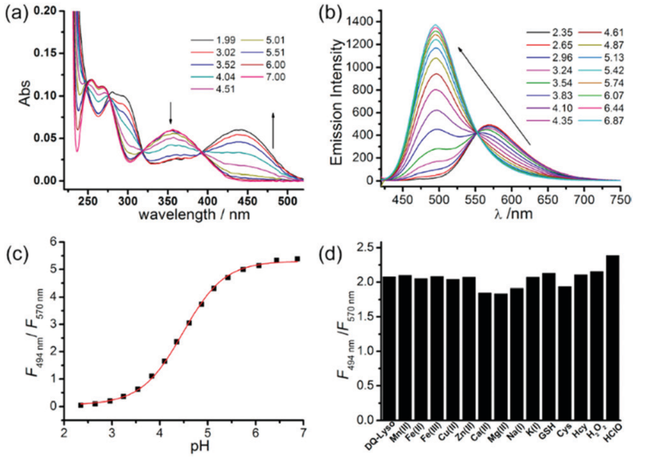

Fig. 44 (a) Absorption spectra of probe **29** (5 μM). (b) Fluorescence emission spectra of probe **29** (2 μM) in Na_2HPO_4–citrate buffer (10 mM Na_2HPO_4 and 10 mM citric acid) at various pH values. (c) Ratio (F_{494nm}/F_{570nm}) changes as a function of the pH values. (d) Emission spectra of probe **29** (2 μM) in the presence of various metal ions (100 μM Mn^{2+}, Fe^{3+}, Fe^{2+}, Cu^{2+}, Zn^{2+}, and 1 mM Mg^{2+}, Ca^{2+}, Na^+, and K^+), 5 mM thiols (GSH, Cys, Hcy), and 100 μM H_2O_2 and NaClO in Na_2HPO_4–citrate buffer (pH = 4.2); λ_{ex} = 405 nm. Copyright 2013 American Chemical Society.

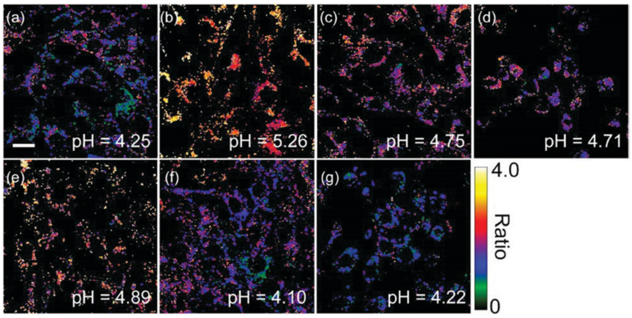

Fig. 45 Ratiometric imaging of NIH 3T3 cells. The cells were incubated with probe **29** (2 μM) at 37 °C for 30 min and then treated with (a) PBS at 25 °C for 3 min, (b) 10 mM NH_4Cl at 25 °C for 1 min, (c) 50 μM chloroquine at 25 °C for 3 min, (d) 100 μM H_2O_2 at 25 °C for 30 min, (g) 100 μM HClO at 37 °C for 30 min. The cells were pretreated with (e) 100 μM NEM and (f) 500 μM NAC at 37 °C for 30 min then incubated with **29** (2 μM) for further 30 min. Average pH values were measured from 10 cells in (a–g) and were calculated from the ratio (F_{green}/F_{red}) according to the intracellular calibration curve. Scale bar: 20 μm, ratio bar: 0–4. Copyright 2013 American Chemical Society.

lysosomal pH changes successfully after treating with H_2O_2 and other oxidative stress. Interestingly, the result indicated that HClO did not obviously affect lysosomal pH.

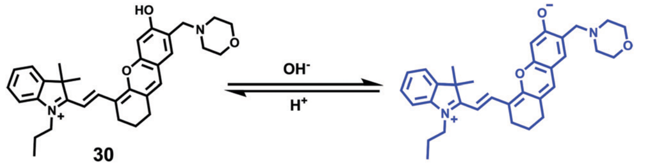

Scheme 23 Fluorescent probe **30** for pH.

Ma *et al.* developed a lysosome-targeting near-infrared ratiometric fluorescent pH probe **30**, by combining a typical lysosome-targeting moiety of morpholine with a hemicyanine skeleton (Scheme 23).[39] This probe showed not only an excellent I_{670}/I_{708} linear ratiometric response in the pH range of 4–6 in living cells, but good reversibility between pH 4.0 and pH 8.0 attributed to the protonation/deprotonation of the hydroxy group (Fig. 46). Moreover, probe **30** had stable fluorescence. It could remain almost constant after 40 minutes of continuous intensive irradiation. This reversible and stable probe **30** was used to investigate the change of lysosomal pH with temperature variation in HeLa and MCF-7 cells (Fig. 47). Notably, they revealed for the first time that the lysosomal pH value increased rather than decreased during heat shock, which meant that the pH rise process was irreversible.

Tiwaria and Liu *et al.* synthesized four near-infrared fluorescent probes **31**, **32**, **33** and **34** containing four different residues in order to investigate the effect of hydrophobic and hydrophilic residues on the cell imaging experiments (Scheme 24).[40] Probes **31**, **32**, **33** and **34** exhibited sensitive fluorescence responses to pH with 71-, 395-, 592- and 229-fold increases in the fluorescence intensity at 743 nm with decreasing pH from 7.4 to 4.1, respectively (Fig. 48a and b), and their pK_{cycl} values were 5.8, 4.6, 4.9 and 5.4, respectively. It was observed that an increase of ethanol concentration in the buffer solution enhanced fluorescence intensity of the four fluorescent probes as the probe solubility had improved (Fig. 48c). All the probes except probe **31** can specially localize in lysosomes (Fig. 49). The fluorescence signal

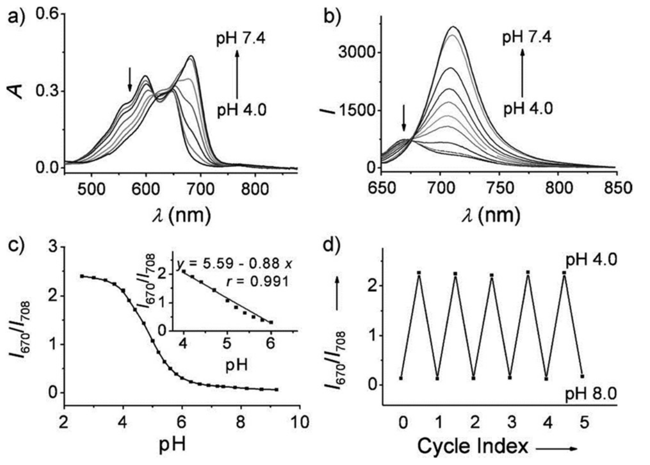

Fig. 46 (a) Absorption and (b) fluorescence emission spectra of probe **30** (10 μM) in phosphate buffer (0.2 M) at different pH values. (c) Plot of I_{670}/I_{708} (ratio of the fluorescence intensity of probe **30** at λ = 670 nm and λ = 708 nm) *versus* pH values in the pH range 2.6–9.2. Inset: The linear relationship between I_{670}/I_{708} and pH values in the pH range 4.0–6.0. (d) pH reversibility study of probe **30** between pH 4.0 and 8.0. λ_{ex} = 635 nm; data are expressed as the mean of three separate measurements ± standard deviation (SD). Copyright 2014 Wiley-VCH.

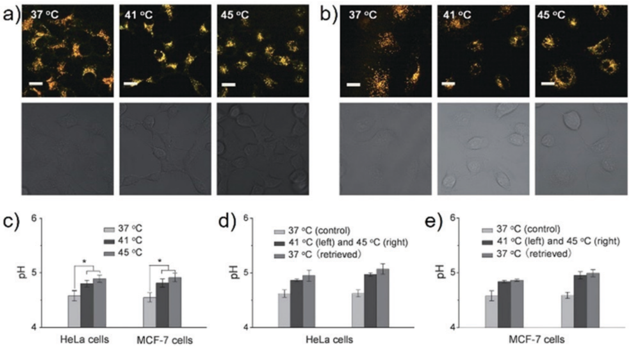

Fig. 47 Relationship between lysosomal pH and heat shock in HeLa and MCF-7 cells monitored by probe **30**. (a and b) The fluorescence images (top, merged; bottom, differential interference contrast) of probe **30**-loaded HeLa cells (a) and MCF-7 cells (b) under heat shock at 37 °C, 41 °C, and 45 °C (left to right) for 20 minutes. The fluorescence images are the merged images from both red (λ_{em} = 650–680 nm) and green (λ_{em} = 690–720 nm) channels at λ_{ex} = 635 nm. (c) Lysosomal pH changes with temperature in HeLa and MCF-7 cells. The lysosomal pH values in control and heat-treated cells were quantified by image analysis with 100–200 cells counted per condition. Results are expressed as the mean of three separate measurements ± SD. Statistical analyses are performed using the Student's *t*-test: $^*P < 0.001$. (d and e) Reversibility of the lysosomal pH change in HeLa cells (d) and MCF-7 cells (e) with temperature. Results are expressed as the mean of three separate measurements ± SD. Scale bars = 20 μm. Copyright 2014 Wiley-VCH.

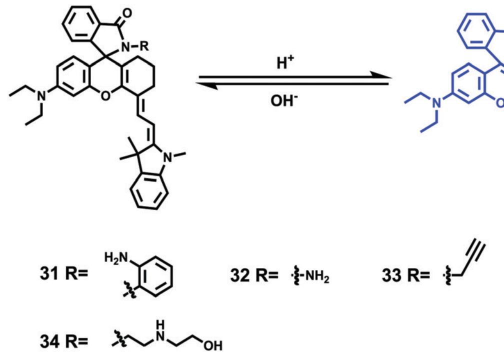

Scheme 24 Fluorescent probes **31–34** for pH.

of probe **34** bearing the *N*-(2-hydroxyethyl) ethylene amide residue was the highest and was followed by probe **32**.

Weng and Zhou *et al.* reported a convenient ratiometric 1,8-naphthalimide derivative **35** with amino groups, as modification with amino groups can usually improve the solubility of molecules in both water and lipids (Scheme 25).[41] **35** had a good fluorescence response to the pH value reversibly with a considerable Stokes shift of 45 nm because of the protonation of the imine (C═N) nitrogen (Fig. 50). It could also be used to distinguish different pH values even by the naked eye under UV excitation. With a pK_a value of 5.88, **35** could measure a wide range of intracellular pH values in HeLa cells and A549 cells (Fig. 51). It showed an obvious fluorescence change from bright red to bright green with the increase of pH value. Moreover, probe **35** could also be used as a lysosome marker in living cells.

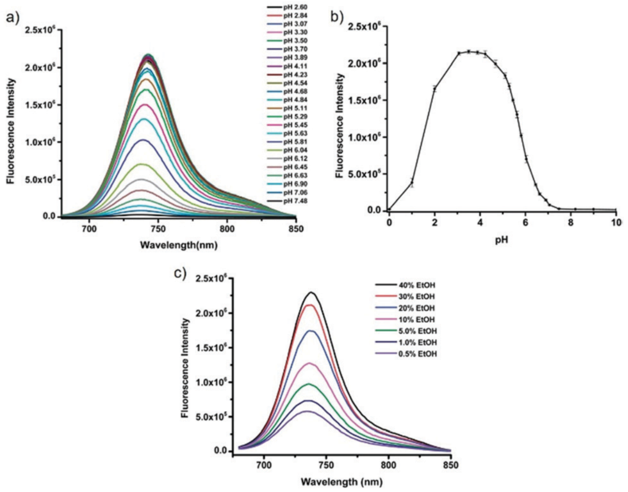

Fig. 48 Fluorescent spectra of 5 μM fluorescent probe **31** at different pH values in 40 mM citrate–phosphate buffer solution containing 40% ethanol (a) and pH effect on fluorescence intensity of fluorescent probe **31** at 743 nm with three repeated measurements (b). Fluorescence spectra of 5 μM fluorescent probe **34** in 40 mM citrate–phosphate buffer solution at pH 4 containing different concentrations of ethanol (c). Copyright 2014 Royal Society of Chemistry.

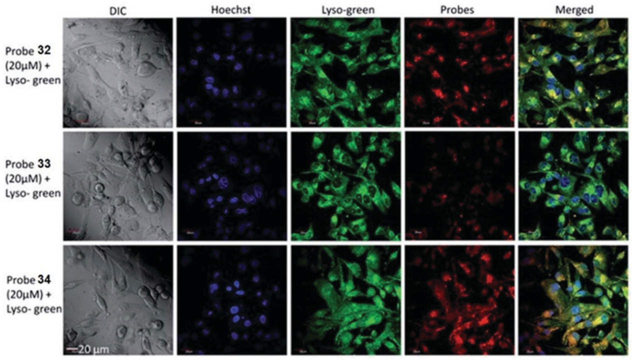

Fig. 49 Fluorescence images of MDA-MB-231 cells incubated with fluorescent probes **32**, **33**, and **34**. Cells were incubated with 20 mM of dyes **32**, **33**, and **34** for 2 h and imaged for co-localization in the presence of 5 μM LysoSensor Green, a lysosomal stain and Hoechst, a nuclear stain. The images were acquired using a confocal fluorescence microscope at 60× magnification. Copyright 2014 Royal Society of Chemistry.

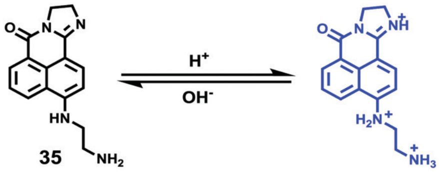

Scheme 25 Fluorescent probe **35** for pH.

Han *et al.* presented an acidic-responsive near-infrared probe **36** conjugated with sialic acid (Sia) (Scheme 26).[42] Probe **36** showed an optimal turn-on fluorescence response to acidic pH within pH 4.0–5.5, because of acidic pH-mediated fluorogenic opening of the intramolecular fluorophore ring (Fig. 52). Containing inflamed tissue targeting domain Sia, probe **36** was utilized for imaging inflammation in mice (Fig. 53). After injecting *Escherichia coli* (*E. coli*), Gram-positive bacteria or lipopolysaccharide (LPS) into

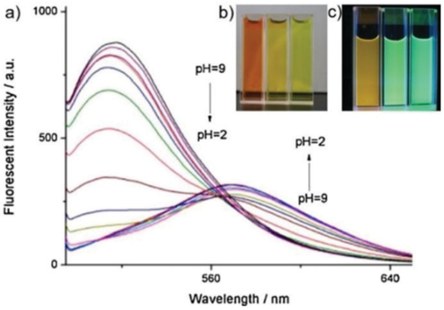

Fig. 50 (a) Fluorescence spectra (λ_{ex} = 480 nm) of probe **35** (2 μM) at different pH values; (b) the color change of probe **35** (1 mM) in 20 mM PBS buffer at different pH values under the condition of visible light; (c) the color change of probe **35** (1 mM) in 20 mM PBS buffer at different pH values under UV light irradiation. Copyright 2014 Elsevier.

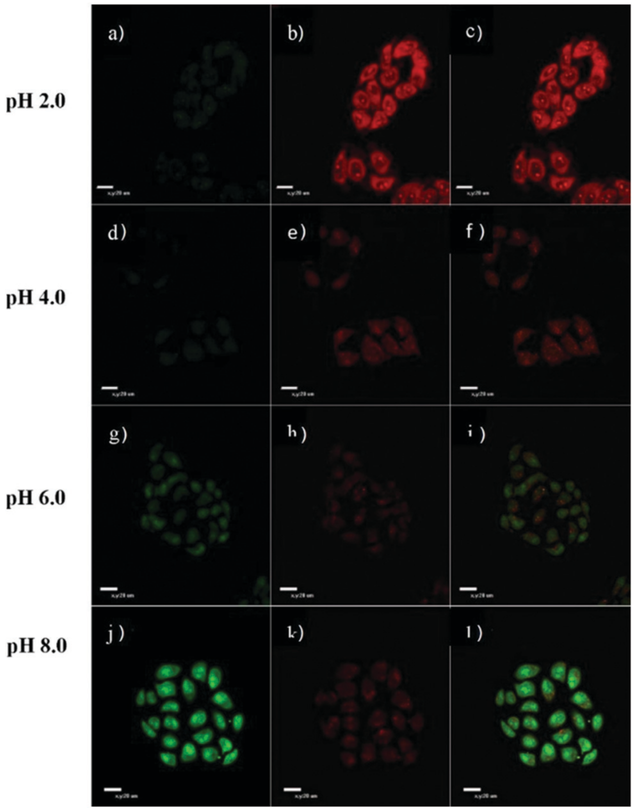

Fig. 51 Confocal laser scanning microscopy analysis of HeLa cells in various pH buffers. HeLa cells incubated with probe **35** (10 μM) for 1 h and then immersed in 20 mM PBS buffers for 5 min at pH 2.0 (a–c), pH 4.0 (d–f), pH 6.0 (g–i), and pH 8.0 (j–l) respectively. All images used Ex 488 nm, Em 515 nm (first column, green fluorescence) and 650 nm (second column, red fluorescence) and the third column was merged with green fluorescence and red fluorescence. Copyright 2014 Elsevier.

the thigh muscle of ICR mice, intense NIR fluorescence of probe 36 was identified in the injection sites respectively, and the fluorescence would be off after immunological elimination. A similar phenomenon was observed when Raw 264.7 cells were incubated with probe 36 and natural Sia, which suggested that probe 36 could be an outstanding cellular uptake substrate even in the presence

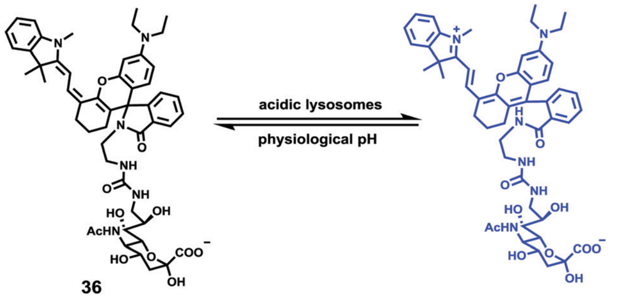

36

Scheme 26 Fluorescent probe **36** for pH.

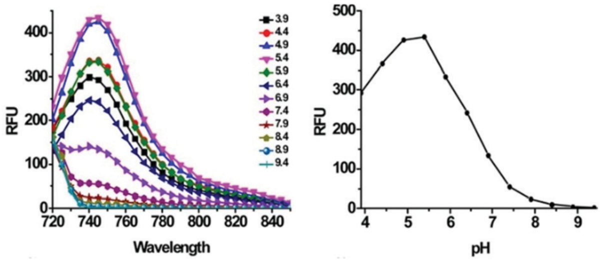

Fig. 52 Acid-activatable fluorescence of probe **36**. A series of phosphate buffer solutions (pH 3.9–9.4) containing **36** (200 μM) was analyzed for fluorescence emission using an excitation wavelength of 715 nm. Copyright 2015 American Chemical Society.

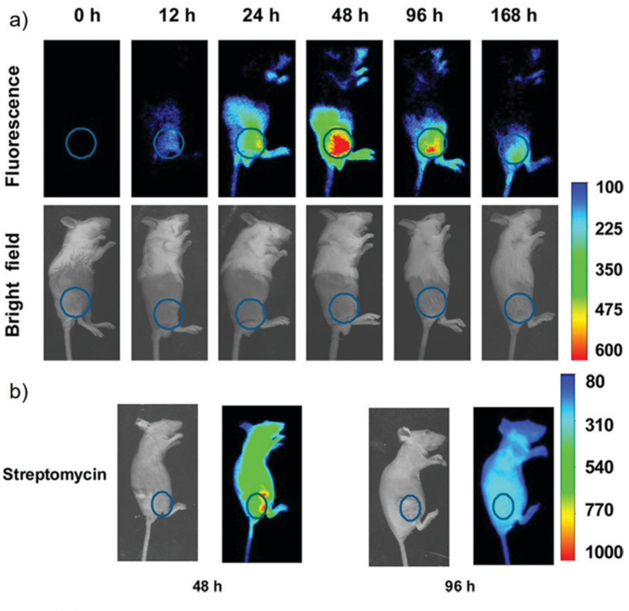

Fig. 53 (a) Differential illumination of *E. coli*-induced inflammation by probe **36**. ICR mice were injected with *E. coli* in the muscle of the right thigh and then administered with **36** (40 mg kg^{-1}) by the tail vein. At indicated time points after probe administration, the mice were imaged for whole-body NIR fluorescence. (b) Antibiotic-mediated fluorescence switch off of probe **36** in inflammatory tissues. ICR mice were injected with *E. coli* in the muscle of the right thigh. Probe **36** (40 mg kg^{-1}) was intravenously injected into mice, and then the mice were injected with streptomycin (20 mg kg^{-1}) in the left thigh 2 days after administration of the bacteria. Whole-body fluorescence was visualized at 48 and 96 h postinjection of streptomycin. Copyright 2015 American Chemical Society.

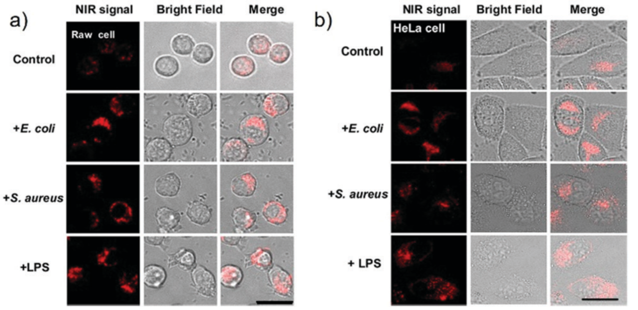

Fig. 54 Elevation of probe **36** fluorescence in live cells in the presence of bacteria and LPS. Raw 264.7 (a) and HeLa cells (b) prestained with probe **36** (100 μM) were cultured in DMEM containing *E. coli*, *S. aureus*, LPS, respectively, or no addition (control). The cells were washed with PBS and then imaged by fluorescence microscopy. Bar: 10 μm. Copyright 2015 American Chemical Society.

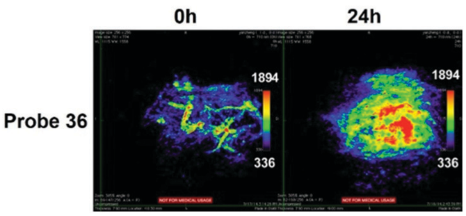

Fig. 55 Optoacoustic imaging of *S. aureus*-elicited inflammation in mice with probe **36**. Nude mice were injected with *S. aureus* in the thigh muscle and then intravenously injected with probe **36** (40 mg kg^{-1}). At 0 and 24 h post probe injection, the inflamed spots were imaged for optoacoustic contrasts. Copyright 2015 American Chemical Society.

of Sia (Fig. 54). Moreover, the inflammation-associated fluorescence of nude mice was quenched after treating with antibiotics. Additionally, probe **36** also displayed turn-on optoacoustic signals under acidic settings (Fig. 55).

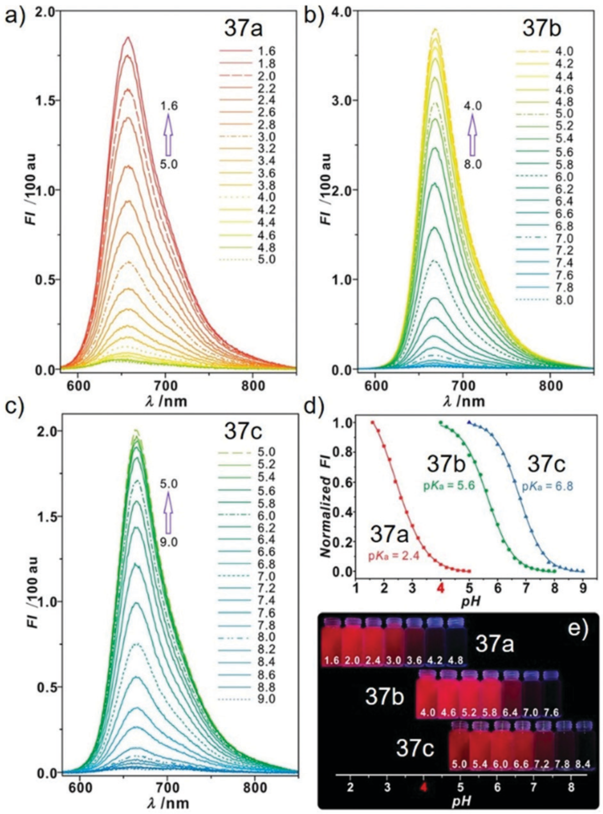

Fig. 56 pH activable emission properties of probes **37a–c** (10 μM, λ_{ex} = 570 nm) in disodium hydrogen phosphate–citric acid buffers containing 10% DMSO: (a) probe **37a**; (b) probe **37b**; (c) probe **37c**; (d) normalized fluorescence intensities of probes **37a–c** at different pH values at (a) 657 nm, (b) 668 nm, and (c) 663 nm; (e) photograph of pH-dependent red emissions under a 365 nm lamp in a darkroom. Copyright 2015 American Chemical Society.

Sun and Ge *et al.* reported lysosome-targetable pH sensors **37a–37c** which were designed aiming at selective detection of cancer cells (Scheme 27).[43] **37a–37c** were based on Darrow Red derivatives and chose a cyano group as a lysosome tracker. Because lysosome maintains an acidic environment of approximately pH 4.5–5.0 in normal cells and pH in cancer cells is lower than that in normal cells, the authors deduced that the lysosome-targetable OFF–ON type sensors for cancer cells should emit no to weak emissions at pH = 4.0. Fluorescent pH titration experiments showed that the fluorescence intensity of **37a** increased 39 times from pH = 5.0 to pH = 1.6 with pK_a value 2.4, fluorescence intensity of **37b** was enhanced by 141-fold from pH = 8.0 to pH = 4.0 with pK_a value 5.6, and fluorescence emission of probe **37c** increased 91 times from pH = 9.0 to 5.0 with a pK_a of 6.8 (Fig. 56). Unsurprisingly, confocal fluorescence imaging in HeLa cancer cells, V79 and KB normal cells showed that **37a** entirely fitted the design aims and was found to be a lysosome tracker for cancer cells. **37b** and **37c** could be used as lysosome-trackers in cancer and normal cells.

Miao and Zhao *et al.* reported a rhodamine B-based probe **38** (Scheme 28).[44] Probe **38** could measure pH values in short time (within 1.5 min at pH values of 4.60, 5.60 and 7.20), and the fluorescence intensity was linearly proportional (R = 0.99523) to pH values in the range of 4.2–6.0 (Fig. 57). Moreover, it had excellent reversibility between pH 4.60 and 7.20 (Fig. 58). In living HeLa cells, **38** could selectively stain lysosomes and the

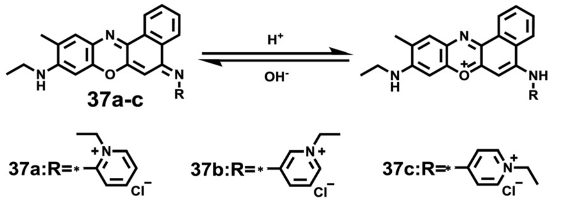

Scheme 27 Fluorescent probes **37a–c** for pH.

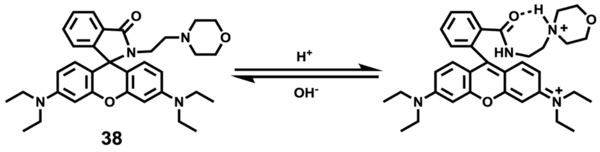

Scheme 28 Fluorescent probe **38** for pH.

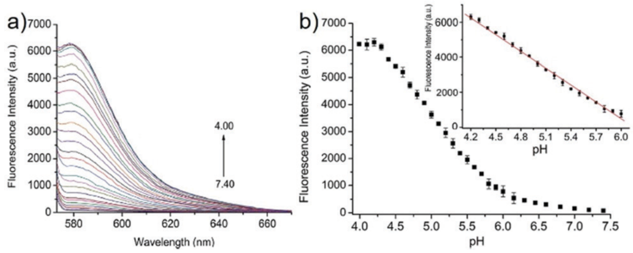

Fig. 57 (a) Fluorescence spectra of probe **38** (1 μM) in buffers at different pH values; (b) fluorescence intensity at 583 nm with pH values according to the fluorescence pH titration (pH 4.00–7.40), λ_{ex} = 563 nm. The inset shows the linear relationship of fluorescence intensity at 583 nm and pH values from 4.20 to 6.00 (R = 0.99523). Copyright 2015 Royal Society of Chemistry.

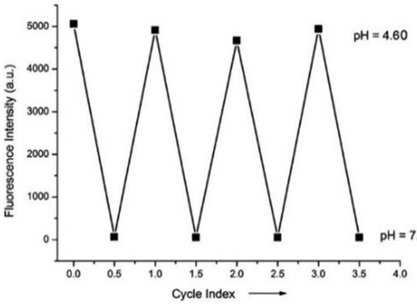

Fig. 58 The pH reversibility of probe **38** between pH 4.60 and 7.20. Copyright 2015 Royal Society of Chemistry.

fluorescence intensity of **38** was also concentration and time dependent. More importantly, **38** could be used to quantitatively monitor the pH changes in lysosomes induced by bafilomycin A1 within HeLa cells (Fig. 59). Lysosomes have proton-pumping vacuolar ATPases and Bafilomycin A1 is a selective inhibitor of the vacuolar-type H^+-ATPase (V-ATPase). Therefore, bafilomycin A1 can inhibit lysosomal acidification, thereby regulating the lysosomal pH environment. Incubating different concentrations of bafilomycin A1 for 6 h, and then 2.5 μM **38** for 1 h, gradually weakened fluorescence intensities with increased concentration of bafilomycin A1 in HeLa cells were observed.

Xiao *et al.* introduced a near-infrared (NIR) lysosomal probe **40** based on their previously reported probe **39** (Scheme 29).[45] The chemical structure of probe **40** was interestingly unusual since it was functionalized with two triphenylphosphonium (TPP) moieties from **39** *via* click chemistry. Because the mitochondrial membrane has typically a negative potential, positively charged TPP moieties are usually used as mitochondrial delivery vehicles instead of lysosome-targeting moieties. In this case, the two TPP moieties endowed the probe with lysosome-targeting capability by mediating the probe's hydrophilic–lipophilic balance. In lysosomes, this probe showed intensive near-infrared (NIR) fluorescence and better photostability compared with commercial lysosomal tracker NR and **39** (Fig. 60). Moreover, probe **40** demonstrated stable targeting ability and stable fluorescence against lysosomal pH changes. This feature was rare but valuable because most currently used lysosomal probes will lose their fluorescence or even leave lysosomes once the pH rises. However, pH values of lysosomes in different physiological status are different. Thus, probe **40** was suitable for tracking lysosomes under different physiological status including apoptosis and poisoning.

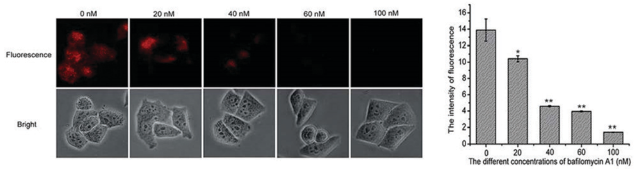

Fig. 59 Fluorescence microscopy images of living HeLa cells first incubated with 0–100 nM bafilomycin A1 for 6 h, and then with 2.5 μM probe **38** for 1 h at 37 °C. The results are presented as means ± SE with replicates n = 3. $*p < 0.05$; $**p < 0.01$. Copyright 2015 Royal Society of Chemistry.

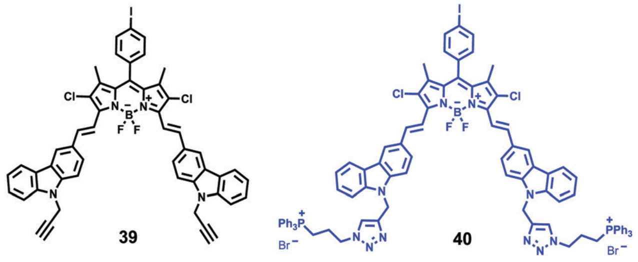

Scheme 29 Fluorescent probe **40** for pH.

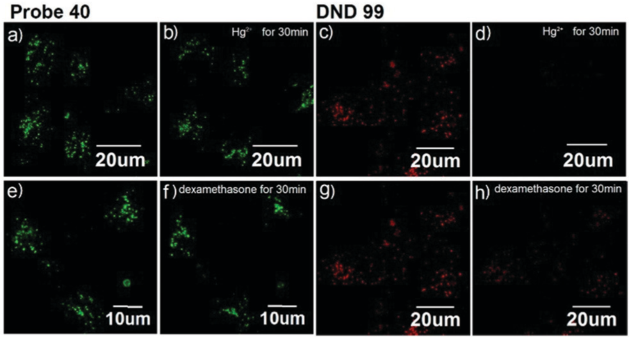

Fig. 60 Fluorescence images of MCF-7 stained with probe **40** (pseudo green) and DND-99 (pseudo red) stimulated with 100 μM Hg^{2+} [(a and b) probe **40**; (c and d) DND-99] and 10 μM dexamethasone [(e and f) probe **40**; (g and h) DND-99]. Copyright 2014 American Chemical Society.

Lin *et al.* developed a novel dual site-controlled and lysosomal-targeted ICT-PET-FRET fluorescent probe **41** for monitoring lysosomal pH in living cells (Scheme 30).[46] The probe employed coumarin and naphthalimide fluorophores as the donor and acceptor to construct the FRET platform, and adopted hydroxyl and morpholine as the two pH sensing sites to control the

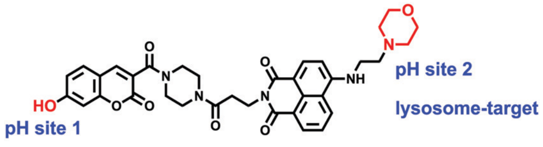

41

Scheme 30 Fluorescent probe **41** for pH.

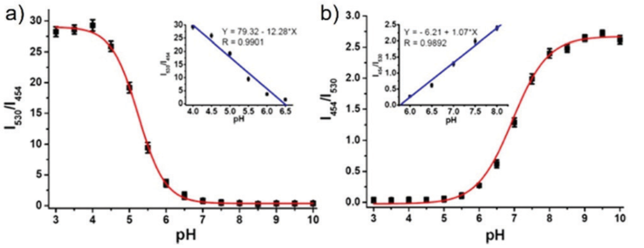

Fig. 61 Fluorescence intensity ratios I_{530}/I_{454} (a) and I_{454}/I_{530} (b) of 5 μM **41** in B–F buffers (5% MeOH) at various pH values. Insets are the linear plots of fluorescence intensity ratio to pH; λ_{ex} = 380 nm. Copyright 2016 American Chemical Society.

fluorescence of coumarin and naphthalimide by ICT and PET, respectively. With the pH changing from 3.0 to 10.0, the fluorescence changed from the green fluorescence of the naphthalimide unit to the blue fluorescence of the coumarin unit. Under the synergistic effect of ICT, PET and FRET, **41** had an excellent response and high sensitivity to pH (Fig. 61). Moreover, the fluorescence ratio of **41** was linearly related to pH over a wide range of pH 4.0 to pH 8.0. Probe **41** had no significant toxicity to living cells and had ideal lysosomal targeting properties, thus was successfully applied to fluorescence imaging of lysosomal pH (Fig. 62).

James, Jia and Huang *et al.* synthesized a new ratiometric fluorescent probe **42** that could be used to detect the interplay between lysosomal behaviour and heat stroke (Scheme 31).[47] The maximum absorption of **42** gradually red-shifted from 430 nm to 538 nm with pH values increasing from 3 to 11. Upon excitation at 473 nm, a decrease of fluorescence emission intensity at 522 nm accompanied by an increase of fluorescence emission intensity at 557 nm was observed when the pH value of the solution increased, indicating the ratiometric fluorescence sensing of probe **42** for pH changes. Colocalization experiments indicated that probe **42** was a lysosomal specific

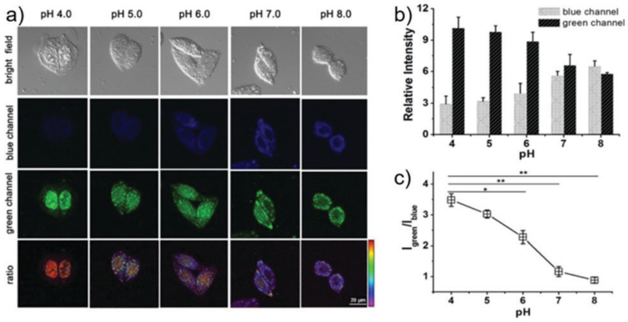

Fig. 62 (a) Fluorescence images for 5 μM **41** in HeLa cells at various pH values: blue channel, emission at 425–475 nm with excitation at 405 nm; green channel, emission at 500–550 nm with excitation at 488 nm. Ratio images represent the ratio of fluorescence intensity between the green channel and blue channel (I_{green}/I_{blue}). (b) Quantified relative fluorescence intensity at various pH values was analyzed using Nikon NIS Element software and presented as mean ± SD, with n = 3. (c) Ratio of I_{green}/I_{blue} at various pH values obtained from panel b. Statistical analyses were performed with Student's t test (n = 3). $^*P < 0.05$, $^*P < 0.01$, and error bars are ±SD. Copyright 2016 American Chemical Society.

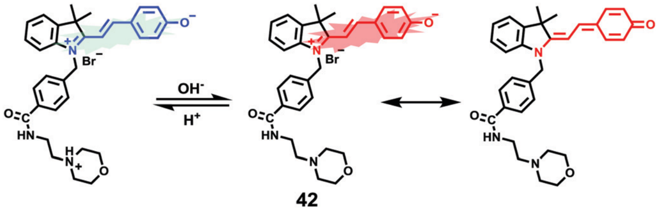

Scheme 31 Fluorescent probe **42** for pH.

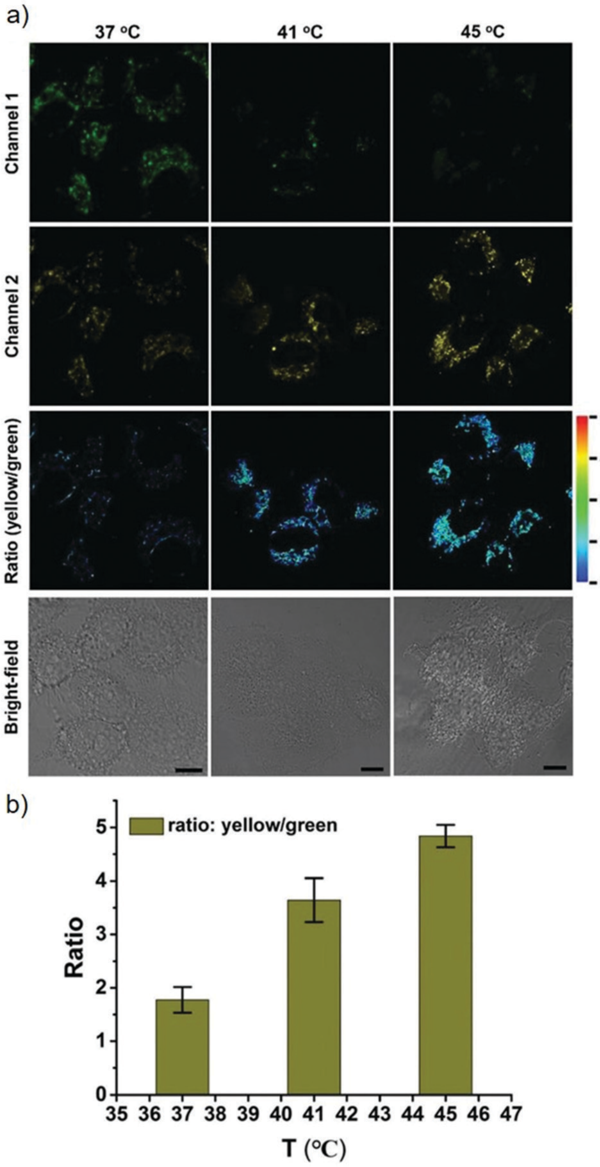

Fig. 63 Relationship between lysosomal pH changes and heat stroke in HeLa cells. (a) Ratiometric fluorescence images of the **42**-stained cells under heat shock at 37 °C, 41 °C, and 45 °C (left to right) respectively for 20 min and then continued culture for another 20 min at 37 °C. Excitation wavelength for probe **42**: 488 nm; emission collection, channel 1 (green, channel 1): 500–550 nm; channel 2 (yellow, channel 2): 570–620 nm. Scale bar is 10 mm. (b) Semiquantitative determination of **42**-stained HeLa cells according to the ratio of average fluorescence intensity of channel 2 (yellow) to channel 1 (green). Error bars represent s.d. Copyright 2018 Royal Society of Chemistry.

labelling probe and could be used for the ratiometric fluorescence sensing of pH changes of lysosomes in live cells, in which the morpholine displayed the ability to improve the lysosome-targeting specificity. More importantly, probe **42** was able to sense the fluctuation of lysosomal pH ratiometrically under heat stroke in live HeLa cells, which showed a gradual decrease in green fluorescence (channel 1, 500–550 nm) and simultaneous enhancement in the yellow fluorescence (channel 2, 570–620 nm) as the temperature increased from 37 °C to 41 °C, then to 45 °C (Fig. 63). The fluorescence emission ratio values of average emission intensity for yellow images (channel 2) and green images (channel 1) were calculated to be increased from 1.78 to 4.84 under heat stress. This work provided an effective ratiometric imaging tool for mapping lysosomal pH changes in live cells under a heat shock stimulus.

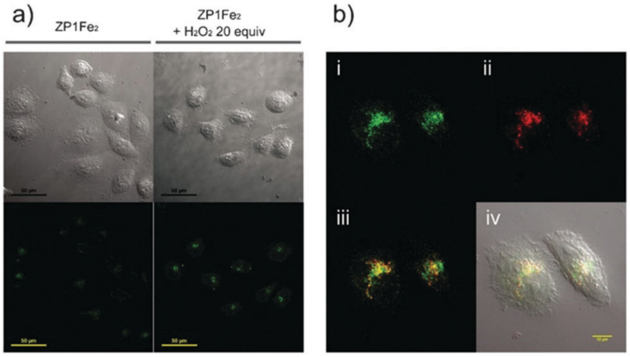

Fig. 64 (a) Fluorescent detection of intracellular H_2O_2 in live HeLa cells: bright field (top) and fluorescence (bottom) micrographs of HeLa cells incubated with probe **43** (10 μM, 30 min). Cells shown in the right panels were treated with H_2O_2 (200 μM, 10 min). Scale bar = 50 μm. (b) Subcellular localized fluorescence signals from the lysosomes. HeLa cells were pre-treated with H_2O_2 (200 μM, 10 min) and incubated with probe **43** (10 μM, 30 min) and LysoTracker-Red (50 nM, 1 h): (i) probe **43** signals; (ii) LysoTracker-Red signals; (iii) merged images (i) and (ii); (iv) bright field image. Scale bar = 10 μm. Copyright 2012 Royal Society of Chemistry.

4. Small-molecule fluorescent probes for the detection of reactive oxygen species (ROS) inside lysosomes

During the metabolism, the body produces different kinds of reactive oxygen species (ROS), including superoxide ($O_2^{\bullet-}$), hydroxyl radicals ($^{\bullet}OH$), peroxy radicals ($^{\bullet}OOR$), single oxygen ($^1O_2$), and hypochlorous acid/hypochlorite ($HOCl/ClO^-$) and hydrogen peroxide (H_2O_2). It has been reported that reactive oxygen species in lysosomes play a crucial role in the pathogenesis of many serious diseases such as cancer, neurodegenerative diseases and cardiovascular diseases.[48] Therefore, effective monitoring of ROS level in living cells and tissues is very important for human health.

4.1 Small-molecule fluorescent probes for the detection of H_2O_2 inside lysosomes

Hydrogen peroxide (H_2O_2) is a major member of reactive oxygen species (ROS) and has a variety of physiological functions, including respiration, host defense, intracellular signaling, and immune responses.[49] Excess H_2O_2 in lysosomes leads to lysosomal dysfunction and even rupture due to autophagy and apoptosis. Therefore, it is important to detect lysosomal H_2O_2 in living cells.

You and Nam *et al.* developed a new fluorescent probe **43** for H_2O_2 (Scheme 32).[50] Unlike previous experiments utilizing H_2O_2 to oxidize Fe^{2+} for the fluorescence detection of H_2O_2, probe **43** was developed based on the cleavage of the paramagnetic Fe ionophore from the fluorophore, which afforded exceptional selectivity for H_2O_2 over other ROSs. The addition of an excess of H_2O_2 to the solution of **43** provoked a significant fluorescence turn-on with a 22-fold increase in the fluorescence quantum yield. However, the addition of $O_2^{\bullet-}$, ^-OCl, *t*-BuOOH, NO, $^1O_2$, $(NH_4)_2Ce^{IV}(NO_3)_6$ (CAN), and 2,3-dichloro-5,6-dicyano-pbenzoquinone (DDQ) did not produce fluorescence turn on, and only a small increase in the fluorescence intensity was observed in the cases of *t*-BuO$^{\bullet}$ and $^{\bullet}OH$. The limit of detection (LOD) of probe **43** for H_2O_2 was determined to be 29 μM. Colocalization experiments showed that the fluorescence patterns of **43** and the LysoTracker-Red signals were overlapped perfectly, which indicated unambiguously that the fluorescence response was localized at the lysosome (Fig. 64).

Zhang *et al.* reported a two-photon cell-permeable fluorescent probe myeloperoxidase **MPO-44** through the combination of MPO with probe **44** since myeloperoxidase (MPO) has many advantages such as specific reactivity and selectivity to convert "H_2O_2 + Cl^-" into hypochlorite, good cell-permeability, and lysosomal retention (Scheme 33).[51] The probe could be used to visualize exogenous or endogenous H_2O_2 with high selectivity and sensitivity. In the presence of MPO, hypochlorite-sensitive ZnSalen **44** showed a selective turn-on response to H_2O_2 in acidic buffer pH (4.5–6.0) aqueous solution, while other bio-related ROS interference can be ignored. Subcellular localization of the probe **MPO-44** assay showed that the probe **MPO-44** exhibited good colocalization with that of LysoTracker Green DND-26, with a Pearson's correlation coefficient of 0.92 and an overlap coefficient of 0.94 (Fig. 65).

p-Dihydroxyborylbenzyloxycarbonyl has been proved to be an efficient moiety for the detection of H_2O_2. Recently, Yin and

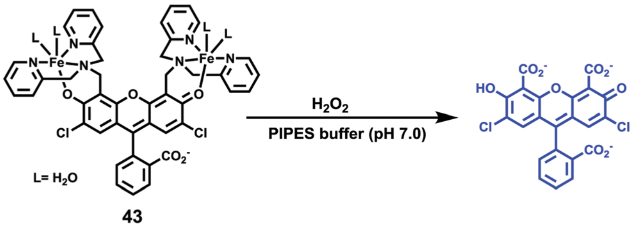

Scheme 32 Fluorescent probe **43** for H_2O_2.

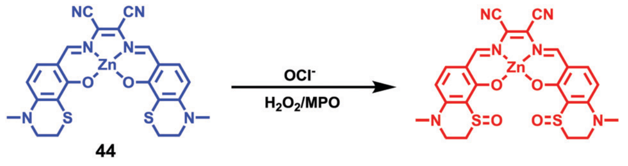

Scheme 33 Fluorescent probe **44** for H_2O_2.

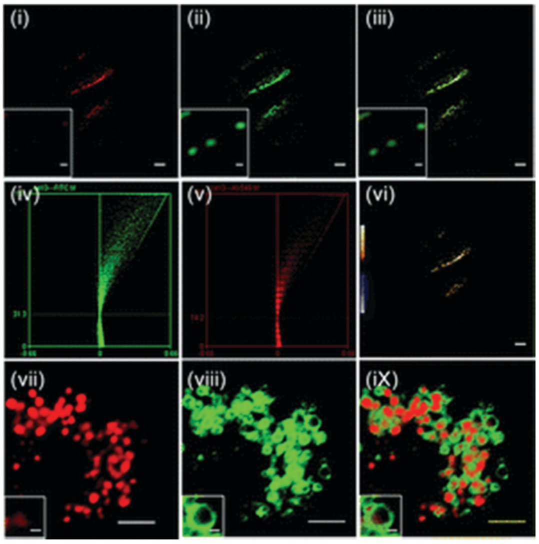

Fig. 65 Probe **44** colocalization assay in HeLa cells. Cells treated with "**MPO-44**" for 12 h and then H_2O_2 for half an hour were stained with LysoTracker Green DND-26 for half an hour: (i) fluorescence image of "**MPO-44**"; (ii) fluorescence image of LysoTracker Green DND-26; (iii) merged image of (i) and (ii); ICA scatter plots of "**MPO-44**" (iv) and LysoTracker Green DND-26 (v); (vi) PDM image. The PDM scale bar is inserted. Cells expressing LAMP2-EGFP were treated with "**MPO-44**" for 12 h and then H_2O_2 for half an hour. (vii) Fluorescence image of "**MPO-44**"; (viii) image of LAMP2-EGFP; (ix) merged image of "**MPO-44**" and LAMP2-EGFP. The scale bar is 10 μm in original pictures, 1 μm in amplified pictures. Copyright 2013 Royal Society of Chemistry.

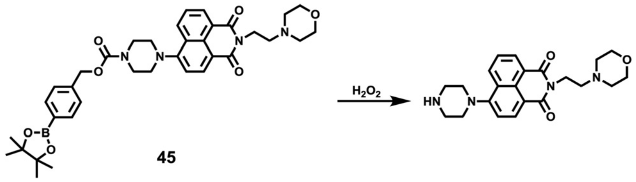

Scheme 34 Fluorescent probe **45** for H_2O_2.

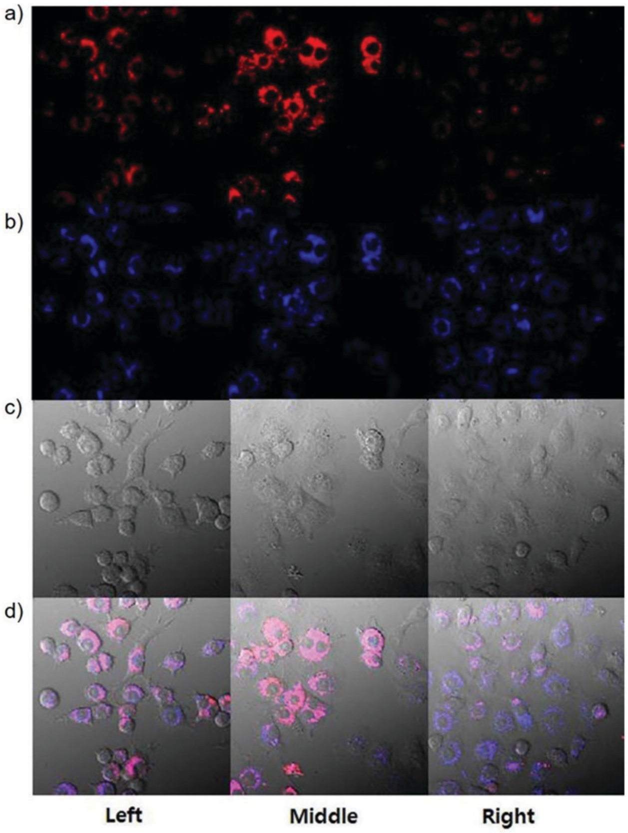

Fig. 67 Probe **45** was localized to lysosomes in RAW264.7 cells. Confocal microscopy images of probe **45** on the endogenous H_2O_2: (a) probe **45** (red, ex405/em490–590 nm); (b) LysoTracker Blue DND-22 (blue, ex405/em430–455 nm); (c) bright field (gray); (d) overlay of (a) and (b) (purple). Left: No treatment; middle: 1 μg mL^{-1} PMA (Phorbol 12-myristate 13-acetate), 1 h; right: 1 μg mL^{-1} PMA, 1 h and 100 μM TEMPO (2,2,6,6-tetramethyl-piperidine-1-oxyl, ROS scavenger), 1 h. (For producing endogenous H_2O_2, the RAW264.7 cells were treated with PMA. All cells were stained with 5 μM probe **45**, 100 nM Lysotracker for 30 min; scale bar: 10 μm.) Copyright 2015 Nature.

Yoon *et al.* reported a borate-based hydrogen peroxide (H_2O_2) probe **45** with a morpholine moiety as the lysosome-directing group (Scheme 34).[52] Probe **45** exhibited high selectivity and sensitivity for H_2O_2. As shown in Fig. 66, the addition of H_2O_2 into the solution of probe **45** induced an obvious increase in the fluorescence intensity. However, under the same condition, slight changes were observed after incubation with various ROSs including $^{\bullet}OH$, $ONOO^-$, $^{\bullet}OOR$, $^{\bullet}NO$, ClO^-, and *t*-ROOH. The investigation of the fluorescence titration of probe **45** upon addition of H_2O_2 showed that an obvious fluorescence enhancement was observed along with increasing H_2O_2. More interestingly, confocal microscopy images of probe **45** indicated that probe **45** was a lysosome-targetable H_2O_2 indicator and could be used as an efficient tool to monitor the level of exogenous and endogenous H_2O_2 in the living cells. As shown in Fig. 67, owing to the existence of endogenous H_2O_2 released from the RAW 264.7 cells, the confocal microscopy image of probe **45** displayed a red emission. Moreover, since more endogenous H_2O_2 was produced by treating RAW 264.7 cells with PMA (Phorbol 12-myristate 13-acetate, 1 mg mL^{-1}), a significant fluorescence enhancement was observed. The subsequent addition of TEMPO (2,2,6,6-tetramethylpiperidine-1-oxyl, 100 mM), a ROS scavenger to block H_2O_2, resulted in a significant decrease in the fluorescence

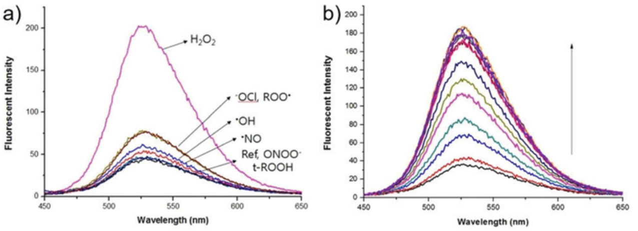

Fig. 66 (a) Fluorescence spectra of probe **45** (2 μM) with various ROS (200 μM) and (b) fluorescence titration of probe **45** (2 μM) upon addition of H_2O_2 (0–100 eq.) in PBS (pH 7.4) solution containing 1% DMF after incubation for 2 h at 25 °C at an excitation wavelength of 405 nm, and excitation and emission slit widths of 3 and 5 mm, respectively. Copyright 2015 Nature.

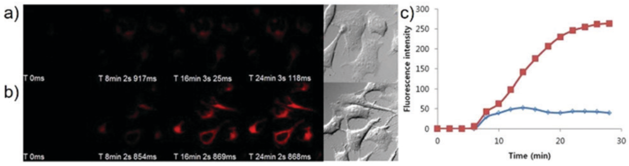

Fig. 68 Time-dependent fluorescence intensity of probe **45** in HeLa cells. HeLa cells were incubated with 0 or 100 μM H_2O_2 for 30 min and 0.2 μM probe **45** was added for 30 min. The time-dependent fluorescence image of probe **45** was acquired by confocal microscopy: (a) no treatment; (b) 100 μM H_2O_2; (c) time-dependent fluorescence intensity graph of probe **45** in HeLa cells (blue color: no treatment; red color: 100 μM H_2O_2). Copyright 2015 Nature.

intensity. Furthermore, probe **45** could be used for monitoring the level of H_2O_2 in the living cells over time. As shown in Fig. 68, the fluorescence image displayed a weak red emission when the HeLa cells were not treated with H_2O_2. However, when the HeLa cells were incubated with H_2O_2, an increasing red emission was observed from the confocal microscopy images and a stronger red emission was observed over time.

4.2 Small-molecule fluorescent probes for the detection of HOCl inside lysosomes

Hypochlorous acid (HOCl) is one of the important reactive oxygen species (ROS) that can be synthesized by hydrogen peroxide and chloride under myeloperoxidase (MPO) catalysis. HOCl is a weak acid ($pK_a = 7.6$) and mainly distributed in the acidic organelle lysosome of macrophages. Although it is present in extremely low concentration, it plays a key role in the immune defense against invading bacteria and other pathogens.[53] Abnormal accumulation of HOCl in phagocytes can induce various diseases such as rheumatoid arthritis, neuronal degeneration, Parkinson's disease and cerebral ischemia. Therefore, chemosensors that achieve imaging or quantification of HOCl are necessary for investigations of HOCl related biological processes. Until now, a large number of fluorescent probes for sensing of HOCl have been reported based on the HOCl-mediated oxidation reaction with recognition groups, such as special carbon–nitrogen double bonds, sulfide, selenide, rhodamine-based spirane structure, *p*-methoxyphenol, and pyrrole and some other methods.[54] However, only a few fluorescent probes could detect HOCl inside lysosomes.

Chang *et al.* developed the lysosomal targetable two-photon fluorescent HOCl probe **47** (Scheme 35).[55] In this probe, a well-known two-photon fluorophore Acedan was chosen as the fluorescence reporting group due to its excellent photophysical properties whilst 2-mercaptoethanol was employed to be the protecting group because the thiol atom in methionine could be easily oxidized to sulfoxide by HOCl thereby changing the fluorescence of the probe. Lysosome-targetable group morpholine was introduced to ensure the probe's intracellular localization. For comparison, a two-photon fluorescent HOCl probe **46** without the morpholine group was prepared as well. Based on the oxidative deprotection mechanism, a fast response (within a few seconds) and good sensitivity (<20 nM) of these probes to HOCl were achieved with excellent selectivity over other ROS and biomolecules. Cell imaging experiments showed that probe **47** displayed good cell penetration and lysosomal localization ability in living cells and could be successfully utilized to detect HOCl in lysosomes. In particular, two-photon imaging of **47** indicated that more HOCl can be detected in the lysosome of macrophages during inflammatory conditions in a murine model. As shown in Fig. 69, strong fluorescence from **47** in LPS-stimulated macrophage cells was observed in inflammation tissues, which was conducted by subcutaneous injection of 200 μL of LPS (1 mg mL^{-1}) into the right rear paws of mice and subcutaneous injection of **47** into the paw skin after 1 day. Therefore, these probes not only could help elucidate the distribution of subcellular HOCl, but also served as excellent tools to exploit potential functions of HOCl at subcellular and tissue levels.

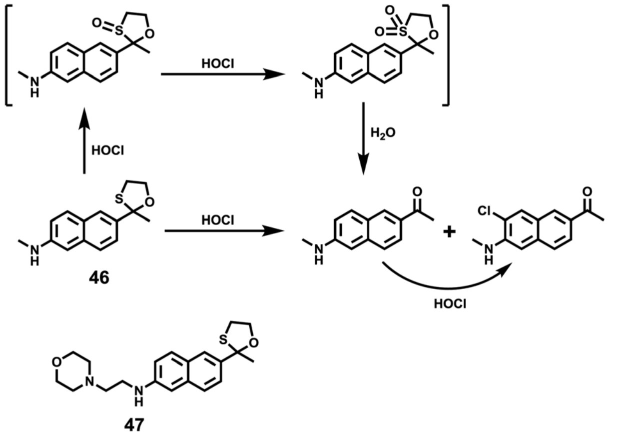

Scheme 35 Fluorescent probe **47** for HOCl.

Based on the intramolecular charge transfer (ICT) mechanism, Tang *et al.* synthesized a two-photon fluorescence probe

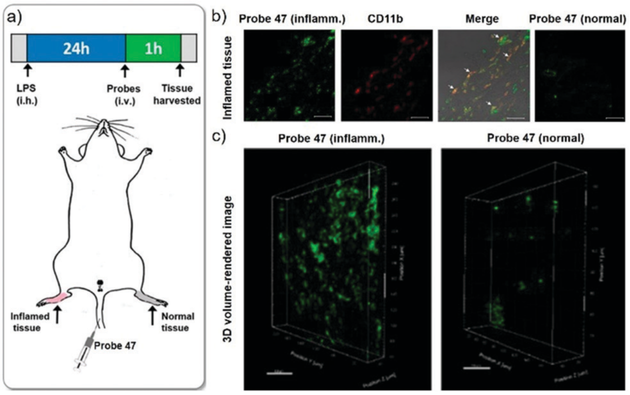

Fig. 69 Detection of LPS-dependent HOCl generation in inflammation tissues *via* probe **47**. (a) 200 μL of LPS (1 mg mL^{-1}) was subcutaneously (i.h.) injected into the right rear paws of mouse to cause inflammation. After 1 day, 200 μL of 1 mM probe **47** was intravenously (i.v.) injected and the paw skin was sectioned 1 h later. (b) Fluorescence images of probe and CD11b in the inflamed tissue. Probe fluorescence, green; antibody CD11b, red. Arrows indicate the merged parts of the HOCl sensitive probe and CD11b. (c) 3D volume-rendered image shows the distribution of macrophages within the inflamed and normal tissues. (+) Inflammation tissues; (−) normal tissues. Scale bar: 30 μm. Copyright 2015 American Chemical Society.

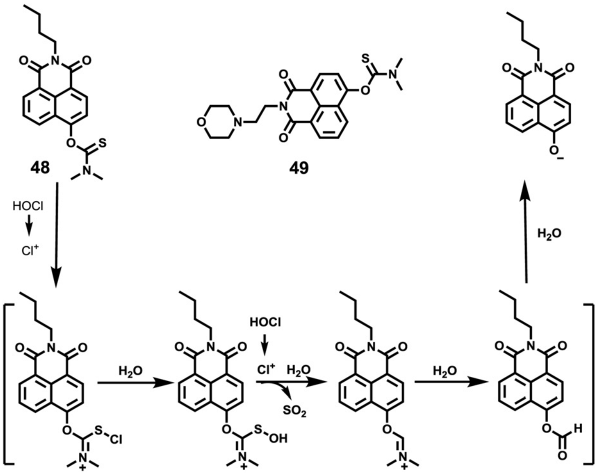

Scheme 36 Fluorescent probes **48** and **49** for HOCl.

O-(*N*-butyl-1,8-naphthalimide)-4-yl-*N*,*N*-dimethylthiocarbamate (probe **48**) employing *N*,*N*-dimethylthiocarbamate (DMTC) as the recognition receptor for HOCl since HOCl can oxidize sulfide-type amino acids through the initiation of an electrophilic addition of chlorinium ion (Cl^+) from the decomposition of HOCl (Scheme 36).[56] Probe **48** displayed excellent selectivity, which may be attributed to oxidative cleavage of the DMTC moiety by electrophilic addition of Cl^+ (Fig. 70). The detection limit of **48** to HOCl was 7.6 pM, which was the first fluorescent probe that can accurately determine the picomolar level of HOCl. The lysosome-targetable fluorescent probe **49** was obtained by introducing an alkylmorpholine group into the **48** platform, and its ability to image HOCl in lysosomes was confirmed. Two-photon confocal fluorescence imaging studies suggested that **49** was capable of monitoring native and the fluctuation of endogenous HOCl levels in lysosomes of live macrophages (Fig. 71).

Lin *et al.* designed and synthesized a lysosomal-targeted ratiometric fluorescent HOCl probe **50** based on the mechanism of ESIPT and rhodol ring opening processes (Scheme 37).[57] Before reacting with HOCl, probe **50** adopted its spirocyclic form and meanwhile the ESIPT process occurred between the phenolic hydroxyl group and the N atom of the benzazole ring. The sensor only displayed the characteristic emission peak of the ESIPT process at around 450 nm and showed no emission band for the rhodol moiety. However, the spirocycle of this probe opened and the ESIPT process stopped after a reaction with HOCl since there were no free protons in close proximity to benzothiazole; meanwhile, a drastic increase in the fluorescence intensity around 586 nm along with a gradual decrease in the emission peak at 450 nm was observed. As shown in Fig. 72a, the addition of 80 mM HOCl induced a 97-fold variation in the emission ratios of the fluorescence intensities at 586 and 450 nm (I_{586}/I_{450}). More importantly, the fluorescence ratios were linear with regard to the concentration of HOCl, which revealed that the limit of detection of **50** toward HOCl could be calculated to be 0.11 μM. Probe **50** displayed high selectivity toward HOCl over other reactive oxygen species (ROSs), reactive nitrogen species (RNSs) and various biologically relevant analytes (Fig. 72b). For example, the addition of Co^{2+}, Cu^{2+}, Ni^{2+}, Br^-, I^-, NO_2^-, NO_3^-, OH^-, S^{2-}, Cys, GHS, Hcy, *t*-butylhydroperoxide, peroxide *tert*-butyl ether, H_2O_2, and NO only caused minimum perturbation in the fluorescence spectra of probe **50** while the addition of HOCl induced a large fluorescence enhancement. The determination of the intracellular location of probe **50** inside cells was conducted by the co-incubation of probe

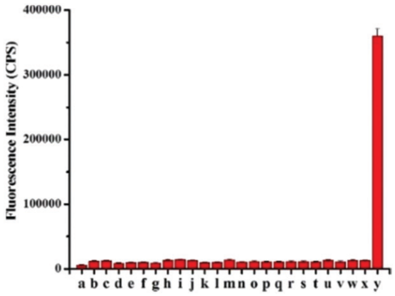

Fig. 70 Fluorescence responses of probe **48** (5.0 μM) toward HOCl (10.0 μM) and other various analytes (500.0 μM except 3000.0 μM GSH) under PBS/ethanol (1 : 1, v/v, pH 7.4) buffer solution: (a) blank, (b) H_2O_2, (c) O_2^-, (d) TBHP, (e) $^{\bullet}O^tBu$, (f) $^{\bullet}OH$, (g) $^1O_2$, (h) NO_2^-, (i) NO_3^-, (j) NO, (k) $ONOO^-$, (l) GSH, (m) K^+, (n) Ca^{2+}, (o) Na^+, (p) Mg^{2+}, (q) Zn^{2+}, (r) glutamate (Glu), (s) alanine (Ala), (t) valine (Val), (u) threonine (Thr), (v) lysine (Lys), (w) leucine (Leu), (x) ascorbic acid (AA), and (y) HOCl; λ_{ex} = 410 nm, slit widths: W_{ex} = W_{em} = 3 nm. Bars represent the fluorescence intensities at 547 nm and each datum was acquired 10 min after HOCl addition. Copyright 2016 American Chemical Society.

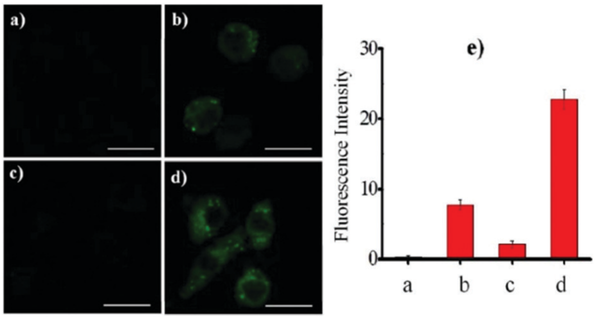

Fig. 71 Two-photon confocal fluorescence images of live macrophages: (a) control macrophages, (b) macrophages pretreated with **49** (20.0 μM) for 20 min, (c) macrophages pretreated with **49** (20.0 μM) for another 20 min after preincubation with 200.0 μM ABAH for 60 min, (d) macrophages pretreated with **49** (20.0 μM) for another 20 min after stimulation with 1.0 μg mL^{-1} PMA for 60 min, and (e) relative fluorescence intensities of macrophages in panels (a)–(d). The provided images of macrophages are representative ones (n = 10 fields of cells). Fluorescence images were obtained with an 800 nm light source. Fluorescence emission windows: 470–650 nm. Scale bar = 20 μm. Copyright 2016 American Chemical Society.

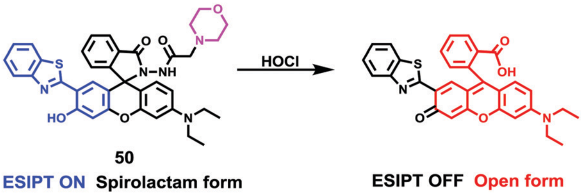

Scheme 37 Fluorescent probe **50** for HOCl.

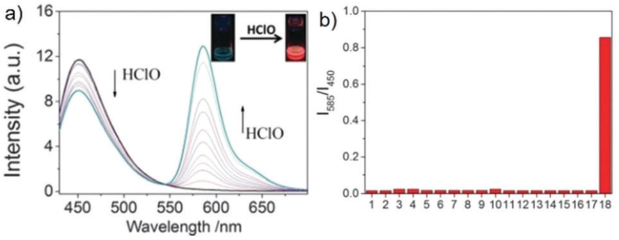

Fig. 72 (a) Emission spectra (excitation at 420 nm) of probe **50** (10 μM) in the presence of various amounts of NaOCl (0 to 80 μM) in PBS buffer (pH 5.0, containing 30% DMSO as a cosolvent). The inset shows the visual fluorescence color of the chemodosimeter **50** (20 μM) before (left) and after (right) the addition of 50 μM of HOCl upon excitation at 365 nm using a hand-held UV lamp. (b) Ratios of fluorescence intensity (I_{585}/I_{450}) of probe **50** (5.0 μM) to various relevant species (100 μM): (1) blank; (2) Co^{2+}; (3) Cu^{2+}; (4) Ni^{2+}; (5) Br^-; (6) I^-; (7) NO_2^-; (8) NO_3^{2-}; (9) OH^-; (10) S^{2-}; (11) Cys; (12) GHS; (13) Hcy; (14) *t*-butylhydroperoxide; (15) peroxide *tert*-butyl ether; (16) H_2O_2; (17) NO and (18) HOCl in pH 5.0 PBS buffer (30% DMF as a cosolvent). Copyright 2016 Royal Society of Chemistry.

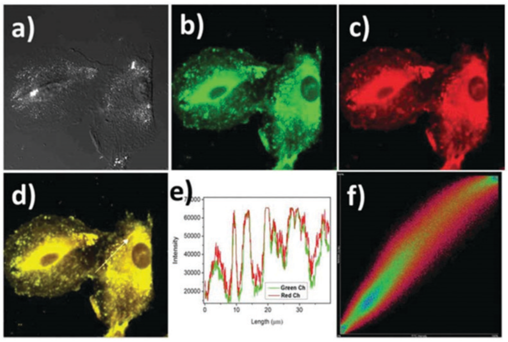

Fig. 73 Bright field and fluorescence images of A549 cells stained with probe **50** and LysoTracker Green. (a) bright-field image; (b) from the green channel (LysoTracker Green imaging of lysosomes); (c) from the red channel (**50** imaging of HOCl); (d) overlay of green and red channels; (e) intensity profile of the linear region of interest across an A549 cell costained with LysoTracker Green and the red channel of **50**; (f) intensity scatter plot of the green and red channels. Copyright 2016 Royal Society of Chemistry.

50 and the commercial lysosomal tracker LysoTracker Green in A549 cells, which suggested that probe **50** could readily permeate the cell membrane and could image HOCl in lysosomes specifically (Fig. 73).

Since some olefinic C=C double bonds are susceptible to oxidative cracking by HOCl under mild conditions, recently, Fan *et al.* developed a BODIPY-based NIR ratiometric probe **51** that could selectively detect HOCl *via* oxidative cleavage of olefins (Scheme 38).[58] Upon the addition of NaOCl into the solution of probe **51**, the absorption intensity displayed a blue-shift from 650 nm to 501 nm, accompanied by a color change from blue to hermosa pink. Meanwhile, the fluorescence intensity at 713 nm decreased while the fluorescence intensity at 511 nm gradually enhanced with increasing NaOCl concentration (Fig. 74). The detection limit of **51** to HOCl was determined to be 10.6 nM. The probe exhibited superior selectivity toward HOCl over other ROS as witnessed by the results that the probe showed more than 300-fold enhancement of the fluorescence ratio (I_{511nm}/I_{713nm}) in the presence of HOCl over other ROS including H_2O_2, $^\bullet OH$, $O_2^{\bullet -}$, TBHP, $TBO^\bullet$, $^1O_2$, $NO^\bullet$ and $ONOO^-$ (Fig. 75). The confocal fluorescence images demonstrated that the probe could penetrate through the plasma membrane and visualize exogenous and endogenous HOCl in lysosomes of living cells with low cytotoxicity (Fig. 76).

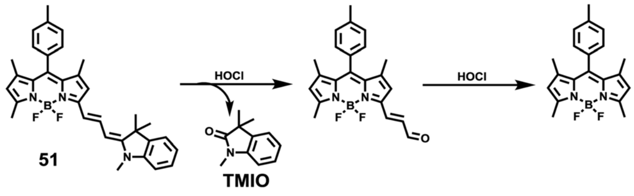

Scheme 38 Fluorescent probe **51** for HOCl.

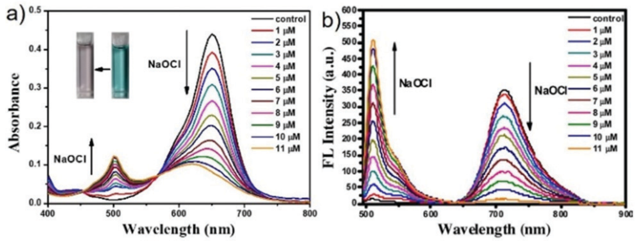

Fig. 74 (a) UV-vis spectra of probe **51** (5 μM) upon addition of NaOCl (0–10 μM) in PBS (10 mM) solution (ethanol/water = 1/1, v/v, pH 7.4). Inset: The color of probe **51** (5 μM) in the absence and presence of NaOCl (10 μM). (b) Fluorescence emission of probe **51** (5 μM) upon the addition of increasing concentrations of NaOCl in PBS (10 mM) solution (ethanol/water = 1/1, v/v, pH 7.4). Copyright 2017 Elsevier.

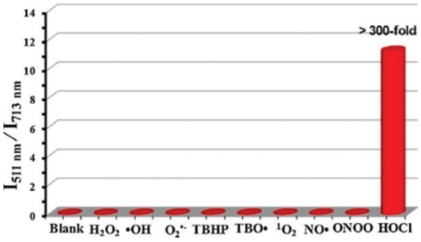

Fig. 75 Fluorescence responses (I_{511nm}/I_{713nm}) of probe **51** (5 μM) toward HOCl (10 μM) and other ROS (100 μM) in PBS (10 mM) solution (ethanol/water = 1/1, v/v, pH 7.4); λ_{ex} = 480 nm, 635 nm. Copyright 2017 Elsevier.

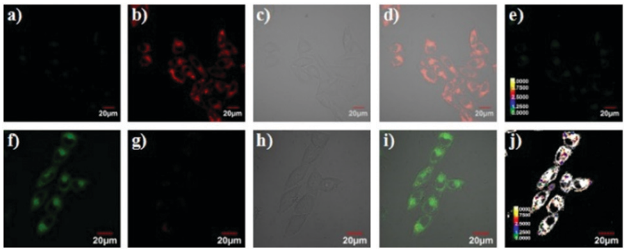

Fig. 76 Confocal fluorescence imaging without (up) and with (down) exogenous NaClO (10 μM) in MCF-7 cells using probe **51** (2 μM) for 60 min at 37 °C; (a and f) green channel (500–550 nm); (b and g) red channel (655–755 nm); (c and h) bright-field images; (d and i) overlay image of (a, b and c; f, g and h); (e and j) ratio images generated from green/red channel; λ_{ex} = 488 nm, 635 nm. Scale bar = 20 μm. Copyright 2017 Elsevier.

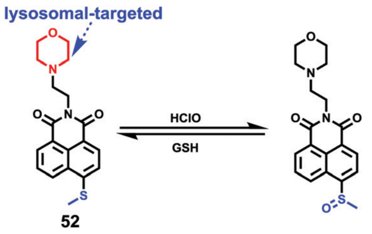

Scheme 39 Fluorescent probe **52** for HOCl.

Although a few fluorescence probes for sensing of HOCl have been reported, relatively few fluorescence probes for reversible HClO/GSH redox cycle monitoring have been established. Ye *et al.* designed and synthesized a two-photon reversible fluorescent probe **52** based on intramolecular charge transfer (ICT) for the selective detection of HOCl (Scheme 39).[59] In probe **52**, methyl thioether was chosen as an ideal receptor for HOCl since it could be easily oxidized to sulfoxide by HOCl and then the sulfoxide can be reduced to thioether by reductants. As shown in Fig. 77, upon the addition of OCl^- into the solution of probe **52**, absorption peak at 405 nm simultaneously decreased and a new absorption peak at 350 nm increased. Moreover, an intense fluorescence quenching at 505 nm was observed with the addition of OCl^-. The detection limit of probe **52** for the determination of OCl^- was estimated to be 0.674 μM based on the fluorescence titration experiments. Due to the selective oxidation of thioether, **52** exhibited higher selectivity to HOCl than other ROS, RNS and anions including H_2O_2, $HClO_4$, O^{2-}, NO, $S_2O_8^{\ 2-}$, F^-, Cl^-, Br^-, I^-, $PO_4^{\ 3-}$, $HPO_4^{\ 2-}$, $H_2PO_4^{\ -}$, $NO_3^{\ -}$, $CO_3^{\ 2-}$, $HCO_3^{\ -}$, AcO^-, and $SO_4^{\ 2-}$. Interestingly, the addition of GSH into the mixture solution of probe **52** and ClO^- induced the restoration of the fluorescence intensity to almost the original level. However, the addition of other reductants, such as Cys, Hcy, H_2S, $HSO_3^{\ -}$, Fe^{2+}, $S_2O_4^{\ 2-}$, and Vc, could not regenerate the probe's fluorescence. These results suggested that probe **52** could be used to monitor the redox cycles between OCl^- and GSH continuously. Furthermore, co-localization experiments by co-staining the 4T1 cell with Lyso Tracker Red DND-99 and probe **52** showed that probe **52** could image OCl^- in lysosomes very well (Fig. 78).

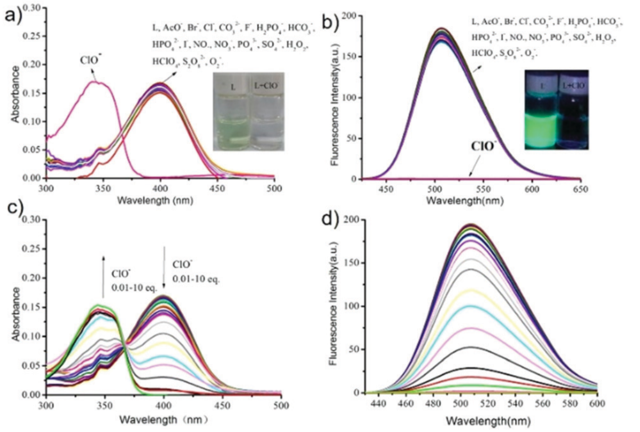

Fig. 77 (a) UV/vis spectra of **52** (10 μM) in PBS with different anions (100 μM). Inset: The photo of **52** (left) and **52** + ClO^- (10 equiv.) (right). (b) Fluorescence spectra of **52** (10 μM) in the presence of 100 μM different anions in PBS (λ_{ex} = 405 nm, slit = 5 nm). (c) UV-vis spectra of **52** (10.0 μM) in the presence of ClO^- (0.1–10 equiv.) in PBS buffer (0.1, 0.2, 0.3, 0.4, 0.5, 0.6, 0.7, 0.8, 0.9, 1.0, 1.5, 2.0, 2.5, 3.0, 3.5, 4.0, 4.5, 5.0, 5.5, 6.0, 6.5, 7.0, 7.5, 8.0, 8.5, 9.0, 9.5, and 10.0). (d) Fluorescence spectra of **52** (10 μM) with gradual addition of various amounts of ClO^- (from bottom 0 to 7 equiv.) in PBS (pH = 7.4, 10 mM). Copyright 2017 American Chemical Society.

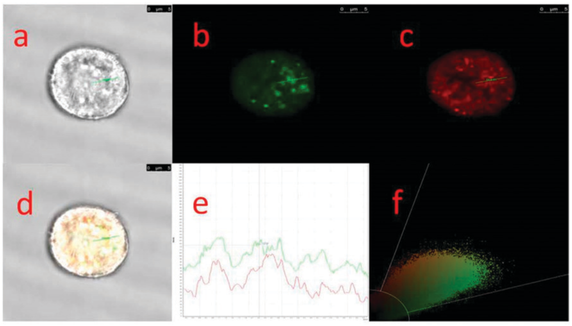

Fig. 78 Confocal fluorescence images of live 4T1 cells pretreated with **52** (10.0 μM) and Lyso-Tracker Red DND-99 (500.0 nM) for 20 min: (a) bright-field image; (b) green channel for probe fluorescence; (c) red channel for Lyso-Tracker fluorescence; (d) merged image from panels b and c; (e) intensity profile of the linear region of interest across the 4T1 cell costained with Lyso-Tracker Red and probe **52**; (f) intensity correlation plot of **52** and Lyso-Tracker Red. Pearson's correlation: 0.8789, overlap coefficient: 0.8937. Scale bar = 5 μm. Copyright 2017 American Chemical Society.

4.3 Small-molecule fluorescent probes for the detection of superoxide inside lysosomes

As the product of the one-electron reduction of dioxygen O_2, $O_2^{\bullet-}$ is associated with the pathogenesis of many diseases such as cardiovascular diseases, diabetes, cancer and immune system decline.[60] Moreover, $O_2^{\bullet-}$ is an important marker for early ROS generation and a parent species of other ROS. Thus, it is crucial to detect superoxide with high selectivity and sensitivity in biological systems.

Chen, Dong and Zhao *et al.* developed a fluorescein-based water-soluble fluorescent probe **53** for detecting superoxide (Scheme 40).[61] This probe contained a (*N*-methylpyridinium-3-yl)sulfonate moiety as a novel superoxide trapper. Probe **53** was fairly stable under neutral and acidic conditions and responded selectively to superoxide with a detection limit of 2.2 μM (Fig. 79). Cell imaging experiments suggested that the probe possessed good cell penetration and could detect $O_2^{\bullet-}$ in the lysosome of PMA-stimulated HepG2 cells (Fig. 80). Moreover, it should be noted that probe **53** could also image $O_2^{\bullet-}$ in the mitochondria of cells due to the presence of the *N*-methylpyridinium unit, which is a well-known mitochondria-targeted

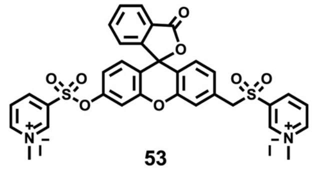

Scheme 40 Fluorescent probe **53** for $O_2^{\bullet-}$.

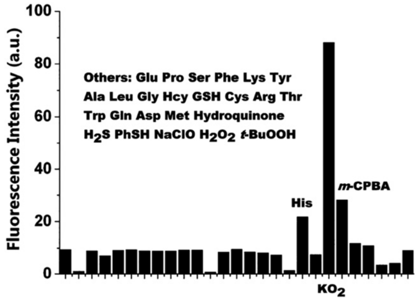

Fig. 79 Fluorescence responses of probe **53** (10 μM) to KO_2, H_2O_2, NaClO, *t*-BuOOH, *m*-CPBA, hydroquinone, H_2S, PhSH, GSH, and amino acids (100 μM each) at room temperature in PBS buffer. Data were recorded at 10 min after addition of various analytes (λ_{ex} = 492 nm, λ_{em} = 513 nm, slit: 2.5 nm/2.5 nm). Copyright 2018 American Chemical Society.

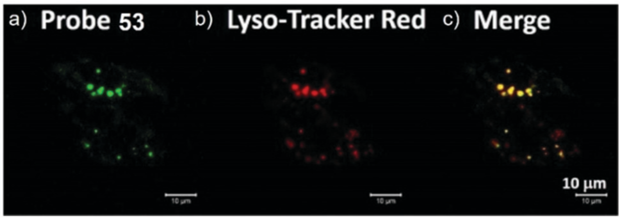

Fig. 80 Confocal fluorescence images of HepG2 cells with multiple labels. HepG2 cells were stimulated for 1 h with PMA (100 ng mL^{-1}) and incubated for 20 min with probe **53** (20 μM), organelle-tracker (5 μM) simultaneously. Images shown above are signals from (a) probe **53**, green channel; (b) Lyso-Tracker Red DND-99, red channel; (c) merged image of (a) and (b). Scale bar = 10 μm. Copyright 2018 American Chemical Society.

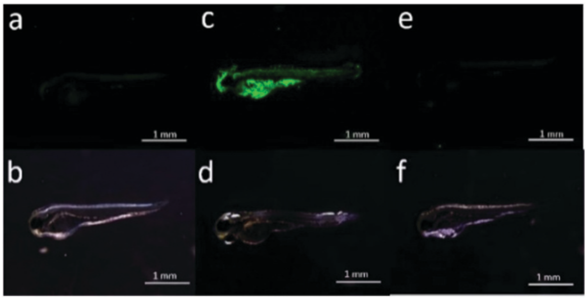

Fig. 81 Confocal imaging of endogenous $O_2^{\bullet -}$ in 72 h post-fertilization zebrafish embryos. (a and b) Zebrafish embryos preloaded with probe **53** (10 μM) for 20 min; (c and d) zebrafish embryos briefly challenged with PMA (200 ng mL^{-1}) for 20 min after preloaded with probe **53** (10 μM) for 20 min; (e and f) zebrafish initially stimulated with PMA (100 ng mL^{-1}) for 20 min, treated with Tiron (100 μM) for 20 min and loaded with probe **53** (10 μM) for 20 min. (a, c and e): green channel, (b, d and f): bright channel. Scale bar = 1 mm. Copyright 2018 American Chemical Society.

functional group. In addition, this probe was successfully applied to detect $O_2^{\bullet -}$ in living zebrafish embryos under PMA-stimulated conditions (Fig. 81). This study presented the first successful example on the detection of $O_2^{\bullet -}$ both in lysosome and mitochondria in living cells.

4.4 Small-molecule fluorescent probes for the detection of lipid peroxynitrite inside lysosomes

Lipid peroxidation (LPO) in lysosomes is closely related to the pathogenesis of many diseases.[62] For example, in the initial stage of atherosclerosis, lysosomes swell by accumulating a lot of lipoproteins, which promotes the free-radical chain propagation of LPO. Although several fluorescent LPO probes have been previously reported,[63] they were unable to detect LPO in lysosomes owing to their unspecific intracellular localizations. Therefore, precise and quantitative assessment of dynamic LPO levels in lysosomes is of great interest for the early diagnosis of atherosclerosis and related pathological or pharmacological studies.

Xiao *et al.* developed a lysosome targetable fluorescent probe **54** for LPO (Scheme 41).[64] This probe had a basic tertiary amino unit to target acidic lysosomes and a diene group to respond to LPO. Because of the extended conjugation with the diene and phenyl moieties, this BODIPY probe displayed bright red fluorescence with an emission maximum at 586 nm. As expected, probe **54** demonstrated a sensitive and selective response to the LPO (Fig. 82). In the presence of hemin and cumene hydroperoxide (CumOOH), which is a similar situation as lipid peroxidation in living cells, a continuous increase in fluorescence intensity at 512 nm and a decrease at 586 nm was observed until equilibrium was reached as time went on. The hypsochromic shift of the emission of the probe was attributed to the cleavage of the π-structure. Cell imaging experiments showed that **54** was able to dynamically visualize morphological changes of lysosomes during the evolution of foam cells as well as to relatively quantify local LPO in a single lysosome through ratiometric imaging (Fig. 83). More importantly, **54** provided a

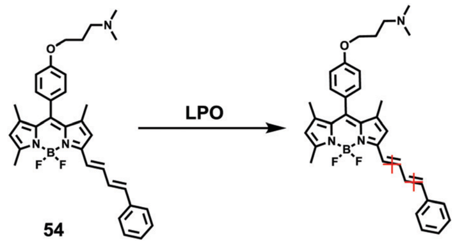

Scheme 41 Fluorescent probe **54** for LPO.

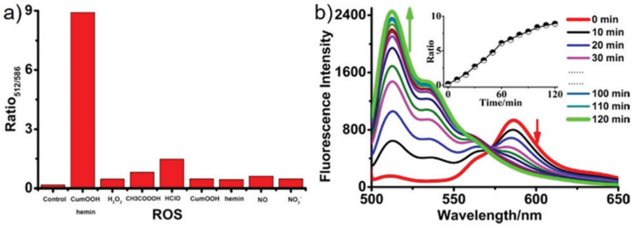

Fig. 82 (a) Fluorescence ratio (512/586) change of probe **54** towards different ROS. (b) Changes of fluorescence wavelength of probe **54** in pH ~5 PBS (containing 30% methanol) in the presence of 1 μM hemin and 1 mM CumOOH, excited at 488 nm. Copyright 2015 American Chemical Society.

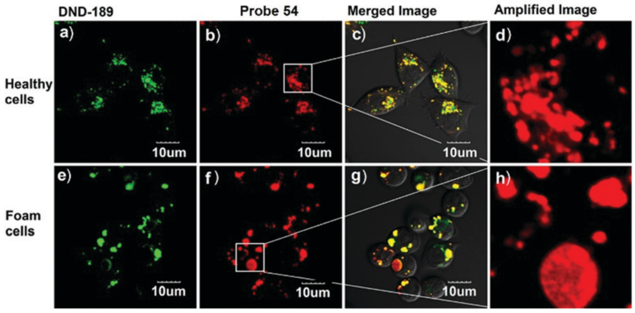

Fig. 83 Fluorescence images of healthy macrophage cells (a, b, and c) and foam cells (e, f, and g) co-stained by DND-189 (a and e, green channel, λ_{ex} = 405 nm, λ_{em} = 500–560 nm) and probe **54** (b and f, red channel, λ_{ex} = 488 nm, λ_{em} = 570–630 nm). (c) Merged image of panels a and b and bright field. (g) Merged image of panels e and f and bright field. Panels d and h are amplified images of regions in panels b and f. Copyright 2015 American Chemical Society.

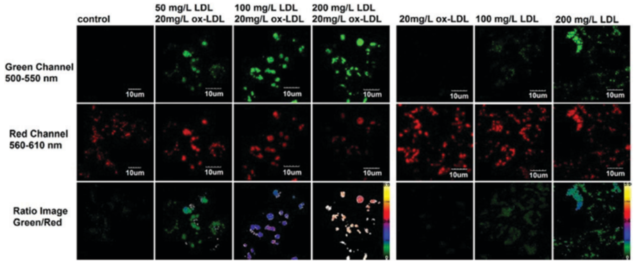

Fig. 84 Fluorescence images of stained (probe **54**, 1 μM for 5 min) macrophage cells being incubated with ox-LDL (20 mg L^{-1}) and different amount of LDL (50–200 mg L^{-1}) for 24 h, cells are stained with probe **54** at the 12th hour. Copyright 2015 American Chemical Society.

new opportunity to distinguish and clarify the different roles played by low-density lipoprotein (LDL) and its oxidized form (ox-LDL) for the LPO processes of foam cells, which was beneficial for understanding the initiation and control factors of atherosclerosis (Fig. 84).

5. Small-molecule fluorescent probes for the detection of reactive sulfur species (RSS) inside lysosomes

Active sulfur species (RSS) include H_2S, SO_2, cysteine (Cys), homocysteine (Hcy), glutathione (GSH) and so on. RSS play important roles in physiological and pathological processes, such as regulating oxidative stress and controlling signal transduction.[65] Therefore, the establishment of convenient detection methods for RSS is on demand.

5.1 Small-molecule fluorescent probes for the detection of hydrogen sulfide inside lysosomes

Hydrogen sulfide (H_2S), which is produced endogenously in mammalian systems from L-cysteine in reactions catalysed mainly by two pyridoxal-50-phosphate-dependent enzymes, cystathionine β-synthase (CBS) and cystathionine γ-lyase (CSE), has been considered the third most important gasotransmitter for regulating cardiovascular, neuronal, immune, endocrine, and gastrointestinal systems. The endogenous level of H_2S has been found to be related to some diseases such as Alzheimer's disease, Down's syndrome, diabetes, and liver cirrhosis.[66] Recently, research revealed that H_2S also functioned in lysosome organelles, and it could induce cell death in association with the activation of calpain proteases and lysosomal destabilization along with the release of lysosomal proteases.[67] For example, H_2S induced lysosomal membrane destabilization leads to an autophagic event of precipitation apoptosis coupled with calpain activation, thus ensuring cellular demise. Therefore, detecting and imaging lysosomal H_2S is meaningful and provides a potential powerful tool for probing the relationship between H_2S and disease states.

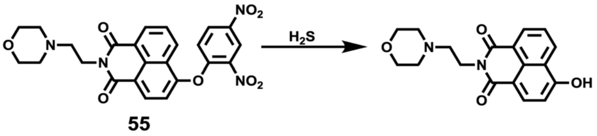

Scheme 42 Fluorescent probe **55** for H_2S.

Xu, Spring and Cui *et al.* developed a lysosome-targetable fluorescent probe **55** based on naphthalimide for imaging H_2S in living cells (Scheme 42).[68] In probe **55**, the dinitrophenyl ether group was introduced into the 4-position of 1,8-naphthalimide acting as the H_2S reactive site, and 4-(2-aminoethyl)morpholine was introduced as the lysosome-targetable group. The fluorescence at 555 nm of **55** remained unaffected at pH 8.2–4.2 and then gradually increased from pH 4.2 to 2.03 which indicated that probe **55** could be used in lysosomes. Probe **55** displayed high sensitivity and selectivity to H_2S in aqueous solution (Fig. 85). The addition of H_2S into the solution of **55** induced a 42-fold enhancement of the emission band centered at 555 nm due to the thiolysis of the dinitrophenyl ether by H_2S. However, the addition of 100 equiv. of Na^+, Ca^{2+}, K^+, Mg^{2+}, HCO_3^-, F^-, Cl^-, Br^-, I^-, NO_3^-, $S_2O_3^{2-}$, $S_2O_4^{2-}$, $S_2O_5^{2-}$, SO_3^-, N_3^-, CO_3^{2-}, CH_3COO^-, OH^-, SO_4^{2-}, H_2O_2, HSO_4^-, homocysteine,

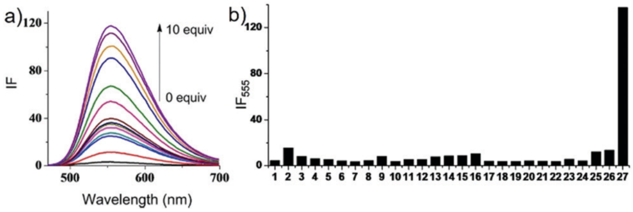

Fig. 85 (a) Fluorescent emission spectra of 10 μM probe **55** in the presence of 0–10 equiv. of H_2S in aqueous solution (CH_3CN/PBS = 1 : 9, pH = 7.4, 37 °C) (NaHS was dissolved in water at a concentration of 10 mM). Excitation at 450 nm. (b) Fluorescence responses of 10 μM **55** to various analytes in aqueous solution (CH_3CN/PBS = 1 : 9, pH = 7.4, 37 °C). Excitation at 450 nm. Bars represent the final fluorescence intensity of **55** with 1 mM analytes over the original emission of free **55**. (1) Free **55**; (2) Zn^{2+}; (3) Na^+; (4) Ca^{2+}; (5) K^+; (6) Mg^{2+}; (7) HCO_3^-; (8) F^-; (9) Cl^-; (10) Br^-; (11) I^-; (12) NO_3^-; (13) $S_2O_3^{2-}$; (14) $S_2O_4^{2-}$; (15) $S_2O_5^{2-}$; (16) SO_3^-; (17) N_3^-; (18) CO_3^{2-}; (19) CH_3COO^-; (20) SO_4^{2-}; (21) H_2O_2; (22) HSO_4^-; (23) homocysteine; (24) ascorbic acid; (25) cysteine; (26) glutathione; and (27) NaHS. Copyright 2013 American Chemical Society.

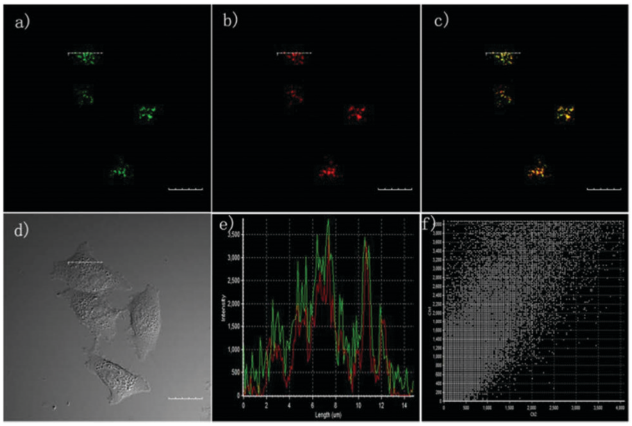

Fig. 86 Probe **55** colocalizes to lysosomes in MCF-7 cells. (a) 5.0 μM probe **55** with 20 μM of H_2S incubated for 10 min at 37 °C (channel 1: λ_{ex} = 450 nm, λ_{em}= 520–560 nm). (b) 5.0 μM NR (channel 2: λ_{ex} = 559 nm, λ_{em} = 565–610 nm). (c) Merged images of (a) and (b). (d) Bright field image. (e) Intensity profile of regions of interest (ROI) across MCF-7 cells. (f) Intensity correlation plot of dyes **55** and NR. Scale bars = 20 μm. Copyright 2013 American Chemical Society.

and ascorbic acid produced a nominal change in the fluorescence spectra of **55**. The detection limit of H_2S with probe **55** was calculated to be 0.48 μM. The fluorescence localization experiments indicated that the probe was applicable to H_2S detection in live cell imaging and had the ability to detect intracellular H_2S in lysosomes. As shown in Fig. 86, the fluorescence patterns of **55** and the commercially available lysosome-specific dye Neutral Red (NR) signals overlapped perfectly, indicating that the fluorescence response of **55** to H_2S was localized at the lysosome.

Yang *et al.* developed a simultaneous H_2S and proton-activatable probe **56** for selective recognition of H_2S in a lysosomal pH environment by utilizing the spironolactam moiety of **56** to bind hydrogen protons and an azide group to react with H_2S (Scheme 43).[69] Probe **56** displayed highly sensitive and selective fluorescence response to H_2S in a lysosomal pH environment. As shown in Fig. 87, the addition of NaHS to the aqueous solution of **56** at pH 4.5 elicited a dramatic enhancement of the emission spectra and the detection limit was calculated to be 0.5 μM. However, the addition of other potentially competing species did not induce observable fluorescence enhancement. Cell imaging experiments showed that **56** was membrane permeable and enabled visualization of exogenous and endogenous H_2S in lysosomes of living cells (Fig. 88 and 89). It should be noted that this simultaneous target and location-activatable approach showed in this study would ensure that fluorescence can only be lighted up by the analyte present in a specific location, which provides advantages of elimination of false signals and improvement of spatial resolution and sensitivity.

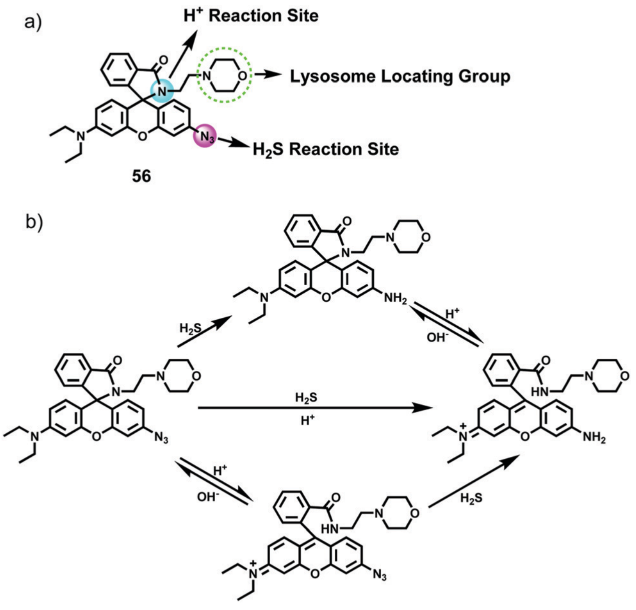

Scheme 43 Fluorescent probe **56** for H_2S.

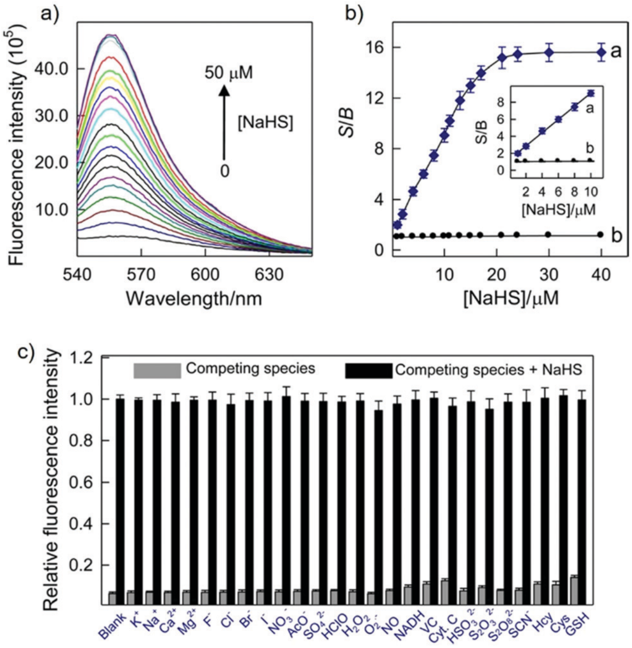

Fig. 87 (a) Fluorescence emission changes of 5.0 μM probe **56** in the presence of different concentrations of NaHS (0–50 μM) in buffer solution (10% DMF, pH 4.5). (b) Signal-to-background ratios (S/B) of probe **56** as a function of NaHS concentrations (0–50 μM) at pH 4.5 (a) and pH 7.4 (b), respectively. Inset: Linear responses of S/B of 5 μM probe **56** to changing NaHS concentrations (0–10 μM) at pH 4.5 (a) and pH 7.4 (b), respectively. The magnitudes of the error bars were calculated from the uncertainty given by three independent measurements. (c) Fluorescence enhancements of probe **56** with selected species (100 μM for ROS and RNS, 5.0 mM for GSH, 1.0 mM for other) in the absence (gray bar) or the presence (black bar) of 50 μM NaHS in buffer solution (pH 4.5). The magnitudes of the error bars were calculated from the uncertainty given by three independent measurements; $\lambda_{ex}/\lambda_{em}$ = 530 nm/555 nm. Copyright 2014 American Chemical Society.

Zhou and Zhang *et al.* synthesized a H_2S fluorescent probe **57** based on a coumarin derivative containing disulfide bonds (Scheme 44).[70] The probe chose a special selective reaction instead of a lysosomal targeting group as a lysosomal-targeted tool to track lysosomal location and disruption in cells. Probe **57** exhibited excellent selectivity towards H_2S with a detection limit of 7.9×10^{-7} M. Colocalization imaging experiments indicated that probe **57** could be applied to monitor endogenous

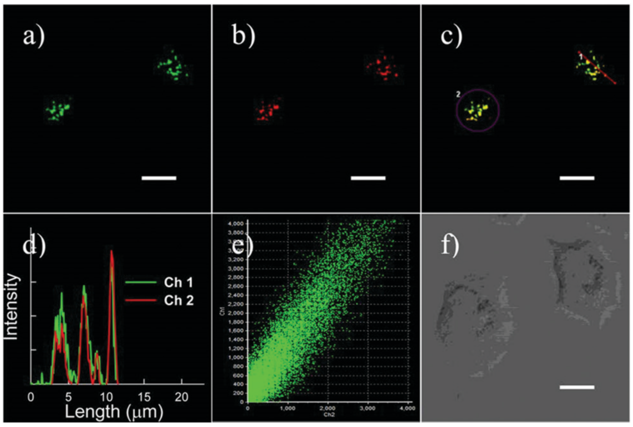

Fig. 88 Probe **56** colocalizes to the lysosome in HeLa cells. Cells were stained with (a) LysoTracker Green (1.0 μM, channel 1 (Ch1, green), λ_{ex} = 488 nm; λ_{em} = 505–530 nm) and (b) probe **56** (5.0 μM, channel 2 (Ch2, red), λ_{ex} = 515 nm; λ_{em} = 540–580 nm) with NaHS solution (50.0 μM) for 60 min at 37 °C. (c) Overlay of parts (a) and (b). (d) Intensity profile of the linear region of interest (ROI 1) across the HeLa cell costained with LysoTracker Green and **56**. (e) Intensity scatter plot of Ch1 and Ch2 in ROI 2. (f) Bright-field images. Scale bar: 10 μm. Copyright 2014 American Chemical Society.

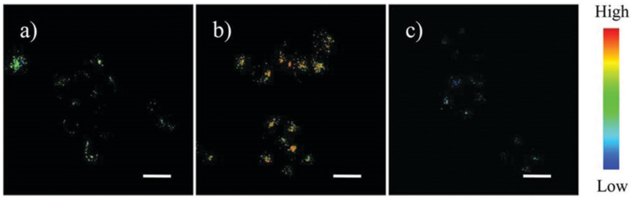

Fig. 89 Relative fluorescence images of endogenous H_2S in lysosomes of HeLa cells using **56** in the absence or presence of H_2S stimulants and inhibitors (images displayed in pseudocolor): (a) incubated with 5.0 μM **56** only; (b) incubated with 5.0 μM **56** in the presence of 200 μM Cys for 60 min; (c) incubated with 5.0 μM **56** in the presence of 2.0 μL (1 μg mL^{-1}) PMA for 60 min. λ_{ex} = 515 nm; λ_{em} = 540–580 nm. Scale bar: 30 μm. Copyright 2014 American Chemical Society.

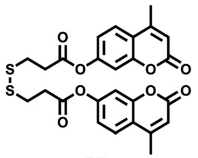

57

Scheme 44 Fluorescent probe **57** for H_2S.

and exogenous H_2S in HeLa cells (Fig. 90), *C. elegans* (Fig. 91), and *D. melanogaster* (Fig. 92). This work provided the first example on the disulfide bond-containing coumarin derivative to trace the accumulation of lysosomes in *D. melanogaster* and endogenous lysosomal injury in mutated *C. elegans* (SRP-6nulls) with a high resolution.

Hua *et al.* designed and synthesized a series of *N*-annulated perylene-based colorimetric and ratiometric NIR fluorescent probes **58** and **59** for the sensitive and selective detection of H_2S (Scheme 45).[71] In the absence of H_2S, probe **58** and its lysosomal targetable derivative **59** showed near-infrared fluorescence at 681 nm due to the strong electron-withdrawing ability of the nitro group. With the addition of only a small amount of H_2S in a few minutes, the dramatic decrease of the NIR fluorescence accompanied by the sharp increase of a new fluorescence peak at 481 nm was observed (Fig. 93). The probe possessed high selectivity to H_2S and the detection limit was determined to be 139 nM. Probe **59** was successfully employed to quantify endogenous H_2S in lysosomes of live cells (Fig. 94) and in fetal bovine serum.

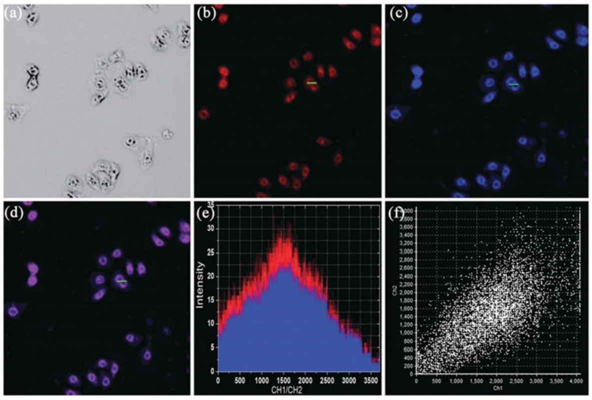

Fig. 90 Colocalization imaging of HeLa cells stained with 10.0 μM **57** and 300 μM of H_2S for 30 min at 37 °C. (a) Bright-field image. (b) The confocal image of 5.0 μM NR on channel 1 (λ_{ex} = 559 nm, λ_{em} = 585–610 nm). (c) The confocal image of **57** on channel 2 (λ_{ex} = 385 nm, λ_{em} = 405–440 nm). (d) The merged image of (b) and (c). (e) The intensity profile of the regions of interest (ROI) across the HeLa cells. (f) The intensity correlation plot of **57** and NR. Copyright 2014 Royal Society of Chemistry.

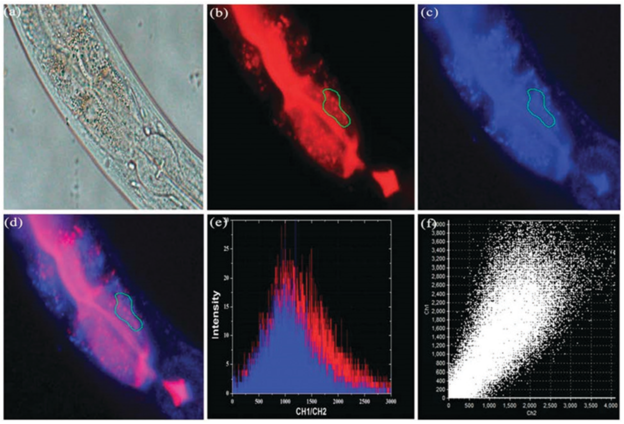

Fig. 91 Colocalization imaging of lysosomes in *C. elegans*. (a) Bright field image. (b) 500 μM AO incubated for 4 h at 20 °C (channel 2: λ_{ex} = 485 nm, λ_{em} = 510–550 nm). (c) 10.0 μM **57** with 300 μM of H_2S incubated for 30 min at 20 °C (channel 1: λ_{ex} = 385 nm, λ_{em} = 405–440 nm). (d) The merged image of channels 1 and 2. (e) The intensity profile of the regions of interest (ROI) across *C. elegans*. (f) The intensity correlation plot of **57** and AO. Copyright 2014 Royal Society of Chemistry.

5.2 Small-molecule fluorescent probes for the detection of sulfur dioxide inside lysosomes

Sulfur dioxide (SO_2) is one of the harmful atmospheric pollutants and exists in the forms of sulfite (SO_3^{2-}) and bisulfite

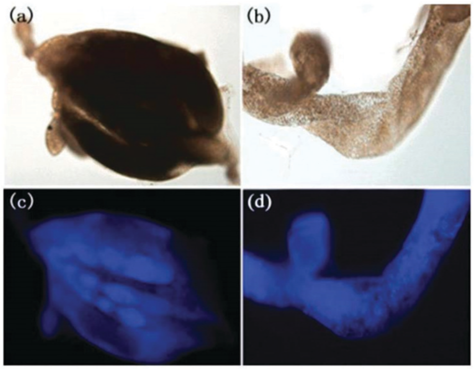

Fig. 92 Detection of H_2S accumulation in the ovary and midgut of *D. melanogaster*. (a) and (b): bright-field images. (c) The fluorescence image of ovary. (d) The fluorescence image of mid gut. Copyright 2014 Royal Society of Chemistry.

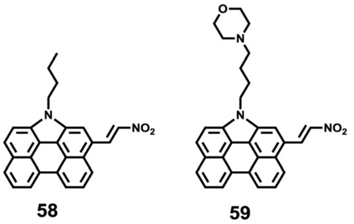

58 **59**

Scheme 45 Fluorescent probes **58** and **59** for H_2S.

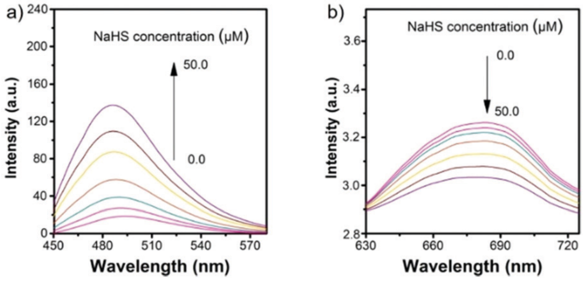

Fig. 93 The changes of fluorescence spectra of **58** in the presence of different concentrations (0.0, 5.0, 10.0, 17.0, 20.0, 40.0, and 50.0 μM) of NaHS in FBS. (a) λ_{ex} = 435 nm; (b) λ_{ex} = 510 nm. Copyright 2017 Royal Society of Chemistry.

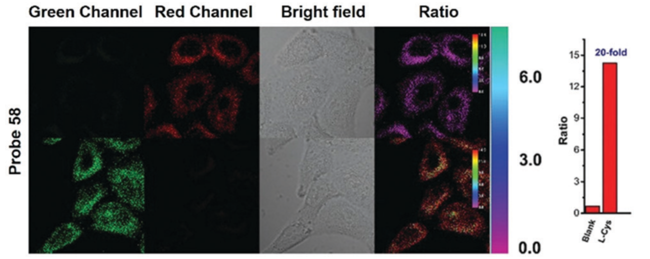

Fig. 94 Confocal fluorescence imaging of the detection of endogenous H_2S using **59** in living HeLa cells. (the first line) Images of HeLa cells strained with probe **59** (10 μM) for 20 min. (the second line) Images of HeLa cells firstly pretreated with L-cysteine (100 μM) for 30 min and then incubated with **59** (10 μM) for 20 min. The green channels represent the fluorescence emission at 480–530 nm (λ_{ex} = 458 nm), while the red channel represents the fluorescence at 630–700 nm (λ_{ex} = 510 nm). The pseudocolored ratiometric images generated from green/red channels using the image analysis software, Image J. (right) Average intensity ratios of images. Copyright 2017 Royal Society of Chemistry.

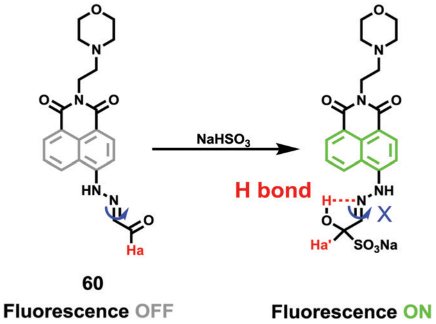

Scheme 46 Fluorescent probe **60** for SO_2.

(HSO_3^-) in organisms. As a gaseous signalling molecule, SO_2 can modulate a wide range of physiological processes, such as anti-atherosclerosis, regulating cardiovascular structure and function, and increasing antioxidant capacity.[72] Excessive intake of sulfur dioxide or its derivatives may bring about respiratory diseases, neurological diseases, vascular diseases and even lung cancer. However, the lack of methods for detecting SO_2 in lysosomes has brought obstacles to the research of related physiological processes and pathological mechanisms. Therefore, the development of methods for detecting SO_2 and its derivatives in lysosomes is of great significance.

Lin *et al.* developed a lysosomal-targeted two-photon fluorescent probe **60** for the detection of SO_2 derivatives (Scheme 46).[73] Probe **60** was designed based on a unique C=N isomerization mechanism, in which bisulfite reacted with aldehydes and formed intramolecular hydrogen bonds to inhibit C=N isomerization. Probe **60** possessed remarkable selectivity and sensitivity since it was only responsive to HSO_3^-. As shown in Fig. 95, the addition of $NaHSO_3$ into the solution of probe **60** triggered a dramatic increase in the fluorescence intensity. However, almost no marked fluorescence enhancement was observed by treating probe **60** with Ca^{2+},Co^{2+}, Cu^{2+}, Fe^{3+}, Fe^{2+}, I^-, Mg^{2+}, Cl^-, SO_3^{2-}, NO_3^-, F^-, NO^{2-}, Sn^{2+}, Zn^{2+}, TBHP, DTBP, H_2O_2, ClO^-, Hcy, GSH, Cys,

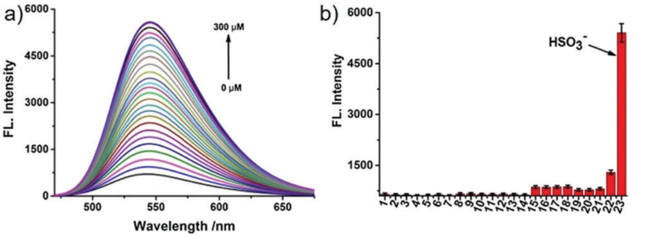

Fig. 95 (a) Fluorescence spectra of probe **60** (10 μM) upon addition of various concentrations of $NaHSO_3$ (0–300 μM). (b) Fluorescence responses of probe **60** (10 μM) in the presence of various relevant species in PBS buffer (10 mM, pH 5.5, 5% CH_3CN). Legend: 1. only **60**; 2. $CaCl_2$; 3. $CoCl_2$; 4. $CuSO_4$; 5. $Fe_2(SO_4)_3$; 6. $FeSO_4$; 7. KI; 8. $MgCl_2$; 9. Na_2SO_3; 10. KNO_3; 11. NaF; 12. $NaNO_2$; 13. $SnCl_2$; 14. $ZnSO_4$; 15. TBHP; 16. DTBP; 17. H_2O_2; 18. NaClO; 19. Hcy; 20. GSH; 21. Cys; 22. NaHS; 23.$NaHSO_3$; λ_{ex} = 440 nm. Copyright 2018 Elsevier.

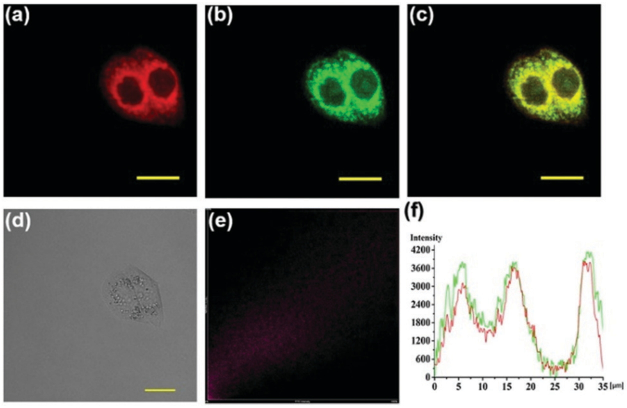

Fig. 96 Confocal images of HeLa cells treated with probe **60** (10 μM), $NaHSO_3$ (500 μM) and Lyso Tracker Red (75 nM). (a) Red channel (570–620 nm) for Lyso-Tracker Red under 561 nm excitation. (b) Green channel (500–550 nm) for probe **60** under 488 nm excitation. (c) The overlay image of red and green channels. (d) Bright-field of HeLa cells. (e) The intensity scatter plot of two channels. (f) Intensity profile of ROI across the cells in the red and green channels. Scale bar = 20 μm. Copyright 2018 Elsevier.

and NaHS. Importantly, fluorescence co-localization studies showed that **60** could be effectively used to image of SO_2 in lysosomes of living cells (Fig. 96) for the first time and to detect SO_2 derivatives in living zebrafish (Fig. 97).

5.3 Small-molecule fluorescent probes for the detection of thiols inside lysosomes

Low molecular weight biothiols, such as cysteine (Cys), homocysteine (Hcy) and glutathione (GSH), are important components of many peptides that play key roles in many physiological processes, including cellular growth, redox hemeostasis, and signal transduction.[74] Once the levels of biothiols are abnormal, they will lead to many serious diseases. For example, low level of Cys can cause symptoms such as liver damage, edema, skin lesions, slow growth in children, and discoloration of hair.[75] More importantly, many reports have been indicated that cystine-containing proteins have their disulphide bonds reduced during proteolysis in lysosomes.[75b] High level of Hcy is closely related to neural tube defects, cardiovascular diseases, and Alzheimer's disease.[76] Abnormal level of GSH, the most abundant intracellular non-protein thiol, is directly related to aging, heart disease, and cancer.[77] Furthermore, thiols were closely associated with proteolysis in the lysosome which reduced disulphide bonds.[77b] Therefore, the development of methods for detecting levels of thiols in living cells and tissues is of great significance, providing more basic information for further exploration of the pathogenesis of related diseases.

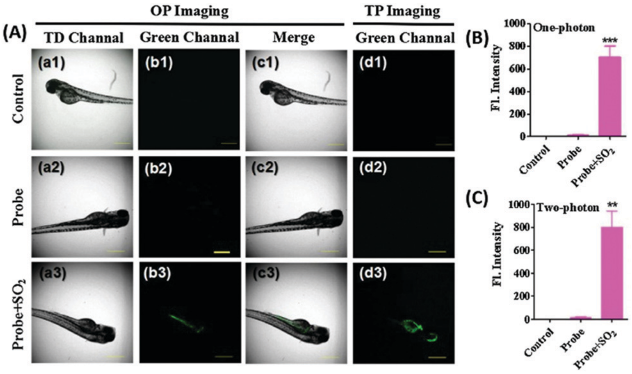

Fig. 97 (A) Fluorescence images of zebrafish treated with probe **60**. (a1–d1) are the fluorescence images of only zebrafish. (a2–d2) are the fluorescence images of zebrafish treated with 10 μM **60**. (a3–d3) are the fluorescence images of zebrafish treated with 500 μM $NaHSO_3$ and then treated with 10 μM **60**. OP green channel: λ_{ex} = 488 nm, λ_{em} = 500–550 nm; TP green channel: λ_{ex} = 760 nm, λ_{em} = 500–550 nm. Scale bar = 500 μm. (B) Quantification of fluorescence intensities for (A) in OP mode. (C) Quantification of fluorescence intensities for (A) in TP mode. The results were presented as means ± SE with replicates n = 3. $^{**}p < 0.01$, $^{***}p < 0.001$. Copyright 2018 Elsevier.

Fan *et al.* developed a two-photon fluorescent probe **61** based on 1,8-naphthalimide, in which morpholine acted as a lysosomal directing group and piperazine acted as a linker to introduce 2,4-dinitrobenzenesulfonyl (DNBS) into the 4-position of naphthalimide (Scheme 47).[78] The fluorescence was essentially quenched due to the photo-induced electron transfer (PET) between DNBS and naphthalimide. Once the thiol reacted with DNBS, the PET process was inhibited bringing about a dramatic increase in fluorescence emission at 540 nm. This probe possessed superior selectivity to Cys, GSH and Hcy compared to other amino acids (Fig. 98). More importantly, the probe was successfully applied to imaging of thiols in lysosomes of living cells and tissues (Fig. 99).

Liu *et al.* designed and synthesized a coumarin-based fluorescent probe **62** for the detection of cysteine (Cys) in lysosomes (Scheme 48).[79] A fast conjugate addition–cyclization reaction

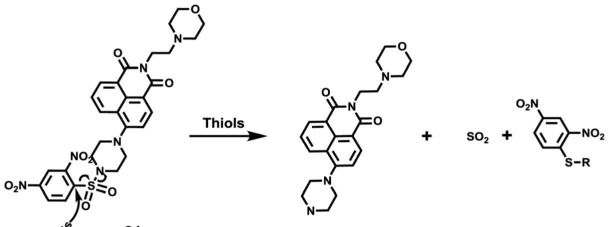

61

Scheme 47 Fluorescent probe **61** for thiols.

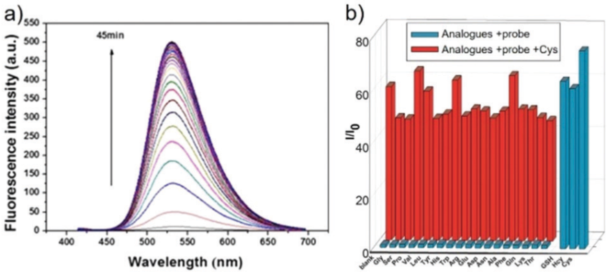

Fig. 98 (a) Time-dependent emission spectra (λ_{ex} = 400 nm) of probe **61** (10 μM) upon treatment with Cys (100 equiv.) in DMSO–HEPES (10 mM, pH 7.4, 3 : 7, v/v) at 37 °C. Spectra were recorded every min (0–45 min). (b) Blue bars represent probe **61** + analogues; red bars represent probe **61** + Cys in the presence of other analogues (100 μM). Data were collected at 45 min after addition of each analogue in DMSO–HEPES (10 mM, pH 7.4, 3 : 7, v/v) at 37 °C. Copyright 2016 Nature.

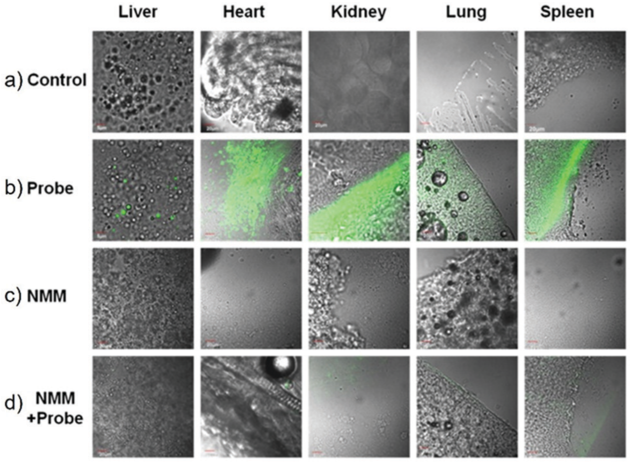

Fig. 99 Fluorescence images of the liver, heart, kidney, lung and spleen. (a) Dissected from mouse not injected with **61**, (b) mouse injected with **61**, (c) mouse injected with NMM, and (d) mouse injected with **61** after pre-injection with NMM. The TPM images were collected at 520–560 nm upon excitation at 805 nm with fs pulse. Copyright 2016 Nature.

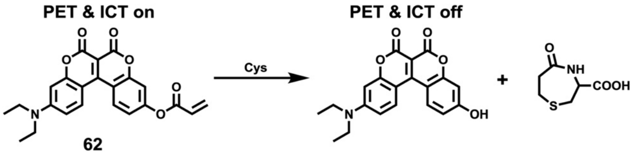

Scheme 48 Fluorescent probe **62** for Cys.

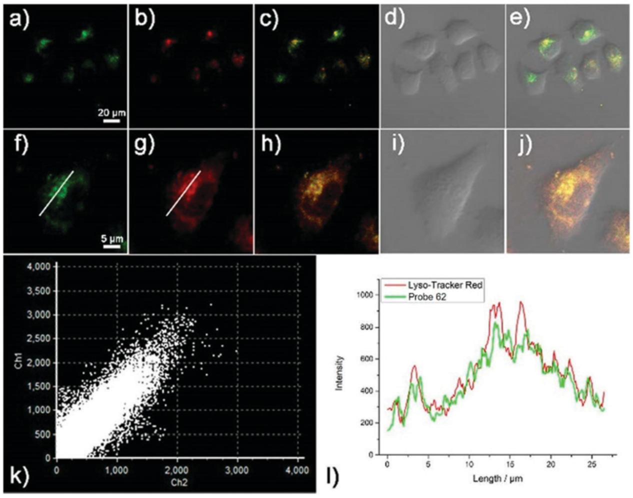

Fig. 101 Fluorescence image of colocalization experiment in (a and f) green channel, (b and g) red channel, and (c and h) overlap; (d and i) bright-field image, (e and j) overlap. (k) Fluorescence intensity correlation plot. (l) Intensity profile of regions of interest (ROI) across HeLa cells. Copyright 2018 American Chemical Society.

between **62** and Cys was achieved for detection of Cys in the micromolar range in aqueous buffer. Probe **62** possessed remarkably higher selectivity for Cys over cysteine (Hcy), glutathione (GSH) and various other natural amino acids under physiological conditions (Fig. 100). The probe was nearly non-fluorescent under excitation at 445 nm due to the influence of the PET effect resulting from the acryloyl group. After the addition of Cys, a significant increase in fluorescence emission at 520 nm was observed. The detection limit of **62** for Cys was calculated to be 0.411 μM. Two-photon fluorescence experiments and co-localization experiments demonstrated the good biocompatibility and the ability to target lysosomes of **62** (Fig. 101). In addition, this probe was then successfully applied to fluorescence imaging of Cys in HeLa cells and mice tissues, indicating that **62** has the potential to detect Cys in living cells and tissues.

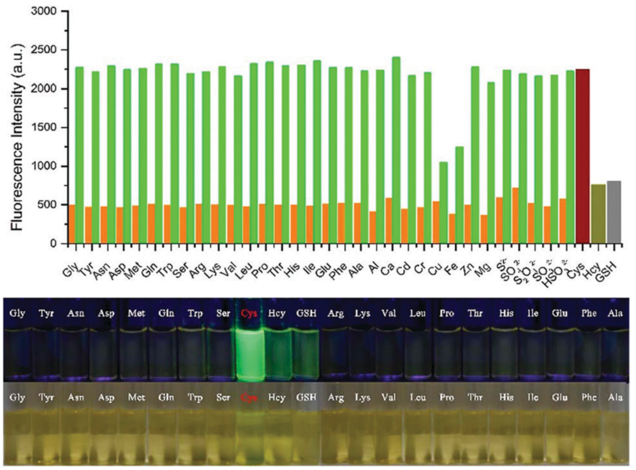

Fig. 100 Top: Selectivity and competitiveness of **62** (2 μM) to various analytes (40 μM) in PBS buffer. (The orange bars represent the fluorescence intensity of **62** after being treated with analytes. Then the solution was treated with Cys, and the green bars show the fluorescence intensity of orange bars treated with Cys.) Bottom: Color changes and fluorescence changes when excited using a UV lamp (365 nm) of **62** upon addition of Cys, Hcy, GSH, and various amino acids. Copyright 2018 American Chemical Society.

6. Small-molecule fluorescent probes for the detection of reactive nitrogen species (RNS) inside lysosomes

Reactive nitrogen species (RNS), including nitric oxide (NO), peroxynitrite ($ONOO^-$), and nitric acid (HNO), play important roles in physiological and pathological processes.[80] Abnormal level of RNS may lead to severe diseases such as inflammation, neurodegenerative diseases, cardiovascular diseases and cancer. Therefore, there is an urgent demand to develop a suitable method for *in vivo* detection of RNS to elucidate their roles in physiological and pathological processes further.

6.1 Small-molecule fluorescent probes for the detection of nitric oxide inside lysosomes

Nitric oxide (NO), a cellular messenger molecule prevalent in the cardiovascular, nervous, and immune systems, is involved in a variety of physiological processes, including inflammation, blood pressure regulation, neurotransmission, and immune regulation.[81] Abnormal levels of intracellular NO may result in a variety of diseases such as Gaucher's disease, Danon and lysosomal storage disorders. It has been reported that NO could react with several related

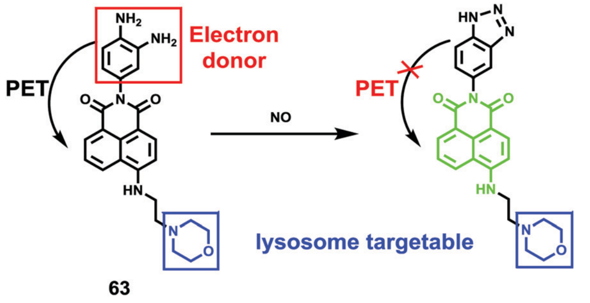

Scheme 49 Fluorescent probe **63** for NO.

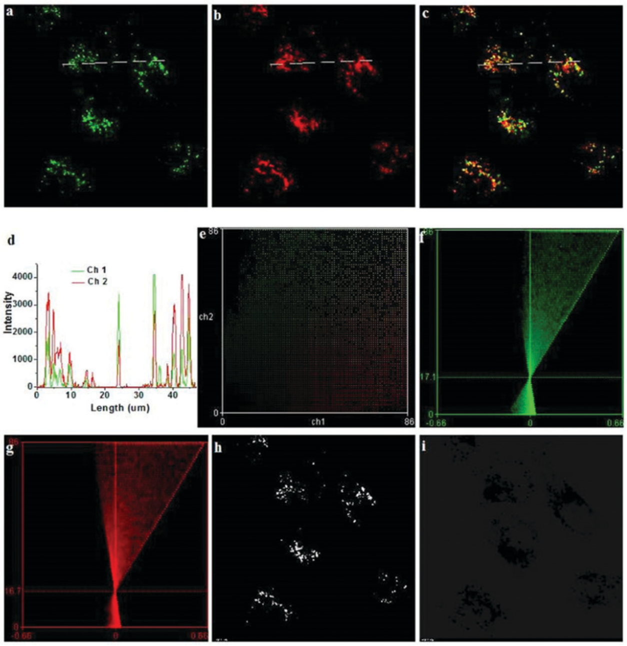

Fig. 103 **63** co-localizes to lysosomes in MCF-7 cells. MCF-7 was stained with (a) 5.0 μM **63** with NO solution (20 μM) for 5 min at 37 °C (Channel 1: λ_{ex} = 840 nm, λ_{em} = 520–560 nm) and (b) 5.0 μM NR (Channel 2: λ_{ex} = 559 nm, λ_{em} = 565–610 nm). (c) Overlay of (a) and (b). (d) Intensity profile of regions of interest (ROI) across MCF-7 cells. (e) Intensity correlation plot of stain **63** and NR. ICA plots of (f) stain **63** and (g) stain NR. PDM images with (h) positive PDM values in the pixels and (i) negative PDM values in the pixels. Copyright 2012 American Chemical Society.

proteins outside lysosomes to drive the autolysosome process.[82] However, on account of the reaction characteristics and high diffusion of NO, the effects of NO on lysosomes are not yet fully understood. Therefore, it is essential to develop effective means for monitoring the level of NO in lysosomes of living cells to further explore the pathological mechanisms of related diseases.

Xiao and Jin *et al.* designed and synthesized a naphthalimide-based lysosomal-targeted two-photon fluorescent probe **63** (Scheme 49).[83] Probe **63** showed higher selectivity and sensitivity for NO over other ROS/RNS and the limit of detection was determined to be 5 nM. As shown in Fig. 102, the addition of NO caused a remarkable enhancement of the emission spectrum of **63** at 530 nm, and a significant increase of the fluorescence quantum yield from 0.02 to 0.3. However, the addition of various reactive oxygen and reactive nitrogen species, such as H_2O_2, NO_2^-, NO_3^-, $^1O_2$, $^\bullet OH$, and $ONOO^-$, didn't induce an observable spectral change. Compared to commercial lysosomal probes, **63** possessed lower cytotoxicity and perfect lysosomal localization. Co-localization experiments showed that **63** was a lysosome-specific probe for NO and the byproduct of NO in lysosomes did not interfere with its photo-properties (Fig. 103). Probe **63** could monitor the releasing process of NO from NOC13 in lysosomes of MCF-7 cells (Fig. 104). More importantly, due to the high selectivity and sensitivity of **63**, the first capture of NO within lysosomes of macrophage cells has been achieved using both two-photon fluorescence microscopy and flow cytometry.

6.2 Small-molecule fluorescent probes for the detection of peroxynitrite inside lysosomes

Peroxynitrite ($ONOO^-$) is the reaction product of nitric oxide (NO) and superoxide ($O_2^{\bullet -}$) under diffusion control without enzymatic catalysis. As a strong oxidant and nitrating agent, it plays a vital role in many physiological and pathological processes.[84] Besides, $ONOO^-$ is associated with many diseases such as neurodegenerative diseases, nitrification stress, cardiovascular diseases, inflammatory disorders and cancer. Lysosomes were attractive pharmacological targets for selective killing of cancer cells *via* the lysosomal cell death pathway that was closely associated with reactive oxygen species (ROS).[84c] Therefore, it is necessary to achieve rapid detection of $ONOO^-$ in living cell lysosomes due to its remarkably short half-life (<20 ms) under physiological conditions.

Yang and Zhang *et al.* successfully developed a versatile fluorescent probe **64** based on naphthalimide-hemicyanine, which was specifically localized in lysosomes for the detection

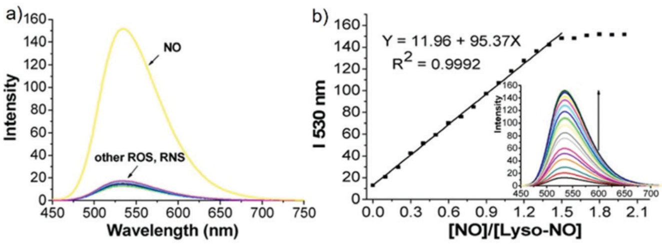

Fig. 102 (a) Selectivity of **63** (11 μM) fluorescence response for NO over other reactive nitrogen and oxygen species (5.0 equiv.) in 20 : 80 CH_3CN–H_2O solution at pH 5.0 (in 10 mM phosphate buffer). (b) Intensity at 530 nm *vs.* NO concentration under the same conditions. Inset: Changes in fluorescence spectra of **63** (11 μM) upon addition of different amounts NO solution (0–2.0 equiv.). Copyright 2012 American Chemical Society.

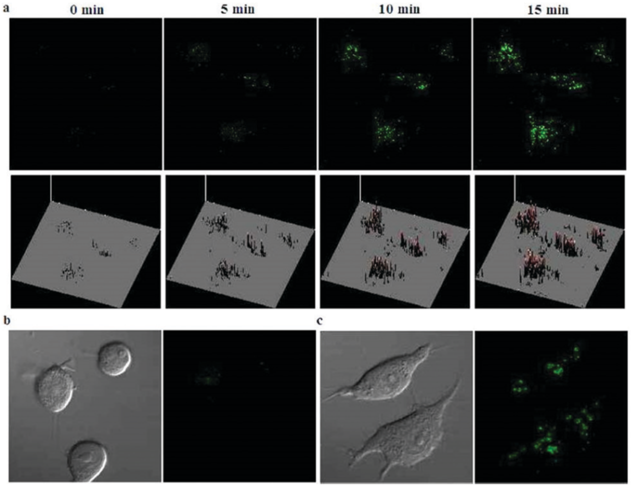

Fig. 104 (a) Time-dependent exogenous NO released from NOC13 (20 μM) in MCF-7 cells stained with **63** (5.0 μM). (b) DIC image and two-photon fluorescent image of RAW 264.7 macrophages stained with **63** (5.0 μM) for 4 h at 37 °C. (c) DIC image and two-photon fluorescent image of RAW 264.7 macrophages co-stained with **63** (5.0 μM) and stimulants containing final concentrations of 5000 μg mL^{-1} L-Arg, 150 units per mL INF-r, and 20 μg mL^{-1} LPS for 12 h, λ_{ex} = 840 nm, λ_{em} = 520–560 nm. Copyright 2012 American Chemical Society.

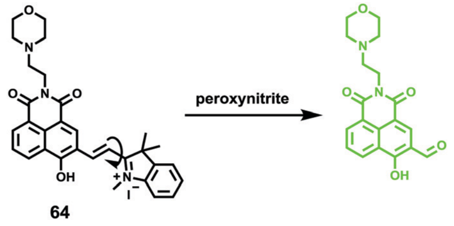

Scheme 50 Fluorescent probe **64** for $ONOO^-$.

of peroxynitrite ($ONOO^-$) (Scheme 50).[85] When excited at 440 nm, the fluorescence of **64** at 510 nm increased by about 3.5-fold with the increase of $ONOO^-$. Probe **64** was more selective for $ONOO^-$ than other ROS and RNS due to the selective cleavage of the double bond between the naphthalimide moiety and the indolium ring by peroxynitrite (Fig. 105). Cell imaging experiments showed that **64** possessed low cytotoxicity and good cell permeability, which was successfully applied to detect peroxynitrite in lysosomes of living cells (Fig. 106).

6.3 Small-molecule fluorescent probes for the detection of nitroxyl inside lysosomes

Nitroxyl (HNO) is one of the least studied RNS. HNO is reported to display unique potential bio-pharmacological effects.[86] On the one hand, HNO can act as an electrophile to resist superoxide infraction in mammalian vascular systems. On the other hand, it can also function as a nucleophile to coordinate and reduce metal ions. More importantly, numerous research studies indicate that HNO is beneficial for heart failure cure. Although it has been reported that HNO can be formed directly from NO and H_2S by a redox reaction, rapid dimerization and dehydration to nitrous oxide (N_2O) resulting from high chemical reactivity of HNO in biological systems always impede the accurate detection of HNO in cells and *in vivo*. Therefore, the development of suitable methods for the detection of HNO in cells and *in vivo* remains a challenging task.

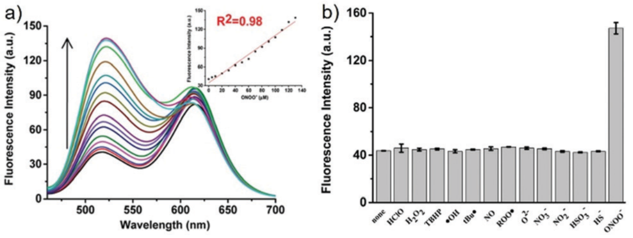

Fig. 105 (a) The fluorescence spectra of **64** (5 μM) in the presence of different concentrations of $ONOO^-$ (0–150 μM) in H_2O : ethanol (5 : 5 v/v) containing 0.5% DMSO (pH = 5.0), and 10 mM CPBS at room temperature. The insert shows the plot of fluorescence intensity at 510 nm *versus* various concentrations of $ONOO^-$. The excitation wavelength = 440 nm, excitation and emission slit widths were both 5 nm. Each spectrum was acquired 3 min after $ONOO^-$ addition at room temperature. (b) Fluorescence intensity of **64** (5 μM) at 510 nm in the presence of $ONOO^-$ (150 μM) and various ROSs (200 μM), HSO_3^- (200 μM), HS^- (200 μM), NO_3^- (200 μM), NO_2^- (200 μM). Excitation wavelength = 440 nm, excitation and emission slit widths were both 5 nm. Each spectrum was acquired 10 min after the addition of the various ROSs and RNSs at room temperature. Copyright 2018 Royal Society of Chemistry.

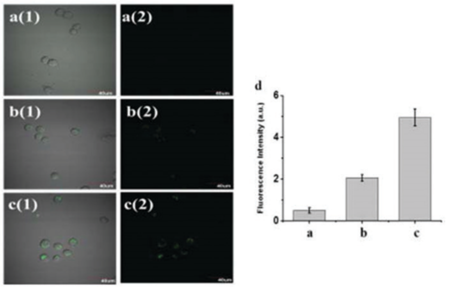

Fig. 106 Confocal fluorescence images of RAW 264.7 cells: (a) RAW 264.7 cells stained with **64** (5 μM) for 15 min. (b) RAW 264.7 cells stimulated with 1 μg mL^{-1} LPS and 50 ng mL^{-1} IFN-γ for 4 h, and then 10 nM PMA for 30 min before incubation with **64** (5 μM) for 15 min. (c) RAW 264.7 cells stained with **64** (5 μM) for 15 min and then $ONOO^-$ (10 μM) was added for 20 min. (d) Relative fluorescence intensity of cells in panels (a–c). (1) Overlay field. (2) Green channel. Green channel: 460–540 nm, excitation at 404 nm. Copyright 2018 Royal Society of Chemistry.

Chen *et al.* presented a NIR fluorescent probe **65** for the detection of nitroxyl groups (HNO) in cells and *in vivo* (Scheme 51).[87] In probe **65**, the diphenylphosphinobenzoyl group was used as the HNO recognition unit since it could react with HNO to form aza-ylide, which will nucleophilically attack the carbonyl of the ester, thereby releasing Lyso-1. **65** exhibited good sensitivity with a detection limit of 60 nM and excellent selectivity in the presence of various biologically relevant species (Fig. 107 and 108). Colocalization experiments demonstrated that **65** could be lysosome targetable and suitable for the detection of HNO in living cells. More importantly, fluorescence/X-ray imaging studies showed that **65** achieved noninvasive visualization of HNO in living mice (Fig. 109).

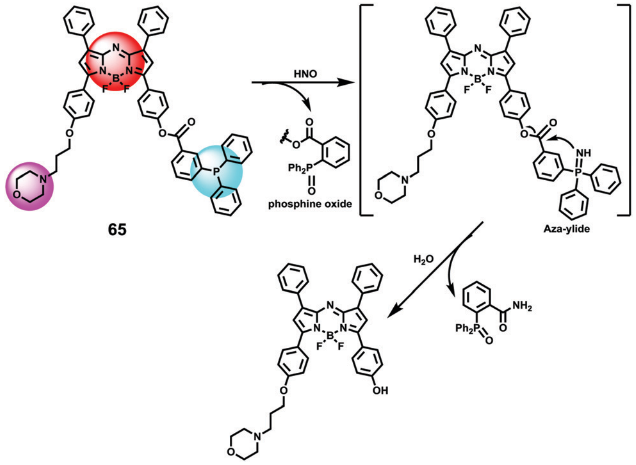

Scheme 51 Fluorescent probe **65** for HNO.

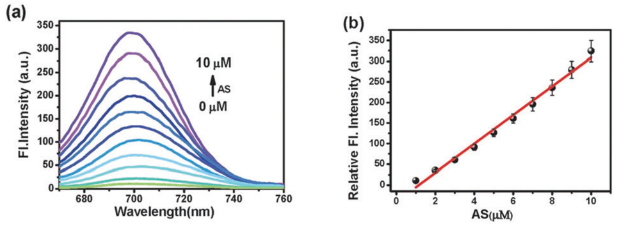

Fig. 107 (a) Fluorescence responses of **65** (2 μM) to different concentrations of Angeli's salt (AS) with emission ranging from 670 to 760 nm. λ_{ex} = 690 nm. (b) Relationship between the relative fluorescence intensity at 700 nm and concentrations of AS (0, 1, 2, 3, 4, 5, 6, 7, 8, 9, 10 μM). Fluorescence spectra were acquired in HEPES buffer solution (10 mM, 0.5% DMSO, 0.5% TW 80, pH 5.0). Copyright 2014 Royal Society of Chemistry.

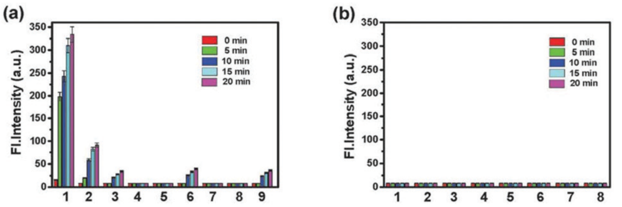

Fig. 108 (a) Time-dependent fluorescence response of 2 μM **65** to the testing species in HEPES buffer solution (10 mM, 0.5% DMSO, 0.5% TW 80, pH 5.0): 1, 10 μM AS; 2, 20 μM GSNO; 3, 200 μM $ONOO^-$; 4, 50 μM NOC-5; 5, 500 μM NO_2^-; 6, 200 μM H_2O_2; 7, 100 μM O_2^-; 8, 20 μM MeLOOH; 9, 200 μM ClO^-. (b) 1, 50 μM L-cys; 2, 100 μM GSH; 3, 500 μM NaHS; 4, 200 μM ascorbic acid; 5, 200 μM tocopherols; 6, 100 μM citrate; 7, 200 μM tyrosine (Tyr); 8, 50 μM hydroxylamine (HA). Bars represent fluorescence intensity during 0, 5, 10, 15, and 20 min after addition of various compounds. λ_{ex} = 690 nm, λ_{em} = 700 nm. Copyright 2014 Royal Society of Chemistry.

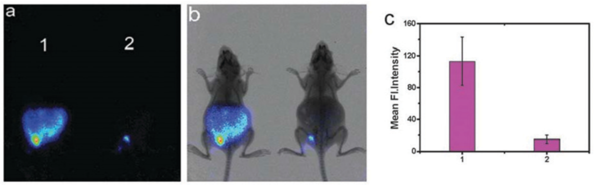

Fig. 109 Fluorescence/X-ray imaging in the peritoneal cavity of the BALB/c mice. (1) Mice injected i.p. with **65** (50 μM, 50 μL in 1 : 9 DMSO/saline v/v), and then loaded with AS (1 mM, 50 μL in saline) for 30 min. (2) Mice injected i.p. with **65** (50 μM, 50 μL in 1 : 9 DMSO/saline v/v) for 40 min. (a) Fluorescence imaging; (b) merged fluorescence imaging with X-ray imaging; (c) quantification of total photon flux from the region of interest for each group. *n* = 5, error bars are ±SD. Images constructed from the 670 nm fluorescence window, λ_{ex} = 660 nm. Copyright 2014 Royal Society of Chemistry.

7. Small-molecule fluorescent probes for the detection of metal ions inside lysosomes

7.1 Small-molecule fluorescent probes for the detection of Zn^{2+} inside lysosomes

A zinc ion (Zn^{2+}) is not only an essential element that plays a key role in various basic biological processes, but also a cofactor for structuring and functioning of different proteins expressed in the cytoplasm.[88] Although lysosomes contain Zn^{2+}, the homeostasis of zinc in lysosomes is still not well established. Therefore, in order to obtain high-precision information from complex lysosomes, molecular fluorescence imaging is a promising method on account of its high sensitivity and high spatial resolution and real-time monitoring capability.

Jiang *et al.* designed and synthesized a lysosomal-targeted ratiometric fluorescent probe **66**, composed of a quinoline scaffold as the ratiometric signaling unit for Zn^{2+} (Scheme 52).[89] In acidic aqueous solution (pH = 5.2), **66** displayed a fluorescence emission maximum at 542 nm. The titration of Zn^{2+} into the solution of probe **66** resulted in quenching of emission around 543–700 nm and a new blue-shifted emission peak at 495 nm with a hypsochromic shift of 47 nm (Fig. 110a). **66** possessed higher selectivity toward Zn^{2+} over other metal ions and good sensitivity with a

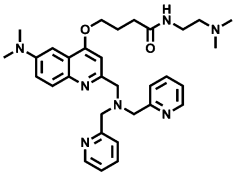

66

Scheme 52 Fluorescent probe **66** for Zn^{2+}.

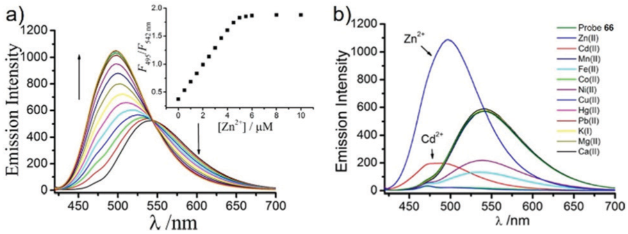

Fig. 110 (a) Fluorescence spectra of 5 μM **66** upon titration of Zn^{2+} (0–10 μM) in aqueous buffer (20 mM MES, 0.1 M NaCl, pH = 5.2), λ_{ex} = 405 nm. Inset: The emission ratio (F_{495}/F_{542nm}) changes as a function of Zn^{2+} concentration. (b) Fluorescence spectra of **66** (5 μM) in the presence of various metal ions (5 μM Mn^{2+}, Fe^{2+}, Co^{2+}, Ni^{2+}, Cu^{2+}, Zn^{2+}, Cd^{2+}, and 1 mM Mg^{2+}, Ca^{2+}, and K^+) in MES buffer (pH = 5.2, λ_{ex} = 405 nm). Copyright 2012 American Chemical Society.

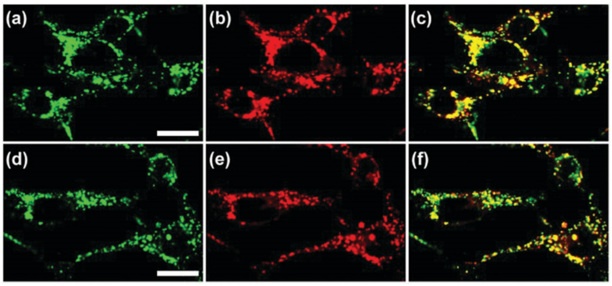

Fig. 111 Probe **66** localizes to lysosomes in live NIH 3T3 cells. The cells were stained with (a) 10 μM **66**, (b) 1 μM LysoTracker Red, (d) 10 μM **66** and further treated with 30 μM $ZnSO_4$ and 15 μM 2-mercaptopyridine *N*-oxide for 5 min, (e) LysoTracker Red, for 30 min at 37 °C in DMEM. (c) Overlay of (a) and (b), (f) overlay of (d) and (e). Scale bar: 20 μm. Copyright 2012 American Chemical Society.

detection limit of 16 nM (Fig. 110b). Probe **66** showed low cytotoxicity and good cell permeability. Confocal imaging experiments indicated that **66** was able to localize to lysosomes and could be applied to ratiometric detection of lysosomal Zn^{2+} changes in the presence of exogenous or endogenous Zn^{2+} (Fig. 111).

Cho and Ahn *et al.* developed a novel two-photon fluorescent probe **67** for selective detection of Zn^{2+} in lysosomes over those in the cytosol (Scheme 53).[90] The probe was a naphthalimide-based dye consisting of an *N*,*N*-di-(2-picolyl)ethylenediamine (DPEN) ligand, which was known to bind Zn(II). The probe emitted negligible fluorescence at various pH values. Upon addition of Zn^{2+}, the probe emitted strong fluorescence in the lysosomal pH range (pH = 4.5–5.5) due to the inhibition of PET processes from the coordination of Zn^{2+} with DPEN and the protonated morpholine unit. It should be noted that, being different from some reported lysosomal Zn(II) probes that show strong fluorescence after binding with Zn(II) even at the cytosolic pH (pH = 7.2–7.4), probe **67** displayed a low fluorescence intensity at cytosolic pH (7.4) even after binding with Zn(II) ions. Strong fluorescence could only be observed when probe **67** bound with Zn(II) ions inside lysosomes (pH 4.5–5.5). The probe exhibited high selectivity to Zn^{2+} over other metal ions and high sensitivity with a detection limit of 0.18 μM (Fig. 112). Co-localization experiments indicated that probe **67** was capable of detecting intracellular lysosomal Zn(II) ions with high fidelity (Fig. 113). Moreover, two-photon microscopic imaging experiments demonstrated that probe **67** had potential applicability in the imaging of endogenous Zn(II) ions in tissues.

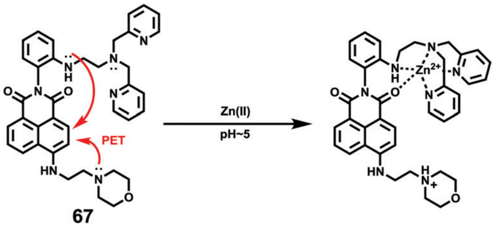

Scheme 53 Fluorescent probe **67** for Zn^{2+}.

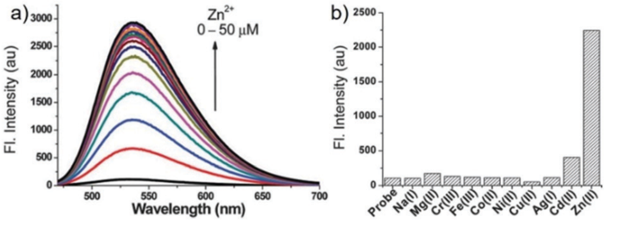

Fig. 112 (a) Fluorescence titration of probe **67** (10 μM) with $Zn(ClO_4)_2$ in a pH 5.0 MES buffer containing 1% EtOH. (b) Fluorescence intensity changes of probe **67** (10 μM) with various metal ions (10 μM) in 1% EtOH containing a pH 5.0 MES buffer. All the fluorescence data were obtained under excitation at 450 nm. Copyright 2016 Royal Society of Chemistry.

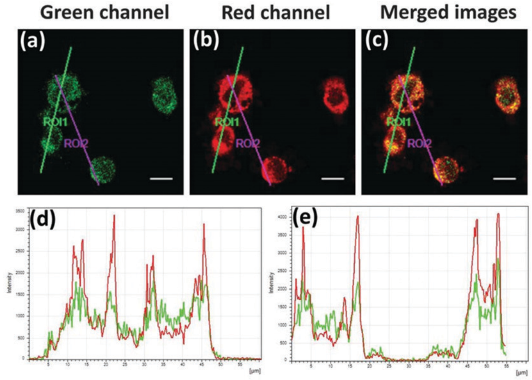

Fig. 113 Pseudo-colored fluorescence images of NIH 3T3 cells: (a) TPM images of cells co-incubated with probe **67** (30 μM) followed by $Zn(ClO_4)_2$ and pyrithione (1 : 1) solution (60 μM), collected in the green channel window (500–630 nm) under excitation at 900 nm. (b) OPM images of cells incubated with LysoTracker Deep Red (1 μM) for 10 min at 37 °C, collected in the red channel window (670–750 nm) under excitation at 633 nm. (c) Merged images. Scale bar: 10 μm. (d and e) Intensity profiles measured across the NIH 3T3 cells: (d) ROI 1 and (e) ROI 2. Copyright 2016 Royal Society of Chemistry.

7.2 Small-molecule fluorescent probes for the detection of Cu^{2+} inside lysosomes

Copper, as the indispensable trace element, plays an important role in various physiological processes, such as pigmentation, cellular respiration, neurotransmitter synthesis and metabolism, iron homeostasis, connective tissue formation, and peptide biogenesis.[91] Most of the copper in the cytoplasm binds to metallothionein, but excess copper is mainly excreted into the bile through the lysosome-to-bile pathway. The disorder of copper homeostasis in cells is closely associated with many serious diseases, including Alzheimer's disease, Menkes disease, Wilson's disease and familial amyotrophic lateral sclerosis. Copper usually accumulates in lysosomes of patients with later stage Wilson's disease. In addition, human copper transporter 2 (hCTR2) localizes in lysosomes and promotes cellular uptake of Cu^{2+}. Therefore, it is highly desirable to develop a reliable method for detecting Cu^{2+} in lysosomes.

Lin *et al.* developed the fluorescence-enhanced and lysosomal-targeted Cu^{2+} probe **68** with unique dual-channel emission (Scheme 54).[92] With excitation at 360 nm, **68** displayed a weak

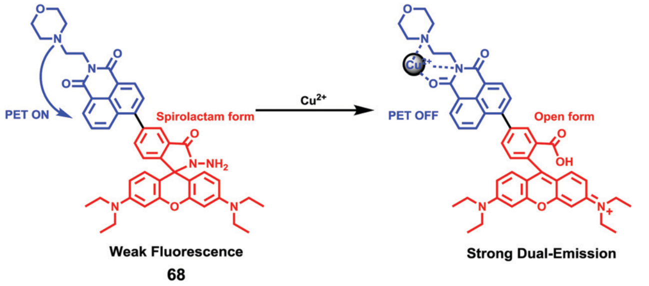

Scheme 54 Fluorescent probe **68** for Cu^{2+}.

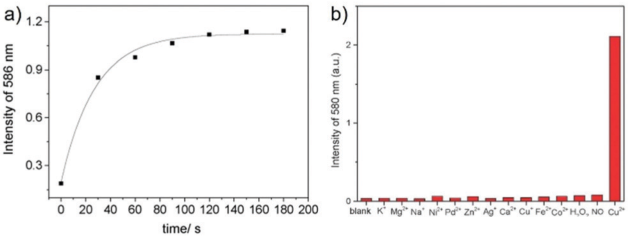

Fig. 114 (a) Fluorescence intensities at 586 nm of **68** (10 μm) in the presence of Cu^{2+} (30 equiv.) for continuous monitoring at time interval periods (0–180 s) in PBS buffer, pH 4.7, containing 50% CH_3CN as a cosolvent. Excitation at 360 nm. (b) Fluorescence intensity of the probe **68** (10 mM) at 580 nm in the presence of various analytes (30 equiv.) in PBS buffer (pH 4.7, containing 50% CH_3CN as a cosolvent). Copyright 2015 Royal Society of Chemistry.

fluorescence emission band at around 440 nm on account of a quenching photoinduced electron-transfer (PET) process from the amino group to the 1,8-naphthalimide fluorophore and rhodamine B in the ring-closed form. Upon addition of Cu^{2+}, not only was the fluorescence at 440 nm dramatically enhanced due to the inhibition of the quenched PET channel, but also a significant fluorescence enhancement was observed at about 580 nm owing to the triggering of rhodamine B ring-opened form formation. **68** possessed a fast response and high selectivity to Cu^{2+}. For example, as shown in Fig. 114, the addition of K^+, Mg^{2+}, Na^+, Ni^{2+}, Pd^{2+}, Zn^{2+}, Ag^+, Ca^{2+}, Cu^+, Fe^{2+}, Co^{2+}, H_2O_2, and NO into the solution of probe **68** caused a negligible fluorescence enhancement of probe **68.** However, a significant fluorescence enhancement was observed upon the addition of Cu^{2+} to probe **68.** Co-localization experiments indicated that **68** was membrane-permeable and suitable for visualization of Cu^{2+} in lysosomes of living cells by dual-channel imaging (Fig. 115).

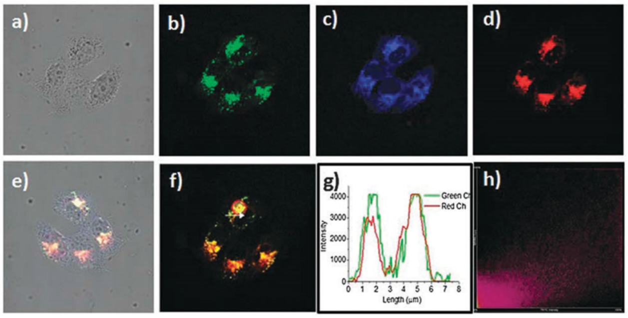

Fig. 115 Bright field and fluorescence images of SiHa cells stained with probe **68:** (a) bright field image; (b) from the green channel (lysosomes staining); (c) from the blue channel; (d) from the red channel; (e) an overlay of bright field, green, blue and red channels; (f) an overlay of green and red channels; (g) intensity profile of the linear region of interest across the SiHa cell co-stained with LysoTracker Green and the red channel of **68**; and (h) an intensity scatter plot of green and red channels. Copyright 2015 Royal Society of Chemistry.

8. Small-molecule fluorescent probes for the detection of enzymes inside lysosomes

8.1 Small-molecule fluorescent probes for the detection of nitroreductase inside lysosomes

Nitroreductase (NTR) is one of the enzymes containing flavin. Nitroaromatic derivatives can be reduced to the corresponding amines by NTR with electrons donated from nicotinamide adenine dinucleotide (NADH).[93] At present, the function and distribution of NTR in lysosomes are poorly understood. Therefore, it is essential to establish a suitable method to detect the change and distribution of NTR in lysosomes.

Ma *et al.* developed a new naphthalimide-based fluorescent probe **69** for the detection of NTR in lysosomes (Scheme 55).[94] The detection mechanism of **69** for NTR was based on the nitroreductase-catalyzed reduction of the probe to 4-amino-1,8-naphthalimide. Before reacting with NTR, **69** was nearly non-fluorescent due to the strong fluorescence quenching of the nitro group. However, the introduction of NTR into the solution of probe **69** gave rise to a large fluorescence enhancement. **69** exhibited superior selectivity to NTR compared to other biologically relevant species (Fig. 116). **69** also possessed high sensitivity with a detection limit of 2.2 ng mL^{-1}. Co-localization experiments demonstrated that **69** was capable of specifically targeting the lysosomes of living cells with good cell-membrane permeability and could detect lysosomal NTR (Fig. 117).

8.2 Small-molecule fluorescent probes for the detection of β-galactosidase inside lysosomes

β-Galactosidase (β-gal) is a glycosidehydrolase enzyme which is encoded by the lacZ gene. β-gal can catalyze the hydrolysis of β-galactosides into monosaccharides through the breaking of a glycosidic bond. It is a vital reporter biomarker for primary ovarian cancers and cell senescence.[95] In addition, cells can generate acid lysosomal β-galactosidase localized in lysosomes.

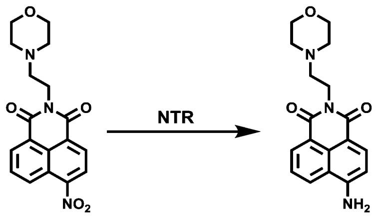

69

Scheme 55 Fluorescent probe **69** for NTR.

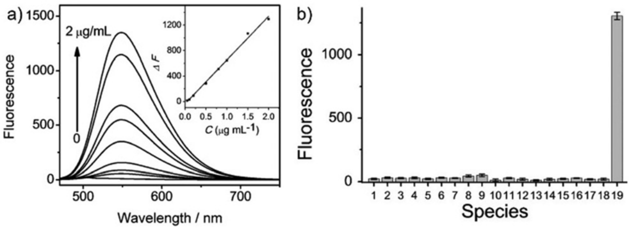

Fig. 116 (a) Fluorescence emission spectra of **69** (10 μM) reacting with NTR at varied concentrations (0, 0.05, 0.1, 0.2, 0.5, 0.8, 1.0, 1.5 and 2.0 μg mL^{-1}). The inset shows the plot of the fluorescence intensity of **69** *versus* the NTR concentration; Δ*F* is the difference of fluorescence intensity of **69** with and without NTR. The reaction was carried out in the presence of 100 μM NADH at 37 °C for 1.0 h. $\lambda_{ex}/\lambda_{em}$ = 425/543 nm. (b) Fluorescence responses of **69** (5 μM) in the presence of NADH (200 μM) to various species: (1) control (**69** + NADH); (2) 2.0 mM $CaCl_2$; (3) 2.0 mM $MgCl_2$; (4) 150 mM KCl; (5) 100 μM HOCl; (6) 100 μM H_2O_2; (7) 100 μm •OH; (8) 1 mM L-cysteine; (9) 1 mM reduced glutathione; (10) 100 μM NaHS; (11) 1 mM glycine; (12) 1 mM vitamin C; (13) 10 mM glucose; (14) 100 μM human serum albumin; (15) 1 U mL^{-1} carboxylesterase; (16) 5 nm matrix metalloproteinase 2; (17) 5 nm thrombin; (18) 0.05 μg mL^{-1} DT-diaphorase; (19) 2.0 μg mL^{-1} NTR. $\lambda_{ex}/\lambda_{em}$ = 425/543 nm. Copyright 2016 Wiley-VCH.

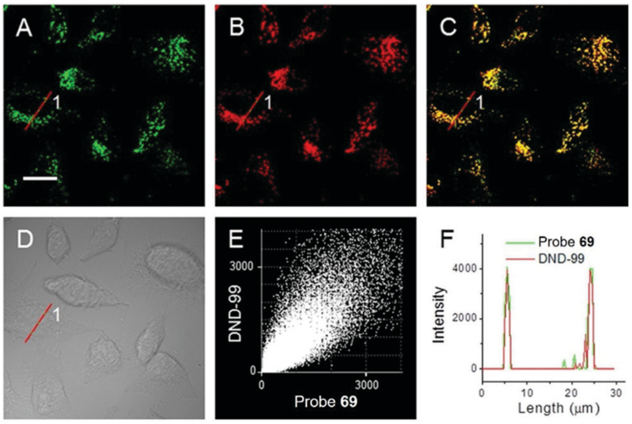

Fig. 117 Colocalization of **69** and DND-99 in A549 cells. Cells were grown under the hypoxic condition of 1% O_2 and then co-stained with **69** (2 μM) and DND-99 (100 nM) at 37 °C. (A) Fluorescence image from the **69** channel (λ_{ex} = 405 nm, λ_{em} = 455–555 nm). (B) Fluorescence image from the DND-99 channel (λ_{ex} = 559 nm, λ_{em} = 570–670 nm). (C) Merged image of images (A) and (B). (D) Corresponding differential interference contrast (DIC) image. (E) Intensity correlation plot of **69** and DND-99. (F) Intensity profiles of **69** and DND-99 within the linear ROI 1 (red lines in A and B) across the cell. Scale bar, 20 μm. Copyright 2016 Wiely-VCH.

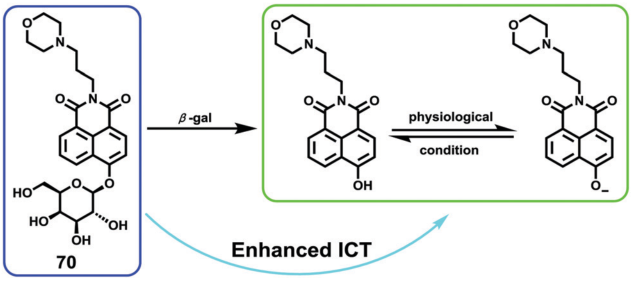

Scheme 56 Fluorescent probe **70** for β-gal.

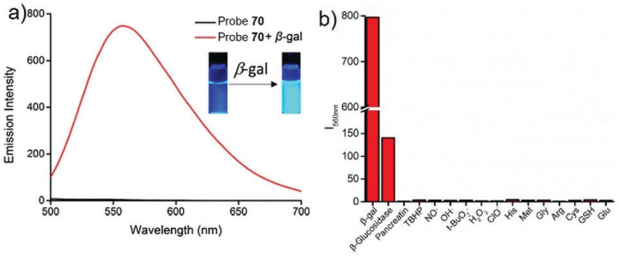

Fig. 118 (a) The emission of probe **70** with or without β-gal (λ_{ex} = 460 nm). Inset: Images irradiated with 365 nm ultraviolet light. (b) Fluorescence intensity of **70** (10 μM) in response to the test species in a PBS buffer solution at 560 nm excited at 460 nm. Copyright 2017 Elsevier.

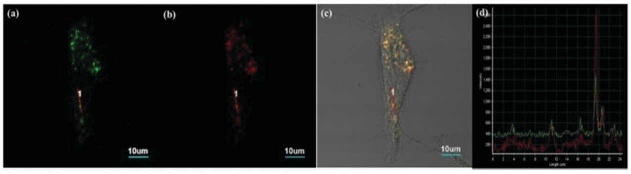

Fig. 119 Fluorescence images of SKOV-3 cells stained with probe **70** and LysoTracker Red DND-99. (a) Image from the green channel; (b) image from the red channel (lysosomes staining); (c) overlay of bright-field, green and red channels; (d) intensity profile of the regions of interest (ROI) across SKOV-3 cells. Copyright 2017 Elsevier.

However, fluorescent probes for monitoring endogenous β-gal in ovarian tumor cells especially in lysosomes were rarely reported.

Gu and Wang *et al.* designed and synthesized a lysosome-targeted two-photon fluorescent probe **70** for detecting β-galactosidase in living ovarian cancer cells (Scheme 56).[96] Probe **70** consisted of a 1,8-naphthalimide fluorophore as the fluorescence reporter, a morpholine ring as the lysosome-targeted group, and a β-gal cleavable unit as the enzyme-active trigger, respectively. Probe **70** exhibited remarkable response to β-gal *in vitro* with a distinct fluorescence change from blue to green. As shown in Fig. 118, in the absence of β-gal, probe **70** exhibited weak fluorescence under the excitation at 460 nm because of its weak ICT. However, after the addition of β-gal, drastically increased fluorescence intensity at 560 nm was observed since the glucosidic bond of the probe could be hydrolyzed by β-gal and transformed into the phenolate group. Probe **70** possessed high sensitivity to β-gal with the detection limit of 4 × 10^{-5} U mL^{-1}. Furthermore, co-localization experiments indicated that probe **70** could be located in lysosomes specifically, imaging endogenous β-gal in living cells as well as monitoring endogenous β-galactosidase in living ovarian cancer cells using two-photon fluorescence microscopy (Fig. 119).

9. Conclusions

Over the past few years, we have focused our research interest on the design and preparation of novel fluorescent probes[97] and construction of supramolecular fluorescent functional materials *via* self-assembly.[98] In this feature article, the recent development of small-molecule fluorescent probes for the selective detection of chemical species inside lysosomes has been systematically summarized. This feature article focuses on the design principle, the recognition mechanism, the properties, and the applications of various kinds of small-molecule fluorescent probes for the detection of pH, reactive oxygen species (ROS), reactive sulfur species (RSS), reactive nitrogen species (RNS), metal ions, and enzymes in lysosomes. Considering their wide applications in chemistry, biology, and medical science, there is no doubt that these kinds of fluorescent probes for detecting chemical species inside lysosomes will attract more attention in the next few decades.

Although a great number of achievements have been made in this research field, many problems are still far from being fully resolved. For example, despite there are general methods, such as the incorporation of weakly alkaline groups and the introduction of rhodamine group, to deliver small-molecule probes to cellular lysosomes, the challenge of developing a selective lysosomal fluorescent probe is still a hard work since the lysosome and cellular environment are highly complex. Moreover, these fluorescent probes still didn't clearly elucidate the relationship between the diseases and the chemical species in lysosomes. In our opinion, three aspects should be considered in further development of small-molecule fluorescent probes for the detection of chemical species inside lysosome. First, in order to develop and expand their biological applications, biocompatible and water-soluble fluorescent probes need to be designed and prepared. Second, near-infrared fluorescent probes for the detection of chemical species inside lysosomes should be constructed. Third, more attention should be paid to the preparation of lysosomal-targeted fluorescent probes for the diagnosis and treatment of related diseases caused by chemical species in lysosomes.

Conflicts of interest

There are no conflicts to declare.

Acknowledgements

Thanks to all excellent authors whose names appear in the references. We acknowledge the financial support of the National Natural Science Foundation of China (No. 21871092 and 21672070), Shanghai Pujiang Program (18PJD015), and the State Key Laboratory of Fine Chemicals (KF 1801).

References

1 (*a*) P. Saftig and A. Haas, *Nat. Cell Biol.*, 2016, **18**, 1025; (*b*) R. E. Lawrence and R. Zoncu, *Nat. Cell Biol.*, 2018, **21**, 133.

2 (*a*) A. Ciechanover, *Cell Death Differ.*, 2005, **12**, 1178; (*b*) M. P. Jackson and E. W. Hewitt, *Essays Biochem.*, 2016, **60**, 173.

3 (*a*) D. W. Lamming and L. Bar-Peled, *Traffic*, 2019, **20**, 27; (*b*) A. M. Thelen and R. Zoncu, *Trends Cell Biol.*, 2017, **27**, 833; (*c*) C.-Y. Lim and R. Zoncu, *J. Cell Biol.*, 2016, **214**, 653.

4 (*a*) H. Appelqvist, P. Wäster, K. Kågedal and K. Öllinger, *J. Mol. Cell Biol.*, 2013, **5**, 214; (*b*) R.-M. N. Boustany, *Nat. Rev. Neurol.*, 2013, **9**, 583; (*c*) R. A. Nixon, *Nat. Med.*, 2013, **19**, 983.

5 (*a*) C. Yang and X. Wang, *Traffic*, 2017, **18**, 348; (*b*) B. Carroll and E. A. Dunlop, *Biochem. J.*, 2017, **474**, 1453; (*c*) S. M. Davidson and M. G. V. Heiden, *Annu. Rev. Pharmacol.*, 2017, **57**, 481; (*d*) C. E. Blaby-Haas and S. S. Merchant, *J. Biol. Chem.*, 2014, **289**, 28129.

6 D. Dahal, L. McDonald, X. Bi, C. Abeywickrama, F. Gombedza, M. Konopka, S. Paruchuri and Y. Pang, *Chem. Commun.*, 2017, **53**, 3697.

7 (*a*) G. Li, S. Ma, J. Tang and Y. Ye, *New J. Chem.*, 2019, **43**, 1267; (*b*) H. Zhang, L. Xu, W. Chen, J. Huang, C. Huang, J. Sheng and X. Song, *ACS Sens.*, 2018, **3**, 2513.

8 J. Liu, S. Zhou, J. Ren, C. Wu and Y. Zhao, *Analyst*, 2017, **142**, 4522.

9 Y. Hong, H. Wang, M. Xue, P. Zhang, W. Liu, S. Chen, R. Zeng, J. Cui, Y. Gao and J. Chen, *Mater. Chem. Front.*, 2019, **3**, 203.

10 H. Duan, Y. Ding, C. Huang, W. Zhu, R. Wang and Y. Xu, *Chin. Chem. Lett.*, 2019, **30**, 55.

11 Y. Li, Y. Zhao, W. Chan, Y. Wang, Q. You, C. Liu, J. Zheng, J. Li, S. Yang and R. Yang, *Anal. Chem.*, 2015, **87**, 584.

12 (*a*) B. Daly, J. Ling and A. P. de Silva, *Chem. Soc. Rev.*, 2015, **44**, 4203; (*b*) H. S. Jung, P. Verwilst, W. Y. Kim and J. S. Kim, *Chem. Soc. Rev.*, 2016, **45**, 1242; (*c*) H.-W. Liu, L. Chen, C. Xu, Z. Li, H. Zhang, X.-B. Zhang and W. Tan, *Chem. Soc. Rev.*, 2018, **47**, 7140; (*d*) J. Zhu, P. Jia, N. Li, S. Tan, J. Huang and L. Xu, *Chin. Chem. Lett.*, 2018, **29**, 1445; (*e*) X. Qian and Z. Xu, *Chem. Soc. Rev.*, 2015, **44**, 4487; (*f*) A. T. Aron, K. M. Ramos-Torres, J. A. Cotruvo Jr. and C. J. Chang, *Acc. Chem. Res.*, 2015, **48**, 2434; (*g*) H. Zhu, J. Fan, J. Du and X. Peng, *Acc. Chem. Res.*, 2016, **49**, 2115; (*h*) L.-Y. Niu, Y.-Z. Chen, H.-R. Zheng, L.-Z. Wu, C.-H. Tung and Q.-Z. Yang, *Chem. Soc. Rev.*, 2015, **44**, 6143; (*i*) M. Kaur and D. H. Choi, *Chem. Soc. Rev.*, 2015, **44**, 58; (*j*) S. T. Manjare, Y. Kim and D. G. Churchill, *Acc. Chem. Res.*, 2014, **47**, 2985; (*k*) K. P. Carter, A. M. Young and A. E. Palmer, *Chem. Rev.*, 2014, **114**, 4564; (*l*) H. Xu, Q. Li, L. Wang, Y. He, J. Shi, B. Tang and C. Fan, *Chem. Soc. Rev.*, 2014, **43**, 2650; (*m*) L. Pu, *Acc. Chem. Res.*, 2012, **45**, 150; (*n*) H. N. Kim, Z. Guo, W. Zhu, J. Yoon and H. Tian, *Chem. Soc. Rev.*, 2011, **40**, 79; (*o*) E. M. Nolan and S. J. Lippard, *Acc. Chem. Res.*, 2009, **42**, 193; (*p*) X. Chen, G. Zhou, X. Peng and J. Yoon, *Chem. Soc. Rev.*, 2012, **41**, 4610; (*q*) Y. V. Suseela, N. Narayanaswamy, S. Pratihar and T. Govindaraju, *Chem. Soc. Rev.*, 2018, **47**, 1098; (*r*) P. Ning, W. Wang, M. Chen, Y. Feng and X. Meng, *Chin. Chem. Lett.*, 2017, **28**, 1943; (*s*) D. Su, C. L. Teoh, L. Wang, X. Liu and Y.-T. Chang, *Chem. Soc. Rev.*, 2017, **46**, 4833; (*t*) Y. Xia, R. Zhang, Z. Wang, J. Tian and X. Chen, *Chem. Soc. Rev.*, 2017, **46**, 2824; (*u*) M. Gao, F. Yu, C. Lv, J. Choo and L. Chen, *Chem. Soc. Rev.*, 2017, **46**, 2237; (*v*) A. Kaur, J. L. Kolanowski and E. J. New, *Angew. Chem., Int. Ed.*, 2016, **55**, 1602; (*w*) Z. Lou, P. Li and K. Han, *Acc. Chem. Res.*, 2015, **48**, 1358; (*x*) Y. Ding, Y. Tang, W. Zhu and Y. Xie, *Chem. Soc. Rev.*, 2015, **44**, 1101.

13 (*a*) H.-Y. Tan, Y.-T. Qiu, H. Sun, J.-W. Yan and L. Zhang, *Chem. Commun.*, 2019, **55**, 2688; (*b*) P. Sharma, N. Gupta, S. Kaur, S. Kaur, P. Ohri, R. D. Parihar, V. Bhalla and M. Kumar, *Sens. Actuators, B*, 2019, **286**, 451; (*c*) P. Ning, L. Hou, Y. Feng, G. Xu, Y. Bai, H. Yu and X. Meng, *Chem. Commun.*, 2019, **55**, 1782; (*d*) S.-H. Park, J. Young and I. Shin, *Chem. Sci.*, 2019, **10**, 56; (*e*) X.-J. Chao, Z.-Y. Pan, L.-L. Sun, M. Tang, K.-N. Wang and Z.-W. Mao, *Sens. Actuators, B*, 2019, **285**, 156; (*f*) S.-L. Shen, X.-Q. Huang, X.-H. Lin and X.-Q. Cao, *Anal. Chim. Acta*, 2019, **1052**, 124; (*g*) G.-J. Mao, Z.-Z. Liang, J. Bi, H. Zhang, H.-M. Meng, L. Su, Y.-J. Gong, S. Feng and G. Zhang, *Anal. Chim. Acta*, 2019, **1048**, 143; (*h*) X.-Q. Hong, X.-H. Yu, K. Zhang and W.-H. Chen, *Org. Biomol. Chem.*, 2018, **16**, 8025; (*i*) K. A. Bertman, C. S. Abeywickrama, H. J. Baumann, N. Alexander, L. McDonald, L. P. Shriver, M. Konopka and Y. Pang, *J. Mater. Chem. B*, 2018, **6**, 5050; (*j*) Y. Ren, L. Zhang, Z. Zhou, Y. Luo, S. Wang, S. Yuan, Y. Gu, Y. Xu and X. Zha, *Anal. Chim. Acta*, 2019, **1056**, 117; (*k*) C. Benitez-Martin, J. A. Guadix, J. R. Pearson, F. Najera, J. M. Perez-Pomares and E. Perez-Inestrosa, *Sens. Actuators, B*, 2019, **284**, 744; (*l*) C. Li, Y. Wang, S. Huang, X. Zhang, X. Kang, Y. Sun, Z. Hu, L. Han, L. Du and Y. Liu, *Talanta*, 2018, **188**, 316; (*m*) M. Zhu, P. Xing, Y. Zhou, L. Gong, J. Zhang, D. Qi, Y. Bian, H. Du and J. Jiang, *J. Mater. Chem. B*, 2018, **6**, 4422; (*n*) F. Wang, S. Yu, Z. Xu, L. Li, Y. Dang, X. Xu, Y. Luo, Z. Cheng, H. Yu, W. Zhang, A. Zhang and C. Ding, *Anal. Chem.*, 2018, **90**, 7953; (*o*) Z. Hu, G. Yang, J. Hu, H. Wang, P. Eriksson, R. Zhang, Z. Zhang and K. Uvdal, *Sens. Actuators, B*, 2018, **264**, 419.

14 E. C. Freundt, M. Czapiga and M. J. Lenardo, *Cell Res.*, 2007, **17**, 956.

15 (*a*) Y. W. Jun, T. Wang, S. Hwang, D. Kim, D. Ma, K. H. Kim, S. Kim, J. Jung and K. H. Ahn, *Angew. Chem., Int. Ed.*, 2018, **57**, 10142; (*b*) D. Lee, K. M. K. Swamy, J. Hong, S. Lee and J. Yoon, *Sens. Actuators, B*, 2018, **266**, 416; (*c*) H. Zhang, J. Liu, C. Liu, P. Yu, M. Sun, X. Yan, J.-P. Guo and W. Guo, *Biomaterials*, 2017, **133**, 60; (*d*) W. Feng and G. Feng, *Dyes Pigm.*, 2019, **164**, 174; (*e*) A. Podder, S. Senapati, P. Maiti, D. Kamalraj, S. S. Jaffer, S. Khatun and S. Bhuniya, *J. Mater. Chem. B*, 2018, **6**, 4514; (*f*) M.-Y. Wu, Y. Wang, Y.-H. Liu and X.-Q. Yu, *J. Mater. Chem. B*, 2018, **6**, 4232.

16 (*a*) X. Chen, T. Pradhan, F. Wang, J. S. Kim and J. Yoon, *Chem. Rev.*, 2012, **112**, 1910; (*b*) L. Xu, Y. Xu, W. Zhu, B. Zeng, C. Yang, B. Wu and X. Qian, *Org. Biomol. Chem.*, 2011, **9**, 8284.

17 Z. Li, S. Wu, J. Han and S. Han, *Analyst*, 2011, **136**, 3698.

18 X.-L. Shi, G.-J. Mao, X.-B. Zhang, H.-W. Liu, Y.-J. Gong, Y.-X. Wu, L.-Y. Zhou, J. Zhang and W. Tan, *Talanta*, 2014, **130**, 356.

19 H.-S. Lv, S.-Y. Huang, B.-X. Zhao and J.-Y. Miao, *Anal. Chim. Acta*, 2013, **788**, 177.

20 H.-S. Lv, S.-Y. Huang, Y. Xu, X. Dai, J.-Y. Miao and B.-X. Zhao, *Bioorg. Med. Chem. Lett.*, 2014, **24**, 535.

21 H.-S. Lv, J. Liu, J. Zhao, B.-X. Zhao and J.-Y. Miao, *Sens. Actuators, B*, 2013, **177**, 956.

22 K.-K. Yu, K. Li, J.-T. Hou, H.-H. Qin, Y.-M. Xie, C.-H. Qian and X.-Q. Yu, *RSC Adv.*, 2014, **4**, 33975.

23 H. Li, C. Wang, M. She, Y. Zhu, J. Zhang, Z. Yang, P. Liu, Y. Wang and J. Li, *Anal. Chim. Acta*, 2015, **900**, 97.

24 Q. Wang, L. Zhou, L. Qiu, D. Lu, Y. Wu and X.-B. Zhang, *Analyst*, 2015, **140**, 5563.

25 X.-X. Zhao, D. Ge, X. Dai, W.-L. Wu, J.-Y. Miao and B.-X. Zhao, *Spectrochim. Acta, Part A*, 2015, **151**, 218.

26 H. Zhu, J. Fan, Q. Xu, H. Li, J. Wang, P. Gao and X. Peng, *Chem. Commun.*, 2012, **48**, 11766.

27 Z. Li, S. Wu, J. Han, L. Yang and S. Han, *Talanta*, 2013, **114**, 254.

28 J. Fan, C. Lin, H. Li, P. Zhan, J. Wang, S. Cui, M. Hu, G. Cheng and X. Peng, *Dyes Pigm.*, 2013, **99**, 620.

29 X.-F. Zhang, T. Zhang, S.-L. Shen, J.-Y. Miao and B.-X. Zhao, *J. Mater. Chem. B*, 2015, **3**, 3260.

30 X.-F. Zhang, T. Zhang, S.-L. Shen, J.-Y. Miao and B.-X. Zhao, *RSC Adv.*, 2015, **5**, 49115.

31 R. Sun, X.-D. Liu, Z. Xun, J.-M. Lu, Y.-J. Xu and J.-F. Ge, *Sens. Actuators, B*, 2014, **201**, 426.

32 L.-Q. Ying and B. P. Branchaud, *Bioorg. Med. Chem. Lett.*, 2011, **21**, 3546.

33 J. Zhang, M. Yang, C. Li, N. Dorh, F. Xie, F.-T. Luo, A. Tiwari and H. Liu, *J. Mater. Chem. B*, 2015, **3**, 2173.

34 L. Chen, J. Li, Z. Liu, Z. Ma, W. Zhang, L. Du, W. Xu, H. Fang and M. Li, *RSC Adv.*, 2013, **3**, 13412.

35 Y. Tian, F. Su, W. Weber, V. Nandakumar, B. R. Shumway, Y. Jin, X. Zhou, M. R. Holl, R. H. Johnson and D. R. Meldrum, *Biomaterials*, 2010, **31**, 7411.

36 R. Sun, W. Liu, Y.-J. Xu, J.-M. Lu, J.-F. Ge and M. Ihara, *Chem. Commun.*, 2013, **49**, 10709.

37 H. J. Kim, C. H. Heo and H. M. Kim, *J. Am. Chem. Soc.*, 2013, **135**, 17969.

38 G. Li, D. Zhu, L. Xue and H. Jiang, *Org. Lett.*, 2013, **15**, 5020.

39 Q. Wan, S. Chen, W. Shi, L. Li and H. Ma, *Angew. Chem., Int. Ed.*, 2014, **53**, 10916.

40 G. K. Vegesna, J. Janjanam, J. Bi, F.-T. Luo, J. Zhang, C. Olds, A. Tiwari and H. Liu, *J. Mater. Chem. B*, 2014, **2**, 4500.

41 J. Hua, F. Wu, S. Feng, J. Xu, Z. Xu, Y. Chen, T. Tang, X. Weng and X. Zhou, *Sens. Actuators, B*, 2014, **196**, 194.

42 M. Yu, X. Wu, B. Lin, J. Han, L. Yang and S. Han, *Anal. Chem.*, 2015, **87**, 6688.

43 D.-D. He, W. Liu, R. Sun, C. Fan, Y.-J. Xu and J.-F. Ge, *Anal. Chem.*, 2015, **87**, 1499.

44 S.-L. Shen, X.-P. Chen, X.-F. Zhang, J.-Y. Miao and B.-X. Zhao, *J. Mater. Chem. B*, 2015, **3**, 919.

45 X. Zhang, C. Wang, Z. Han and Y. Xiao, *ACS Appl. Mater. Interfaces*, 2014, **6**, 21669.

46 B. Dong, X. Song, C. Wang, X. Kong, Y. Tang and W. Lin, *Anal. Chem.*, 2016, **88**, 4085.

47 L. Wu, Y. Wang, T. D. James, N. Jia and C. Huang, *Chem. Commun.*, 2018, **54**, 5518.

48 (*a*) A. Dreyer and K.-J. Dietz, *Antioxidants*, 2018, **7**, 169; (*b*) N. T. Moldogazieva, S. V. Lutsenko and A. A. Terentiev, *Cancer Res.*, 2018, **78**, 6040; (*c*) M. H. Hoffmann and H. R. Griffiths, *Free Radical Biol. Med.*, 2018, **125**, 62.

49 (*a*) L. Fialkow, Y. Wang and G. P. Downey, *Free Radical Biol. Med.*, 2007, **42**, 153; (*b*) S. G. Rhee, *Exp. Mol. Med.*, 1999, **31**, 53; (*c*) A. van der Vliet and Y. M. W. Janssen-Heininger, *J. Cell. Biochem.*, 2014, **115**, 427.

50 D. Song, J. M. Lim, S. Cho, S.-J. Park, J. Cho, D. Kang, S. G. Rhee, Y. You and W. Nam, *Chem. Commun.*, 2012, **48**, 5449.

51 J. Jing and J.-L. Zhang, *Chem. Sci.*, 2013, **4**, 2947.

52 D. Kim, G. Kim, S.-J. Nam, J. Yin and J. Yoon, *Sci. Rep.*, 2015, **5**, 8488.

53 (*a*) C.-H. Sam and H.-K. Lu, *J. Dent. Sci.*, 2009, **4**, 45; (*b*) D. Lapenna and F. Cuccurullo, *Gen. Pharmacol.*, 1996, **27**, 1145.

54 (*a*) M. Ren, K. Zhou, L. He and W. Lin, *J. Mater. Chem. B*, 1716, **2018**, 6; (*b*) H. Li, J. Fan and X. Peng, *Prog. Chem.*, 2017, **29**, 17; (*c*) Y. Yue, F. Huo, C. Yin, J. O. Escobedoc and R. M. Strongin, *Analyst*, 2016, **141**, 1859.

55 L. Yuan, L. Wang, B. K. Agrawalla, S.-J. Park, H. Zhu, B. Sivaraman, J. Peng, Q.-H. Xu and Y.-T. Chang, *J. Am. Chem. Soc.*, 2015, **137**, 5930.

56 B. Zhu, P. Li, W. Shu, X. Wang, C. Liu, Y. Wang, Z. Wang, Y. Wang and B. Tang, *Anal. Chem.*, 2016, **88**, 12532.

57 M. Ren, B. Deng, K. Zhou, X. Kong, J.-Y. Wang, G. Xu and W. Lin, *J. Mater. Chem. B*, 2016, **4**, 4739.

58 Z. Zhang, J. Fan, G. Cheng, S. Ghazali, J. Du and X. Peng, *Sens. Actuators, B*, 2017, **246**, 293.

59 B. Zhang, X. Yang, R. Zhang, Y. Liu, X. Ren, M. Xian, Y. Ye and Y. Zhao, *Anal. Chem.*, 2017, **89**, 10384.

60 (*a*) N. Taniguchi, *Adv. Clin. Chem.*, 1992, **29**, 1; (*b*) L. A. Pham-Huy, H. He and C. Pham-Huy, *Int. J. Biomed. Sci.*, 2008, **4**, 89.

61 X. Lu, Z. Chen, X. Dong and W. Zhao, *ACS Sens.*, 2018, **3**, 59.

62 (*a*) M. Maiorino, M. Conrad and F. Ursini, *Antioxid. Redox Signaling*, 2018, **29**, 61; (*b*) A. Romano, G. Serviddio, S. Calcagnini, R. Villani, A. M. Giudetti, T. Cassano and S. Gaetani, *Free Radical Biol. Med.*, 2017, **111**, 281; (*c*) A. Marjani, *Bioscience Res.*, 2016, **13**, 21.

63 (*a*) G. P. C. Drummen, L. C. M. Liebergen, J. A. F. O. den Kamp and J. A. Post, *Free Radical Biol. Med.*, 2002, **33**, 473; (*b*) M. Takahashi, M. Shibata and E. Nikia, *Free Radical Biol. Med.*, 2001, **31**, 164.

64 X. Zhang, B. Wang, C. Wang, L. Chen and Y. Xiao, *Anal. Chem.*, 2015, **87**, 8292.

65 (*a*) T. Takata, H. Ihara, N. Hatano, Y. Tsuchiya, T. Akaike and Y. Watanabe, *Biochem. J.*, 2017, **474**, 2547; (*b*) X. Jiao, Y. Li, J. Niu, X. Xie, X. Wang and B. Tang, *Anal. Chem.*, 2018, **90**, 533.

66 (*a*) P. Kamoun, M.-C. Belardinelli, A. Chabli, K. Lallouchi and B. Chadefaux-Vekemans, *Am. J. Med. Genet.*, 2003, **116A**, 31; (*b*) A. R. Lippert, E. J. New and C. J. Chang, *J. Am. Chem. Soc.*, 2011, **133**, 10078.

67 (*a*) N. S. Cheung, Z. F. Peng, M. J. Chen, P. K. Moore and M. Whiteman, *Neuropharmacology*, 2007, **53**, 505; (*b*) L.-F. Hu, M. Lu, P. T. H. Wong and J.-S. Bian, *Antioxid. Redox Signaling*, 2011, **15**, 405.

68 T. Liu, Z. Xu, D. R. Spring and J. Cui, *Org. Lett.*, 2013, **15**, 2310.

69 S. Yang, Y. Qi, C. Liu, Y. Wang, Y. Zhao, L. Wang, J. Li, W. Tan and R. Yang, *Anal. Chem.*, 2014, **86**, 7508.

70 X. J. Zou, Y. C. Ma, L. E. Guo, W. X. Liu, M. J. Liu, C. G. Zou, Y. Zhou and J. F. Zhang, *Chem. Commun.*, 2014, **50**, 13833.

71 X. Zhang, H. Tan, Y. Yan, Y. Hang, F. Yu, X. Qu and J. Hua, *J. Mater. Chem. B*, 2017, **5**, 2172.

72 (*a*) X.-B. Wang, H. Cui, X.-H. Liu and J.-B. Du, *Histol. Histopathol.*, 2017, **32**, 1231; (*b*) X.-B. Wang, J.-B. Du and H. Cui, *Life Sci.*, 2014, **98**, 63; (*c*) D. Liu, H. Jin, C. Tang and J. Du, *Mini-Rev. Med. Chem.*, 2010, **10**, 1039.

73 Y. Zhao, Y. Ma and W. Lin, *Sens. Actuators, B*, 2018, **268**, 157.

74 (*a*) G.-J. Kim, K. Lee, H. Kwon and H.-J. Kim, *Org. Lett.*, 2011, **13**, 2799; (*b*) C. S. Lim, G. Masanta, H. J. Kim, J. H. Han, H. M. Kim and B. R. Cho, *J. Am. Chem. Soc.*, 2011, **133**, 11132.

75 (*a*) C.-X. Yin, K.-M. Xiong, F.-J. Huo, J. C. Salamanca and R. M. Strongin, *Angew. Chem., Int. Ed.*, 2017, **56**, 13188; (*b*) J. B. Lloyd, *Biochem. J.*, 1986, **237**, 271.

76 (*a*) Z. Lu, Y. Lu, C. Fan, X. Sun, M. Zhang and Y. Lu, *J. Mater. Chem. B*, 2018, **6**, 8221; (*b*) Z. Zhou, G. Duan, Y. Wang, S. Yang, X. Liu, L. Zhang, R. Sun, Y. Xu, Y. Gu and X. Zha, *New J. Chem.*, 2018, **42**, 18172.

77 (*a*) S. Lee, J. Li, X. Zhou, J. Yin and J. Yoon, *Coord. Chem. Rev.*, 2018, **366**, 29; (*b*) J. Fan, Z. Han, Y. Kang and X. Peng, *Sci. Rep.*, 2016, **6**, 19562.

78 J. Fan, Z. Han, Y. Kang and X. Peng, *Sci. Rep.*, 2016, **6**, 19562.

79 C. Chen, L. Zhou, W. Liu and W. Liu, *Anal. Chem.*, 2018, **90**, 6138.

80 (*a*) Y. Ishimoto, T. Tanaka, Y. Yoshida and R. Inagi, *Clin. Exp. Pharmacol. Physiol.*, 2018, **45**, 1097; (*b*) R. Nemes, E. Koltai, A. W. Taylor, K. Suzuki, F. Gyori and Z. Radak, *Antioxidants*, 2018, **7**, 85.

81 (*a*) P. Narne, V. Pandey and P. B. Phanithi, *Mol. Neurobiol.*, 2019, **56**, 1749; (*b*) H. C. Saternos and W. A. AbouAlaiwi, *Nitric Oxide*, 2018, **80**, 108.

82 T. R. M. da Silva, J. R. de Freitas, Q. C. Silva, C. P. Figueira, E. Roxo, S. C. Leão, L. A. R. de Freitas and P. S. T. Veras, *Infect. Immun.*, 2002, **70**, 5628.

83 H. Yu, Y. Xiao and L. Jin, *J. Am. Chem. Soc.*, 2012, **134**, 17486.

84 (*a*) C. Prolo, N. Rios, L. Piacenza, M. N. Álvarez and R. Radi, *Free Radical Biol. Med.*, 2018, **128**, 59; (*b*) G. Ferrer-Sueta, N. Campolo, M. Trujillo, S. Bartesaghi, S. Carballal, N. Romero, B. Alvarez and R. Radi, *Chem. Rev.*, 2018, **118**, 1338; (*c*) H. Zhang, J. Liu, C. Liu, P. Yu, M. Sun, X. Yan, J.-P. Guo and W. Guo, *Biomaterials*, 2017, **133**, 60.

85 B. Guo, J. Jing, L. Nie, F. Xin, C. Gao, W. Yang and X. Zhang, *J. Mater. Chem. B*, 2018, **6**, 580.

86 (*a*) J. M. Fukuto, *Br. J. Pharmacol.*, 2019, **176**, 135; (*b*) R. Smulik-Izydorczyk, K. Dębowska, J. Pięta, R. Michalski, A. Marcinek and A. Sikora, *Free Radical Biol. Med.*, 2018, **128**, 69.

87 X. Jing, F. Yu and L. Chen, *Chem. Commun.*, 2014, **50**, 14253.

88 (*a*) E. M. Nolan and S. J. Lippard, *Acc. Chem. Res.*, 2009, **42**, 193; (*b*) P. Jiang and Z. Guo, *Coord. Chem. Rev.*, 2004, **248**, 205.

89 L. Xue, G. Li, D. Zhu, Q. Liu and H. Jiang, *Inorg. Chem.*, 2012, **51**, 10842.

90 H.-J. Lee, C.-W. Cho, H. Seo, S. Singha, Y. W. Jun, K.-H. Lee, Y. Jung, K.-T. Kim, S. Park, S. C. Bae and K. H. Ahn, *Chem. Commun.*, 2016, **52**, 124.

91 (*a*) G. Sivaraman, M. Iniya, T. Anand, N. G. Kotla, O. Sunnapu, S. Singaravadivel, A. Gulyani and D. Chellappa, *Coord. Chem. Rev.*, 2018, **357**, 50; (*b*) J. A. Cotruvo Jr, A. T. Aron, K. M. Ramos-Torres and C. J. Chang, *Chem. Soc. Rev.*, 2015, **44**, 4400; (*c*) C. Shen and E. J. New, *Metallomics*, 2015, **7**, 56.

92 M. Ren, B. Deng, J.-Y. Wang, Z.-R. Liu and W. Lin, *J. Mater. Chem. B*, 2015, **3**, 6746.

93 (*a*) E. M. Williams, R. F. Little, A. M. Mowday, M. H. Rich, J. V. E. Chan-Hyams, J. N. Copp, J. B. Smaill, A. V. Patterson and D. F. Ackerley, *Biochem. J.*, 2015, **471**, 131; (*b*) W. Qin, C. Xu, Y. Zhao, C. Yu, S. Shen, L. Li and W. Huang, *Chin. Chem. Lett.*, 2018, **29**, 1451.

94 J. Zhou, W. Shi, L.-H. Li, Q.-Y. Gong, X.-F. Wu, X.-H. Li and H.-M. Ma, *Chem. – Asian J.*, 2016, **11**, 2719.

95 (*a*) J. R. Xavier, K. V. Ramana and R. K. Sharma, *J. Food Biochem.*, 2018, **42**, e12564; (*b*) B. Y. Lee, J. A. Han, J. S. Im, A. Morrone, K. Johung, E. C. Goodwin, W. J. Kleijer, D. DiMaio and E. S. Hwang, *Aging Cell*, 2006, **5**, 187; (*c*) J. J. Going, R. C. Stuart, M. Downie, A. J. Fletcher-Monaghan and W. N. Keith, *J. Pathol.*, 2002, **196**, 394.

96 J. Huang, N. Li, Q. Wang, Y. Gu and P. Wang, *Sens. Actuators, B*, 2017, **246**, 833.

97 (*a*) Z. Xu and L. Xu, *Chem. Commun.*, 2016, **52**, 1094; (*b*) H.-I. Un, S. Wu, C.-B. Huang, Z. Xu and L. Xu, *Chem. Commun.*, 2015, **51**, 3143; (*c*) H.-I. Un, C.-B. Huang, C. Huang, T. Jia, X.-L. Zhao, C.-H. Wang, L. Xu and H.-B. Yang, *Org. Chem. Front.*, 2014, **1**, 1083; (*d*) H.-I. Un, C.-B. Huang, J. Huang, C. Huang, T. Jia and L. Xu, *Chem. – Asian J.*, 2014, **9**, 3397; (*e*) Z. Xu, G. Li, Y.-Y. Ren, H. Huang, X. Wen, Q. Xu, X. Fan, Z. Huang, J. Huang and L. Xu, *Dalton Trans.*, 2016, **45**, 12087; (*f*) Z. Xu, Y.-Y. Ren, X. Fan, S. Cheng, Q. Xu and L. Xu, *Tetrahedron*, 2015, **71**, 5055.

98 (*a*) C.-B. Huang, L. Xu, J.-L. Zhu, Y.-X. Wang, B. Sun, X. Li and H.-B. Yang, *J. Am. Chem. Soc.*, 2017, **139**, 9459; (*b*) L.-J. Chen, S. Chen, Y. Qin, L. Xu, G.-Q. Yin, J.-L. Zhu, F.-F. Zhu, W. Zheng, X. Li and H.-B. Yang, *J. Am. Chem. Soc.*, 2018, **140**, 5049; (*c*) C.-W. Zhang, B. Ou, S.-T. Jiang, G.-Q. Yin, L.-J. Chen, L. Xu, X. Li and H.-B. Yang, *Polym. Chem.*, 2018, **9**, 2021; (*d*) Y.-Y. Ren, N.-W. Wu, J. Huang, Z. Xu, D.-D. Sun, C.-H. Wang and L. Xu, *Chem. Commun.*, 2015, **51**, 15153; (*e*) W.-J. Fan, B. Sun, J. Ma, X. Li, H. Tan and L. Xu, *Chem. – Eur. J.*, 2015, **21**, 12947.